IN-SITU 3D IMAGING OF STRUCTURE AND FAILURE OF MATERIALS USING SYNCHROTRON RADIATION TOMOGRAPHY

A Thesis Submitted to the College of
Graduate Studies and Research
In Partial Fulfillment of the Requirements
For the Degree of Master of Science
In the Department of Mechanical Engineering
University of Saskatchewan
Saskatoon

By

K. M. MOSTAFIJUR RAHMAN

PERMISSION TO USE

In presenting this thesis in partial fulfillment of the requirements for a Postgraduate degree from the University of Saskatchewan, I agree that the Libraries of this University may make it freely available for inspection. I further agree that permission for copying of this thesis in any manner, in whole or in part, for scholarly purposes may be granted by the professor or professors who supervised my thesis work or, in their absence, by the Head of the Department or the Dean of the College in which my thesis work was done. It is understood that any copying or publication or use of this thesis or parts thereof for financial gain shall not be allowed without my written permission. It is also understood that due recognition shall be given to me and to the University of Saskatchewan in any scholarly use which may be made of any material in my thesis.

Requests for permission to copy or to make other use of material in this thesis in whole or part should be addressed to:

Head of the Department of Mechanical Engineering
57 Campus Drive
University of Saskatchewan
Saskatoon, Saskatchewan
Canada, S7N 5A9

ABSTRACT

X-ray micro-tomography has become an increasingly important technique for characterizing the 3D microstructure of materials. This became possible mainly because spatial resolution of the imaging detectors has improved, and synchrotron radiation is more accessible for micro-tomography imaging.

In the presented project a novel experimental system has been designed and built at Biomedical Imaging and Therapy (BMIT)'s 05B1-1 beamline at Canadian Light Source (CLS). This system allows imaging structural transformation during in-situ loading experiments under tensile stress. The system was tested and several examples illustrating the application of this experimental system are presented.

The system has been used to image the structure of porous aluminum and the size and distribution of pores was analyzed. The system was also used to image the structure of $Al/Al_2O_3/TiC$ hybrid composites manufactured by accumulated roll bonding (ARB) process and this allowed analyzing the size distribution of reinforcing particles and voids. It was further demonstrated that in-situ imaging of deformation can be used to image consecutive stages of structural transformation (change in volume, change of position of reinforcing particles, creation of voids etc.) in aluminum alloy and aluminum composites during application of tensile stress and to illustrate the nucleation of failure.

This system of dynamic imaging at BMIT-BM at CLS can help in better description of structural transformation associated with the application of stress and will contribute to better understanding of the failure mechanisms of different types of materials during straining.

ACKNOWLEDGMENTS

The work presented in this thesis has been carried out at Department of Mechanical Engineering, University of Saskatchewan, Saskatoon, Saskatchewan during the years 2010 - 2012 under the kind supervision of Dr. Jerzy A. Szpunar.

First, I would like to express my gratitude to my supervisor, Dr. Jerzy Szpunar for introducing me to this research field and for his continuous support, inspiration, and guidance throughout the project. His vast knowledge and expertise in this field added considerably to my graduate experience.

Special thanks to our research group members, George Belev, Denise Miller, Tomasz Wysokinski and Professor David Cooper.Also I would like to acknowledge help of machine shop staffs Keith, Kevin, and electronics technologist Bob Wilson. We are grateful for the aluminum composites that were provided by Professor M. R.Toroghinejad. Work described in this thesis was performed at the Canadian Light Source. This research is supported by the Natural Sciences and Engineering Research Council of Canada.

I would like also to thank my thesis committee for their insightful comments. I would also like to acknowledge the financial support from the University of Saskatchewan.

Finally, I would like to thank my family for their love, encouragement, and support.

- K. M. Mostafijur Rahman

TABLE OF CONTENTS

Page

PERMISSION TO USE…….. i

ABSTRACT ii

ACKNOWLEDGMENTS iii

LIST OF TABLES vi

LIST OF FIGURES vii

LIST OF ABBREVIATIONS x

1 INTRODUCTION 01

1.1 2D imaging and its limits 01
1.2 3D X-ray tomography 02
1.3 Synchrotron Radiation Computed Tomography 03
1.4 In-situ experiments 03
1.5 Objectives of the present project 04

2 LITERATURE REVIEW 05

2.1 Literature review on 3D tomography imaging in material science 05
2.2 Computed Tomography 09
2.2.1 Overview 09
2.2.2 Reconstruction methods of the projected images 10

3 EXPERIMENTAL FACILITY AND SPECIMEN PEPARATION 14

3.1 BMIT at Canadian Light Source 14
3.2 Specimen used for 3D imaging 17

4 DESIGN OF EXPERIMENTAL STAGE FOR TENSILE LOADING 21

4.1 Overview of the sample stage 21
4.2 Tensile System 22
4.3 Rotational System 23
4.4 Control System 25
4.5 Summary on Equipment Design 26

5 3D STRUCTURAL ANALYSIS OF POROUS ALUMINUM 27

5.1 Summary of the findings 30

6 3D IMAGING OF ALUMINUM COMPOSITES 31

6.1 Al/Al2O3/TiC composite after 4 ARB passes 31
6.2 Al/Al2O3/TiC composite after 8 ARB passes 33
6.3 Al/Al2O3/TiC composite after 10 ARB passes 36
6.4 Comparison and discussion of the composites structure after different passes 39
6.5 Comments on the findings 43

7 IN-SITU STRUCTURAL ANALYSIS OF ALUMINUM ALLOY (AA 6061) UNDER TENSILE LOADING 44

7.1 In-situ 2D Experiment under Tensile stress of AA 6061 in SEM 44
7.2 In-situ 3D Experiment under Tensile stress of AA 6061 using Synchrotron Radiation Tomography 47
7.3 Comments on the findings 49

8 IN-SITU 3D STRUCTURAL ANALYSIS OF ALUMINUM COMPOSITE UNDER TENSILE LOADING 50

8.1 3D view of the composite in different strain using synchrotron radiation tomography 50
8.2 Size distribution of voids in the composite at different strain levels 57
8.3 Discussion on findings 62

9 CONCLUSION 63

10 FUTURE WORK 65

11 LIST OF REFERENCES 66

12 APPENDIX 68

LIST OF TABLES

Table Page

3.1 The parameters of the BMIT-BM beamline used in the present investigation 15

3.2 The parameters for the BMIT-ID beamline under construction 15

5.1 Volume fractions of the porous aluminum 30

6.1 Results of measurements of alumina particles in the ARB composites 38

6.2 Results of measurements of voids in the ARB composites 39

8.1 Results of measurements of voids in different stain levels in the composite 60

LIST OF FIGURES

Figure Page

2.1 Reconstructed tomographic slices before tensile deformation located approximately in the middle plane of the sample for materials 5754, 2024 and 7449 (figure a–c respectively). Each slice is parallel to the tensile axis. The notch radius is 1 mm 05

2.2 Same slices as in Fig 2.1 after deformation for materials 5054, 2024 and 7449 (figure a–c respectively) 06

2.3 (a) 3D microstructures of as-processed composite showing distribution of voids and Fe-rich inclusions. (b) Quantitative analysis of void fraction and inclusion fraction as a function of distance along the gauge length. The distribution of voids and inclusions is quite uniform 07

2.4 (a) 3D microstructures of composite after tensile fracture showing distribution of voids and cracks, and Fe-rich inclusions. (b) Quantitative analysis of void fraction as a function of distance along the gauge length. The damage is intensified over about 1 mm from the fracture surface. At larger distances the damage state is similar to that of the as-processed material 07

2.5 Computed tomography views 10

2.6 Back projection 12

2.7 Filtered backprojection 13

3.1 (a) Canadian Light Source (CLS) (b) Beam Lines 14

3.2 Experimental set-up at BMIT-BM beamline 16

3.3 Manufacturing process of porous aluminum 17

3.4 Manufacturing process of the hybrid composites by ARB 20

3.5 Tensile sample 20

4.1 Experimental sample stage 21

4.2 Tensile system of the sample stage 22

4.3 Rotational system of the sample stage 24

4.4 Control system of the sample stage 26

5.1 Selection of threshold value to segment the voids and aluminum 27

5.2 3D view of the porous aluminum 28

5.3 3D view of the porous aluminum (slice cut from the left side to see inside) 28
5.4 3D view of the porous aluminum (slice cut from both sides to see inside) 29
5.5 Volume distribution of voids in the porous aluminum 29
6.1 3D view of the composite after 4 passes (front view) 31
6.2 3D view of the composite after 4 passes (side view) 32
6.3 Volume of alumina particles distribution chart after 4 passes 32
6.4 Volume of voids distribution chart after 4 passes 33
6.5 3D view of the composite after 8 passes (front view) 34
6.6 3D view of the composite after 8 passes (side view) 34
6.7 Volume of alumina particles distribution chart after 8 passes 35
6.8 Volume of voids distribution chart after 8 passes 35
6.9 3D view of the composite after 10 passes (front view) 36
6.10 3D view of the composite after 10 passes (side view) 36
6.11 Volume of alumina particles distribution chart after 10 passes 37
6.12 Volume of voids distribution chart after 10 ARB passes 37
6.13 Number of alumina particle vs. number of ARB cycle 40
6.14 Mean volume of alumina particle vs. number of ARB cycle 40
6.15 Volume of the largest alumina particle vs. number of ARB passes 41
6.16 Volume % of alumina vs. number of ARB cycle 41
6.17 Number of voids vs. number of ARB cycle 42
6.18 Mean volume of voids vs. number of ARB cycle 42
6.19 Volume of the largest void vs. number of ARB passes 42
6.20 Volume % of voids vs. number of ARB cycle 43
7.1 Tensile sample 44
7.2 2D surface image of AA6061 in different strain levels 45

7.3 Load vs elongation curve of AA 6061 tensile test 45

7.4 Close view of the fracture of the AA 6061 sample 46

7.5 3D images of the AA 6061 in different strain levels (a) without loading (b) after 0.30 mm elongation (c) after 0.40 mm elongation 47

7.6 (a) 3D images of AA 6061 after 0.40 mm elongation (b) Close view of the sample showing crack propagation inside the material in 3D 48

8.1 3D view of the composite without loading 51

8.2 3D view of the composite without loading (witout aluminum matrix) 51

8.3 3D view of voids in the composite without loading 52

8.4 3D view of the composite after 0.30 mm elongation 52

8.5 3D view of the composite after 0.30 mm elongation (without aluminum matrix) 53

8.6 3D view of voids in the composite after 0.30 mm elongation 53

8.7 3D view of the composite after 0.40mm elongation 54

8.8 3D view of the composite after 0.40mm elongation (without aluminum matrix) 54

8.9 3D view of voids in the composite after 0.40 mm elongation 55

8.10 3D view of the coposite after 0.45mm elongation 55

8.11 3D view of the coposite after 0.45mm elongation (without aluminum matrix) 56

8.12 3D view of voids in the composite after 0.45 mm elongation 56

8.13 Volume of voids distribution chart without loading 57

8.14 Volume of voids distribution chart after 0.30 mm elongation 58

8.15 Volume of voids distribution chart after 0.40 mm elongation 59

8.16 Volume of voids distribution chart after 0.45mm elongation 59

8.17 Total number voids vs. the elongation 61

8.18 Total volume of void vs. elongation 61

8.19 Mean volume of voids vs. elongation 61

8.20 Volume of the largest void vs. elongation 62

LIST OF ABBREVIATIONS

Abbreviation	
2D	Two Dimensional
3D	Three Dimensional
ARB	Accumulated Roll Bonding
ART	Algebraic Reconstruction Technique
ASTM	American Standard for Testing Materials
BMIT-BM	Biomedical Imaging and Therapy-Bending Magnet
BMIT-ID	Biomedical Imaging and Therapy-Insertion Device
CCD	Charged Coupled Detector
CLS	Canadian Light Source
CT	Computed Tomography
DP	Dual Phase
ESRF	European Synchrotron Radiation Facility
FFT	Fast Fourier Transform
ILST	Iterative Least Squares Technique
MG	Microstructure Gauge
PSF	Point Spread Function
RT	Rice and Tracy
SEM	Scanning Electron Microscope
SIRT	Simultaneous Iterative Reconstruction Technique
TEM	Transmission Electron Microscope

CHAPTER 1
INTRODUCTION

The micrometer range resolution of synchrotron radiation tomography has allowed development of an important technique for characterizing the three dimensional (3D) microstructure of materials. To optimize materials, it is common to relate mechanical, chemical or physical properties to microstructure. During the manufacturing processes, the structure of materials can be optimized to satisfy requirement for different engineering applications. Understanding of complicated relationships between structure and properties is essential for the optimum design of various engineering structures and systems. Such design is often influenced by service conditions and environment. Understanding of performance and failure of materials in service is crucial for extending the life of various engineering components and preventing unexpected failure. The materials characterization is performed in 2D using optical microscope or scanning electron microscope (SEM) or transmission electron microscopy (TEM) under different environmental conditions e.g. temperature, mechanical load. Though these 2D imaging techniques have very important contribution to materials characterization, we need complementary 3D techniques to understand the materials structure and behavior more accurately [1].

1.1 2D imaging and its limits

Micro-structural information can be obtained by analysis of 2D images. In the following cases 2D measurements give us good approximation of the 3D information:

- The volume fraction of structural elements, when they have isotropic shape [2].
- In some simple cases (sphere, cube) for the size and size distribution using Saltykov methods for spheres or other shape [2 - 4].
- The specific surface Sv, which is defined as the area of the solid–liquid interface per unit volume of solid, and is often related to micro-structural evolutions [2].

However this 2D analysis is not sufficient when direct 3D information is needed:

- The number of objects per surface area cannot be linked to the true 3D number of objects per unit volume since on a 2D section objects might appear separated whereas they may be connected in 3D.

- The size distribution of phases with complex shape in the material cannot be obtained from a 2D section.
- The connectivity of phases cannot be obtained from 2D measurements since this is obviously a 3D parameter.
- Nucleation and propagation of failure in engineering materials cannot be observed 2D in the most important cases of failure if nucleation occurs inside the materials or in other plane than the plane we are looking at.
- Furthermore, sometimes sample preparation for 2D observations may lead to artifacts i.e. observation of porosities is not easy since polishing might create artificial porosities by extracting hard phases such as intermetallics from the material or sometimes eliminating porosities in a soft material by refilling them [1].

In addition, from a mechanical point of view the stress state is not the same when measured on a free surface than in the bulk as it has been already demonstrated [5]. There is a need for 3D characterization of micro-structure which is now possible thanks to the recent developments in high resolution X-ray tomography.

1.2 3D X-ray tomography

In X-ray radiography an X-ray beam is sent on a sample and the transmitted beam through the sample is recorded by a detector (mainly film or CCD based detector for radiography). According to the Beer–Lambert law, the ratio of the number of transmitted to incident photons is related to the integral of the absorption coefficient of the material along the path that the photons follow through the sample. The absorption coefficient μ is linked to the density, the atomic number and the energy of radiation (when the beam is monochromatic) by using an empirical law. The resulting image is superimposed information (projection) of the absorption of the tested section of the sample in a 2D plane. The classical way to get 3D information is to perform a large number of radiographs while rotating the sample between 0˚ and 180˚. We do not need to take any further image projection till 360˚ because those would repeat the similar images as we already got till 180˚. The filtered back-projection algorithm can then be used to reconstruct the structure of the sample from these radiographs [6].

1.3 Synchrotron Radiation Computed Tomography

X-ray beams suitable for micro-tomography experiments are available either from microfocus X-ray apparatus that can be operated in a laboratory environment or at synchrotron radiation sources [7]. Synchrotron X-rays have the advantages of

- high photon flux,
- high brilliance,
- high parallelism,
- large energy range,
- partially coherent beam (at 3rd generation sources).

Because of which it needs shorter exposure time of the detector to take the projection image of the sample with reasonable contrast. Compared to laboratory X-ray micro-focus sources, synchrotron X-rays provide both a significantly higher image resolution and time resolution [8].

1.4 In-situ experiments

Among the reasons to perform the more challenging in-situ 3D imaging experiments [7]:

(i) In in-situ micro-tomography experiments the same gauge volume can be visualized during the experiment.

(ii) Unloading effects such as crack closure or a decrease of pore size due to shrinkage during cooling can be observed.

(iii) Artifacts introduced during the unloading/loading cycle and mounting/dismounting of the sample can be prevented.

However, there are some limitations to in-situ X-ray micro-tomography experiments:

(i) The data acquisition time needed to obtain a tomogram needs to be well adjusted to the time interval of the change of the microstructure.

(ii) Relaxation effects, e.g. during loading of polymers or an increase in sample length may introduce artifacts into the reconstructed image.

(iii) The loading or heat treatment experimental system must be specially designed to allow mounting in the existing tomography set-up.

Selection of materials and optimizing the structure for different service conditions is always necessary for all engineering applications. In particular, it is important to understand the mechanism of failure processes in different environment of service. An example of such applications is imaging the processes of structure transformation (change in volume, change of position of reinforcing particles, creation of voids etc.) and failure of materials during in-situ tensile test. Equipment for such 3D observation, when designed, will allow us to collect information essential for understanding the failure processes in important engineering materials. Although 2D in-situ tensile test can give us information of the sample at different strain levels, many phenomena related to the materials failure processes cannot be observed and analyzed since the 2D imaging is limited to the surface structure. A 3D in-situ imaging technique is needed to get the true 3D volumetric information on the structural transformation during failure processes.

1.5 Objectives of the present project

- To design and fabricate an experimental stage for in-situ experiments under tensile stress at CLS
- To analyze 3D structure of typical engineering materials:
  - (a) Porous aluminum
  - (b)Al/Al_2O_3/TiC hybrid composites
- To perform in-situ 3D structural analysis under tensile loading of the following engineering materials:
  - (a) AA 6061
  - (b) Al/Al_2O_3/TiC hybrid composites

CHAPTER 2
LITERATURE REVIEW

2.1 Literature review on 3D tomography imaging in material science

Over the last 20 years a series of novel and innovative true 3D internal imaging techniques have emerged, and already found a place in medical science. Following this success, the same 3D methods are now gradually applied in the advanced materials field.

In situ tensile experiments by using synchrotron X-ray tomography of three different aluminum alloys (2024, 7449 and 5754) exhibiting different mechanical properties has been done by Eric et al. (2011) [9]. These experiments allowed the observation of damage nucleation, growth and coalescence and produced a wide database on the mechanism of damage. The damage steps (initiation, growth and coalescence) were clearly visualized during in-situ tensile experiments. This method used gives a precise image of the outer shape of the sample and changes that take place during deformation (Fig 2.1), and allows calculating the true strain vs true stress curve and also an approximation of the stress triaxiality using the Bridgman formula.

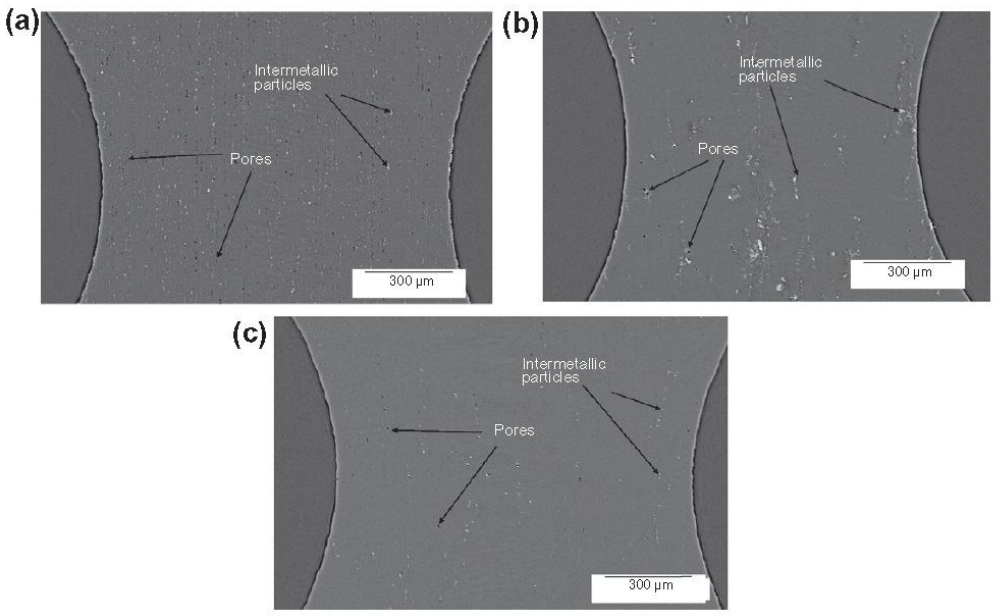

Fig 2.1: Reconstructed tomographic slices before tensile deformation located approximately in the middle plane of the sample for materials 5754, 2024 and 7449 (figure a–c respectively). Each slice is parallel to the tensile axis. The notch radius is 1 mm [9].

The results show that damage can be visualized and also quantified in terms of nucleation and growth, coalescence of microcracks being also evident in the results (Fig 2.2) but still it was hard to quantify. Finally, the authors found that a model for damage growth during ductile straining based on the Rice and Tracey approach can be used to explain the obtained results.

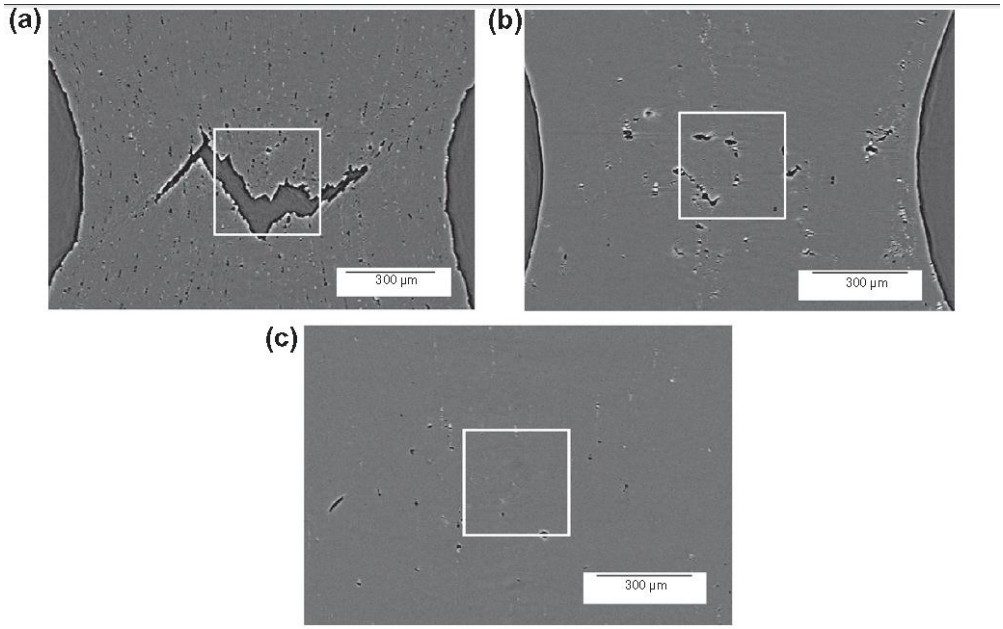

Fig 2.2: Same slices as in Fig 2.1 after deformation for materials 5054, 2024 and 7449 (figure a–c respectively) [9].

A systematic study of the 3D microstructure of SiC particle reinforced 2080 Al alloy matrix composites, as-processed and after tensile damage, was conducted using X-ray synchrotron tomography by Williams et al. (2010) [10]. Despite the similarity in density between Al and SiC, novel segmentation techniques allowed to obtain the 3D microstructure and quantitative analysis of fracture in this composite. Complimentary X-ray techniques, absorption and refraction, were used to analyze different phases in the microstructure (Fig 2.3). Absorption measurements were used to obtain the images of pores, Fe-rich inclusions, and oxide phases. Refraction was used to study the SiC particles, because of the sharp contrast at the particle/matrix interface facilitated observations. The damage zone in the composite was confined to a very small volume close to the fracture plane (Fig 2.4). The zone for void growth and for particle fracture both extended to about 1 mm from the fracture plane. A large number of

particles were sampled by X-ray tomography. Quantitative analysis of particle fracture showed that particles with larger size and larger aspect ratio are more prone to fracture. The strength of the particle appears to be a strong function of the aspect ratio.

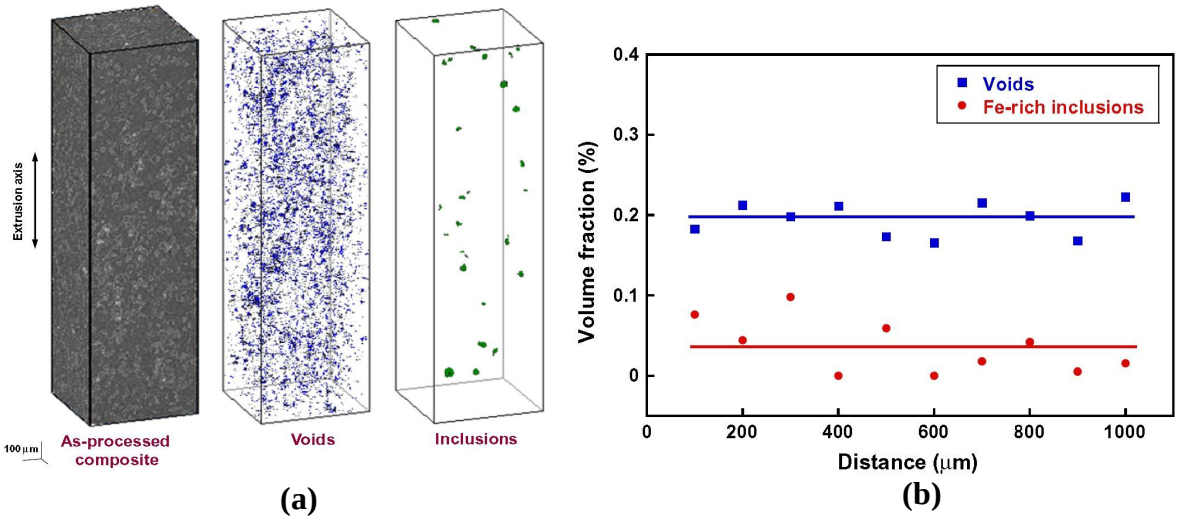

Fig 2.3: (a) 3D microstructures of as-processed composite showing distribution of voids and Fe-rich inclusions. (b) Quantitative analysis of void fraction and inclusion fraction as a function of distance along the gauge length. The distribution of voids and inclusions is quite uniform [10].

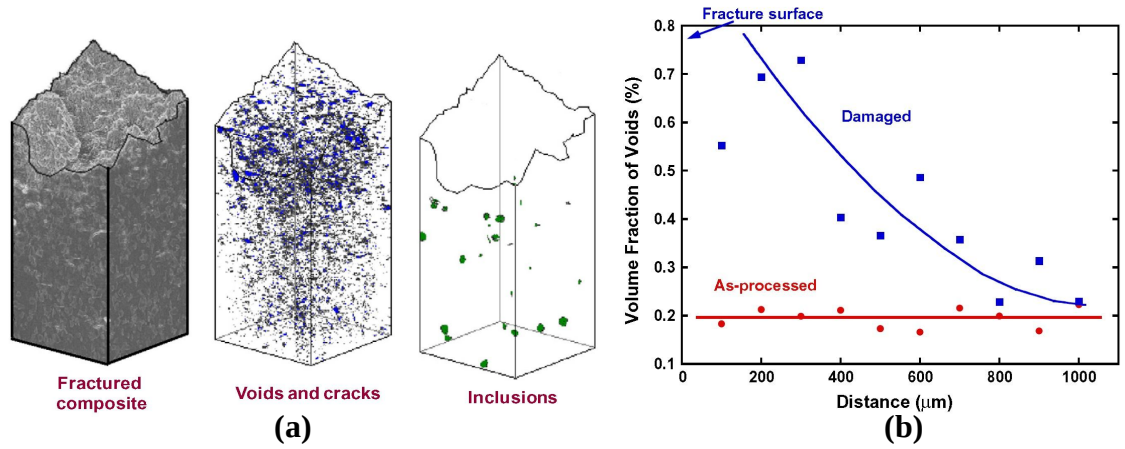

Fig 2.4: (a) 3D microstructures of composite after tensile fracture showing distribution of voids and cracks, and Fe-rich inclusions. (b) Quantitative analysis of void fraction as a function of distance along the gauge length. The damage is intensified over about 1 mm from the fracture surface. At larger distances the damage state is similar to that of the as-processed material [10].

The compressive behavior of closed-cell aluminum foams was investigated by Ohgaki et al. (2006) [11]. The microstructure of cell walls or plateau borders in the foams was visualized in 3D. The shapes and the 3D distribution of micropores, particles, and regions of solute segregation in the foams were evaluated, comparing the cell walls with the plateau borders. Under compressive loads, the damage was been observed using an in-situ test rig. It was found that the microcracks were initiated mainly from the cell walls and the micropores with large diameters. The crack initiation sites were classified from the obtained results. In addition, a method for non-destructive characterization of elastic and plastic deformation in the foams, called a 3D microstructure gauge (MG) method, was presented. The local strain mapping by the MG method indicates that the edges of the micropores with large diameters experience large strain under compression and this is consistent with the observed crack nucleation sites.

An in situ tensile test during X-ray tomography experiments on high-strength steel has been done by E. Maire et al. (2008) [12]. The experiment was done at ID15 beam line at the European Synchrotron Radiation Facility (ESRF) with the beam energy of 50 keV. This study showed that it was possible to qualify and quantify damage in 3D in the bulk of steels. The quantification of the observations led to the determination of some important parameters affecting damage. It was possible to measure not only the evolution of the density and size of the cavities, but also the local strain. The main finding of this quantitative analysis was the quasi-stagnation of the value of the average equivalent diameter of the cavities in the studied dual phase (DP) steel. This has been shown to be due to the competition between the growth of existing cavities and the nucleation of smaller new ones. To account for this competition, a new model has been proposed, inspired by studies on the precipitation process in metallic materials, and also composed of an initiation and a growth phase. The new model is based on the Rice and Tracy (RT) approach, which has been shown to describe the growth of the bigger cavities, and also accounts for the nucleation of cavities. The proposed model is able to predict the stagnation of the diameter of the cavities.

A comparison between the behavior of two constituent's ferrite and martensite, taken separately, was made in the experiment of damage measurement in dual phase steel by using in-situ high-resolution X-ray absorption tomography by Bareggi et al. (2012) [13]. The method was

particularly useful for analyzing the contribution of nucleation and growth of voids to failure in the studied materials. Quantitative analysis of the damage events was carried out on a same 3D region at different deformation steps for different samples cut from three kinds of materials. Void number prediction and growth of voids model was based on local stress triaxiality, and showed a Good agreement with the experimental data.

Accuracy in 3D imaging by X-ray tomography was discussed by Patterson et al. (2010) [14]. The quality of a 3D reconstruction of μCT data depends of many parameters. These parameters include the signal-to-noise of the individual radiographs, dimensional accuracy and contrast of the radiographs, number of radiographs, noise minimization during acquisition. Also of importance is the quality of the reconstruction algorithm. Most of these parameters are inherent to an individual instrument but several require the knowledge and experience of the operator and the selection of the right filters, acquisition settings and time on the instrument, specifically dwell time and number of radiographs. The authors conduct some experiments to establish the dimensional standard for micro X-ray computed tomography. They found that setting the size threshold to avoid noise domination was very difficult but must be optimized. The way to do this is to collect enough images to minimize the noise. More images are needed if the contrasts between objects are similar in X-ray absorption. As the gray scale range is directly proportional to the number of radiographs collected, more radiographs would be required to increase the contrast and we can get it by reducing the angular step size of the image projection around the sample.

2.2 Computed Tomography

2.2.1 Overview

The term *tomography* refers to the general class of devices and procedures for producing 2D cross-sectional images of a 3D object. Tomography systems make it possible to image the internal structure of objects in a non-invasive and non-destructive manner. In conventional x-ray radiography, a stationary source and planar detector are used to produce a 2D projection image of the object. The image has intensity proportional to the amount by which the x-rays are attenuated as they pass through the object, i.e., the 3D spatial distribution of x-ray attenuation coefficients is projected into a 2D image. X-rays passing through an object experience

exponential attenuation proportional to the linear attenuation coefficient of the object. The intensity of a collimated beam of monoenergetic x-radiation exiting a uniform block of material with linear attenuation coefficient μ and thickness d is given by $I = I_o e^{-\mu d}$ where I_0 is the intensity of the incident beam. For objects with spatially variant attenuation μ (*z*) along the path length *z*, this relationship is generalizes to: $I = I_0 e^{-\int \mu(z) dz}$

2.2.2 Reconstruction methods of the projected images

The relationship between the measured views and the corresponding image illustrates in Figure 2.5. Each image projection of the sample acquired in a CT system is equal to the sum of the image values along a ray pointing to those projection directions. For example, view 1 is found by adding all the pixels in each row. Likewise, view 3 is found by adding all the pixels in each column. The other views, such as view 2, sum the pixels along rays that are at an angle.

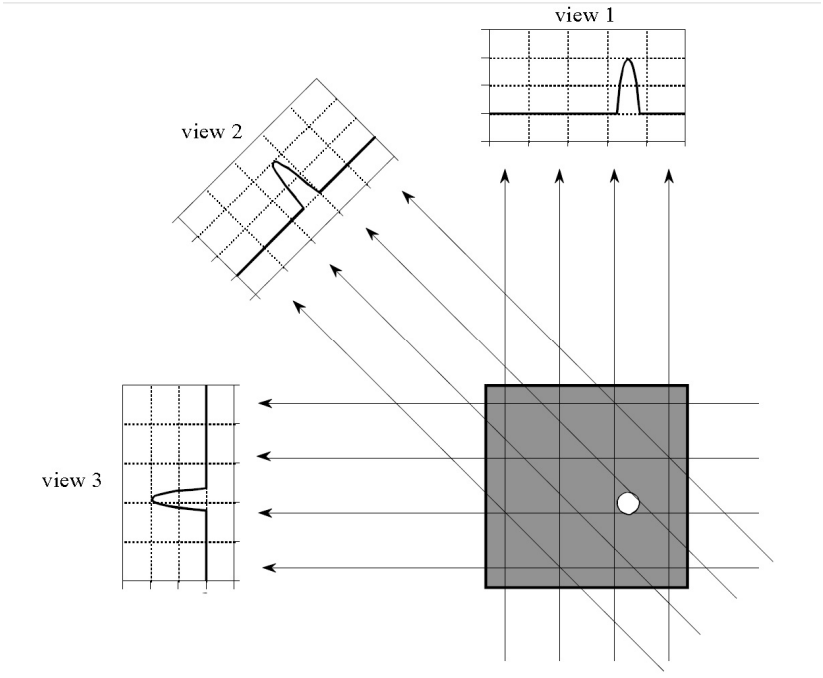

Fig 2.5: Computed tomography views [15].

There are four main approaches to calculate the slice image given the set of its views. These are called CT reconstruction algorithms.

The first method is based on solving many simultaneous linear equations. One equation can be written for each measurement. That is, an image projection of the sample of a particular

profile is the sum of a particular group of pixels in the image. The problem with this first method of CT reconstruction is computation time. Solving several hundred thousand simultaneous linear equations is a daunting task.

The second method of CT reconstruction uses iterative techniques to calculate the final image in small steps. There are several variations of this method: the Algebraic Reconstruction Technique (ART), Simultaneous Iterative Reconstruction Technique (SIRT), and Iterative Least Squares Technique (ILST). The difference between these methods is how the successive corrections are made: ray-by-ray, pixel-by-pixel, or simultaneously correcting the entire data set. In the ART algorithm, all the pixels in the image array are set to some arbitrary value. An iterative procedure is then used to gradually change the image array to correspond to the profiles. An iteration cycle consists of looping through each of the measured data points. For each measured value, the following question is asked: *how can the pixels values in the array are changed to make them consistent with this particular value of measured intensity*? In other words, the measured intensity from the sample is compared with the sum of the image pixels along the ray pointing at the sample. If the sum is lower than the intensity from the measured sample, all the pixels along the ray are increased in value. Likewise, if the ray sum is higher than the measured sample, all of the pixel values along the ray are decreased. After the first complete iteration cycle, there will still be an error between the ray sums and the measured values. This is because the changes made for any one measurement disrupts all the previous corrections made. The idea is that the errors become smaller with repeated iterations until the image converges to the proper solution. Iterative techniques are generally slow, but they are useful when better algorithms are not available.

The third method is called filtered backprojection. It is a modification of an older technique, called backprojection or simple backprojection. Figure 2.5 shows that simple backprojection is a common sense approach, but not very sophisticated. An individual projected image of the sample is backprojected by setting all the image pixels along the ray pointing to the projected image of the sample to the same value. In less technical terms, a backprojection is formed by *smearing* each view back through the image in the direction it was originally acquired. The final backprojected image is then taken as the sum of all the backprojected views.

While backprojection is conceptually simple, it does not correctly solve the imaging problem. As shown in the figure 2.6 a backprojected image is very *blurry*. A single point in the *true* image is reconstructed as a circular region that decreases in intensity away from the center. In more formal terms, the point spread function of backprojection is circularly symmetric, and decreases as the reciprocal of its radius.

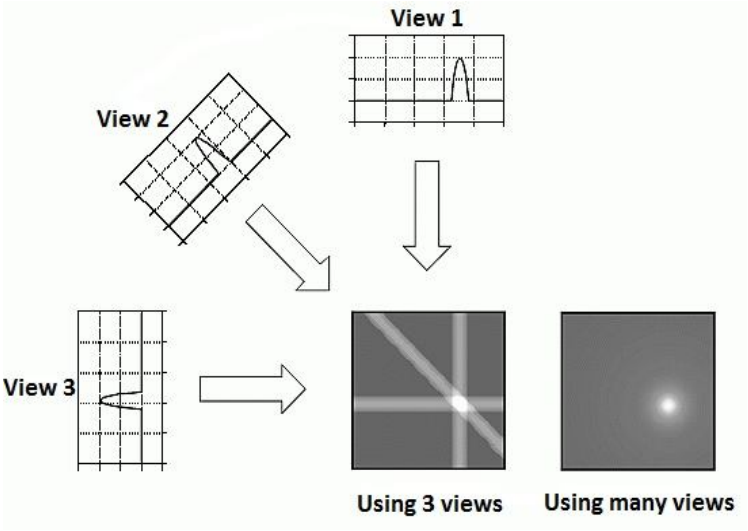

Fig 2.6: Back projection [15].

Filtered backprojection is a technique to correct the blurring encountered in simple backprojection. As illustrated in Fig. 2.7, each view is *filtered* before the backprojection to counteract the blurring Point Spread Function (PSF). That is, each of the one-dimensional views is convolved with a one-dimensional filter kernel to create a set of *filtered views*. These filtered views are then backprojected to provide the reconstructed image, a close approximation to the "correct" image. In fact, the image produced by filtered backprojection is *identical* to the "correct" image when there are an *infinite* number of views and an *infinite* number of points per view. The image in this example is a uniform white circle surrounded by a black background (a pillbox). Each of the acquired views has a flat background with a rounded region representing the white circle. Filtering changes the views in two significant ways. First, the top of the pulse is made flat, resulting in the final backprojection creating a *uniform* signal level within the circle. Second, negative spikes have been introduced at the sides of the pulse. When backprojected, these negative regions counteract the blur.

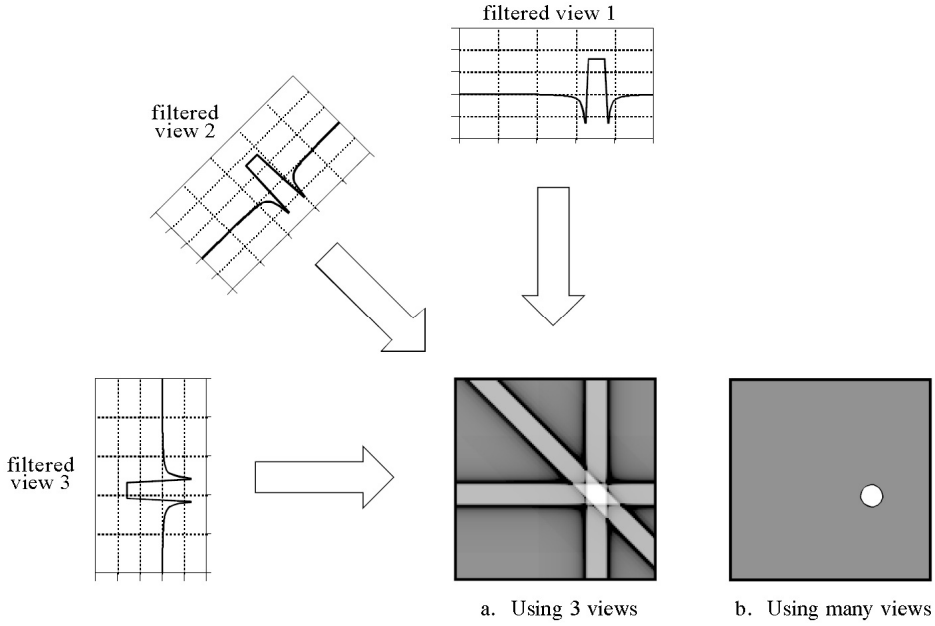

Fig 2.7: Filtered backprojection [15].

The fourth method is called Fourier reconstruction. In the spatial domain, CT reconstruction involves the relationship between a two-dimensional image and its set of one-dimensional views. By taking the two-dimensional Fourier transform of the image and the one-dimensional Fourier transform of each of its views, the problem can be examined in the frequency domain. As it turns out, the relationship between an image and its views is far simpler in the frequency domain than in the spatial domain. The frequency domain analysis of this problem is a milestone in CT technology called the Fourier slice theorem. Fourier reconstruction of a CT image requires three steps. First, the one dimensional FFT is taken of each view. Second, these view spectra are used to calculate the two-dimensional frequency spectrum of the image, as outlined by the Fourier slice theorem. Since the view spectra are arranged *radially*, and the correct image spectrum is arranged *rectangularly*, an interpolation routine is needed to make the conversion. Third, the inverse FFT is taken of the image spectrum to obtain the reconstructed image [15].

CHAPTER 3
EXPERIMENTAL FACILITY AND SPECIMEN PREPARATION

3.1 BMIT at Canadian Light Source

The BMIT beam line at the **Canadian Light Source (CLS)** synchrotron facility was used for our research project (Figure 3.1). The CT setup was installed at BMIT-BM beamline hutch at Canadian Light Source (Fig 3.2). The characteristics of the beamline are given in Table 3.1. The energy range at BMIT-BM at CLS is 8 – 40 KeV, and that energy is suitable for imaging light weight materials like Aluminum, however is not suitable for materials having high atomic weight like iron, zirconium etc. For high atomic weight materials we need higher energy. The process of incrementing the beam energy in BMIT-ID (Insertion Device) to an energy range of 20-100 KeV is in commission. We are optimistic that BMIT-ID (specifications of the beamline are given in Table 3.2) will become an important tool for analyzing high Z materials.

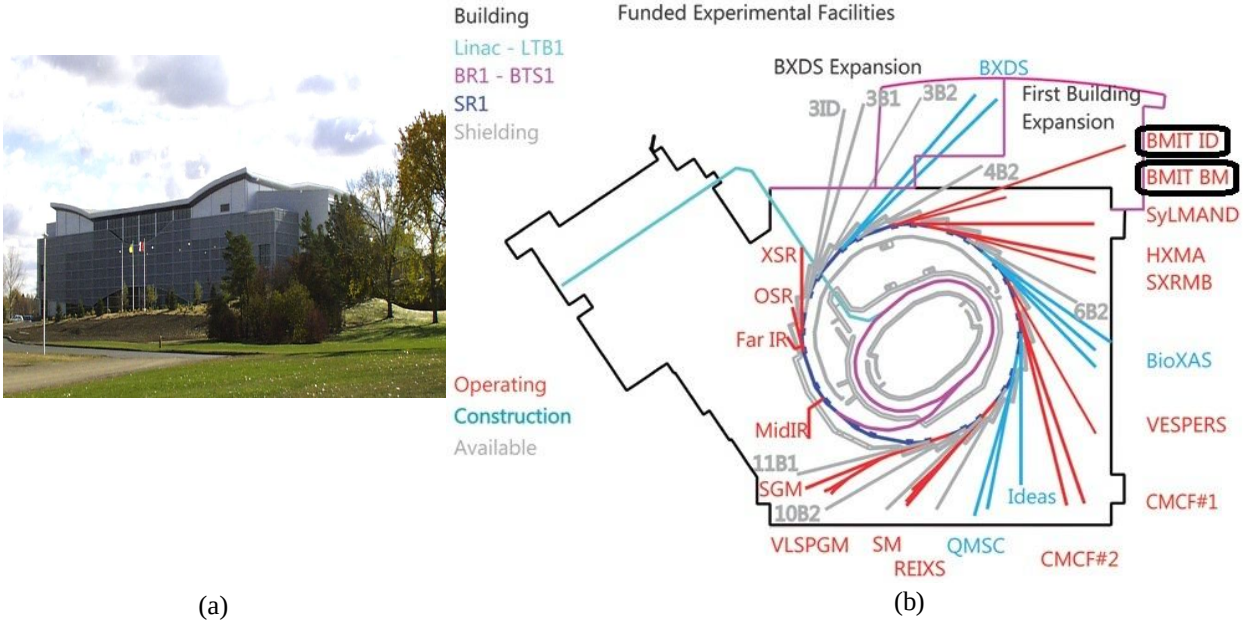

(a) (b)

Fig 3.1: (a) Canadian Light Source (CLS) (b) Beam Lines.

Since our experiments were with aluminum and aluminum composites, beam energy of about 30 KeV was sufficient for obtaining measurable contrasts. The chosen resolution of the BMIT-BM imaging system was about 10 μm, and this was sufficient to analyze the shape of

larger (>10 μm) structural components e.g. precipitates. Unfortunately small (<10 μm) components could not be imaged; they are however less likely to be responsible for crack initiation.

Table 3.1 The parameters of the BMIT-BM beamline used in the present investigation:

Source	Bending Magnet
Energy Range	8 – 40 keV
Wavelength	1.6 – 0.3 Å
Photon Brightness	1.5 x 10^{11} ph/(s * mr^2 * 0.1%bW * mA) @10 keV
Beam Size (Horizontal x Vertical)	231 mm x 4.6 mm @ 23 m

Table 3.2 The parameters for the BMIT-ID beamline under construction:

Source	Superconducting (SC) Wiggler
Energy Range	20 - 100 keV
Wavelength	1.6 – 0.3 Å
Photon Brightness	3 x 10 12 ph (s * mr 2 * 0.1%bW * mA) @ 20 keV
Beam Size (Horizontal x Vertical)	220 mm x 11 mm @ 55 m

Synchrotron radiation micro CT was applied to the tensile sample when held by a tensile testing sample stage (Fig 3.2). In this micro-CT set up the source of synchrotron radiation and the detector was fixed while the sample was rotated to take image projections from different angular positions of the sample. The projection image transmitted through the sample was detected by an image detector with a pixel size of 4.3 μm.

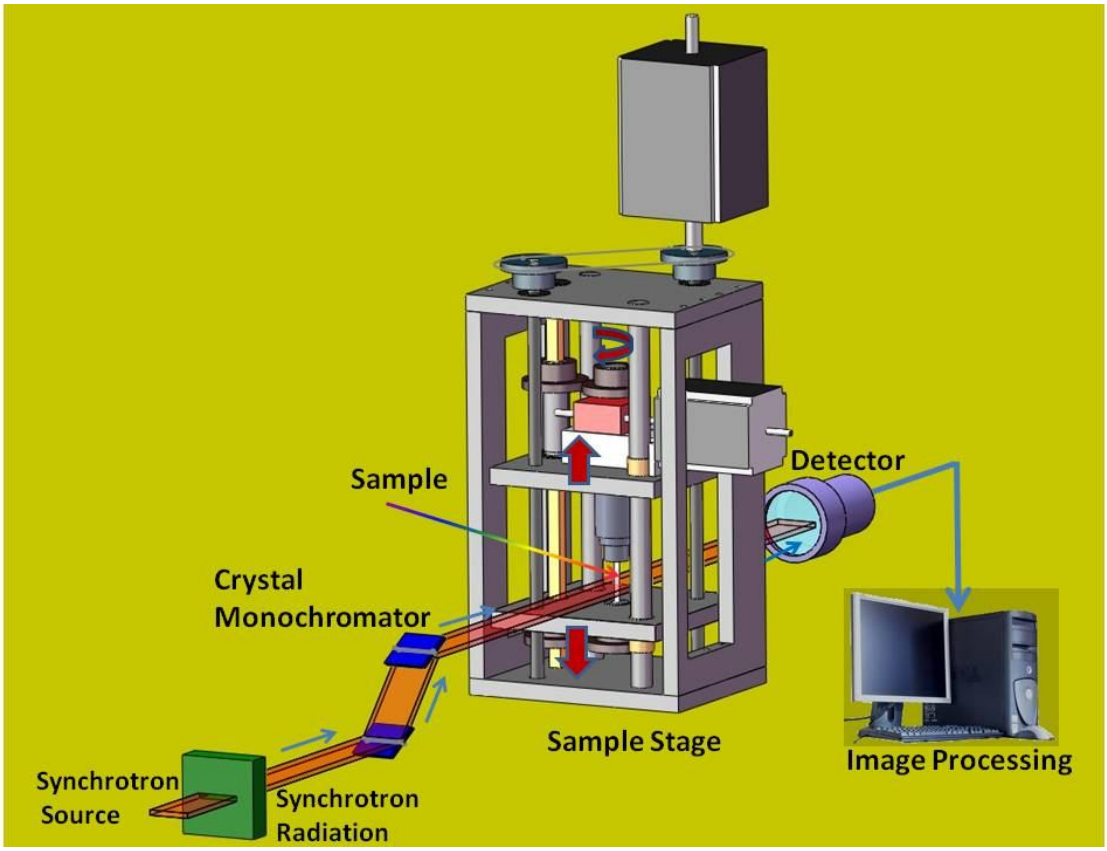

Figure 3.2: Experimental set-up at BMIT-BM beamline.

Required number of projections, at required angular intervals (generally 0.1° to 0.2° depending on the sample size) was measured by rotating the sample from 0° to 180° by the sample stage rotational system. Moreover, twenty projections without the sample were taken before and after CT measurement (ten of which is with the beam and rest is without the beam). In this way absorption and background corrections are introduced. We used syrmep tomoproject software to reconstruct the serial 2D slices. The software used a filtered backprojection reconstruction algorithm. Next, Amira image processing software was used to make 3D structure of the objects from 2D slices. We found the Amira software to be potential tool for segmentation of different constituents' phases of the investigated materials.

3.2 Specimen used for 3D imaging

Porous aluminum

Porous aluminum was made by sintering the aluminum powder at 550 ˚C for an hour in argon environment in a tube furnace after cold pressing it at 150 MPa (Fig 3.3). This porous aluminum was made from commercially pure aluminum powder. The pressure was applied by a Universal Tensile Testing Machine located at the engineering building in the University of Saskatchewan. After cold pressing the powder it became solid and then it was sintered in a tube furnace (having capacity of 800 ˚C) in argon environment located at pilot plant of Chemical engineering department at the University of Saskatchewan.

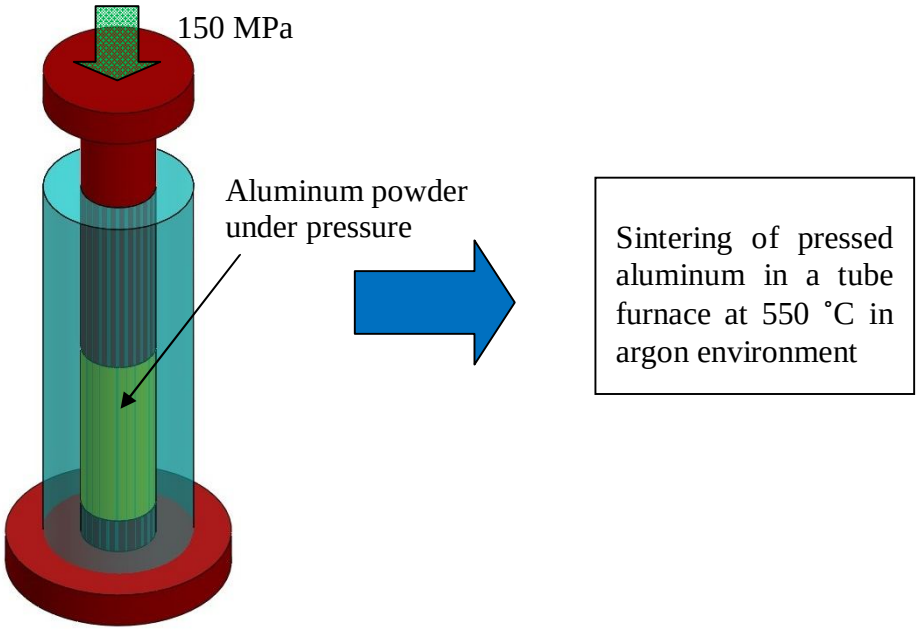

Fig 3.3: Manufacturing process of porous aluminum.

Hybrid composite of $Al/Al_2O_3/TiC$ produced by anodizing and accumulative roll bonding (ARB) processes

Strips of fully-annealed 1050-aluminum alloy with the initial dimensions of 200mm×50mm×1mm parallel to the sheet-rolling direction and TiC powder with average particle size between 50 to 75 μm were used as the primary materials. The specimens were provided by Professor M. R.Toroghinejad (Department of Materials Engineering, Isfahan

University of Technology, Isfahan, Iran) and were prepared according to the processing scheme described below.

First the anodizing process was carried out by subjecting the annealed aluminum strips to 180 g/l of sulphuric acid electrolyte under an applied voltage of 15 V, at a low electrolyte temperature (18°C) in order to generate alumina on top of the aluminum strips.

The anodized aluminum strips were degreased in acetone. After surface preparation, the rolling process was carried out immediately to avoid the formation of oxide layer on surfaces of the strips.

The procedure of ARB process used for fabricating $Al/Al_2O_3/TiC$ hybrid composites is shown in Fig. 3.4. This process consists of three steps. In the first step (Fig. 3.4(a)), the anodized aluminum strip with alumina layer at both sides was placed between the as-prepared surfaces of two aluminum strips. This combination has a thickness of about 3mm. TiC particles were also uniformly dispersed between each pair of the strips. The stacked strips were firmly attached to each other by steel wires and then rolled-bonded with 66% reduction, to produce a roll-bonded strip with the thickness of 1mm (first cycle). Afterwards, the length of the roll-bonded samples was sectioned into two halves. In the second step (Fig. 3.4(b)), the two roll-bonded strips obtained from step1 were roll-bonded again with a rolling reduction of 50% at room temperature. This was done after surface preparation, dispersing the TiC particles between them and stacking strips on each other as described in first step. This procedure was repeated up to forth step without anodized the strip. In the last step (Fig. 3.4(c)), the aim was to achieve a uniform distribution of reinforcement particles (Al_2O_3 and TiC) in the matrix, and also to eliminate porosities at the interfaces of aluminum layers and aluminum–reinforcement particles. The second step was repeated up to eighth cycle (without adding TiC particles). It is worthwhile to notice that all rolling cycles were performed parallel to the rolling direction of the as-received aluminum sheets and the direction of stripes was unchanged during ARB process. Also in the first step of the process (initial 4 cycles), a quarter of 1vol. % TiC particles was distributed between the aluminum strips in each cycle. Rolling was conducted in non-lubricated conditions using a laboratory rolling mill with a roll diameter of 127 mm and a loading capacity of 20 tons with rolling speed about 4 m/min.

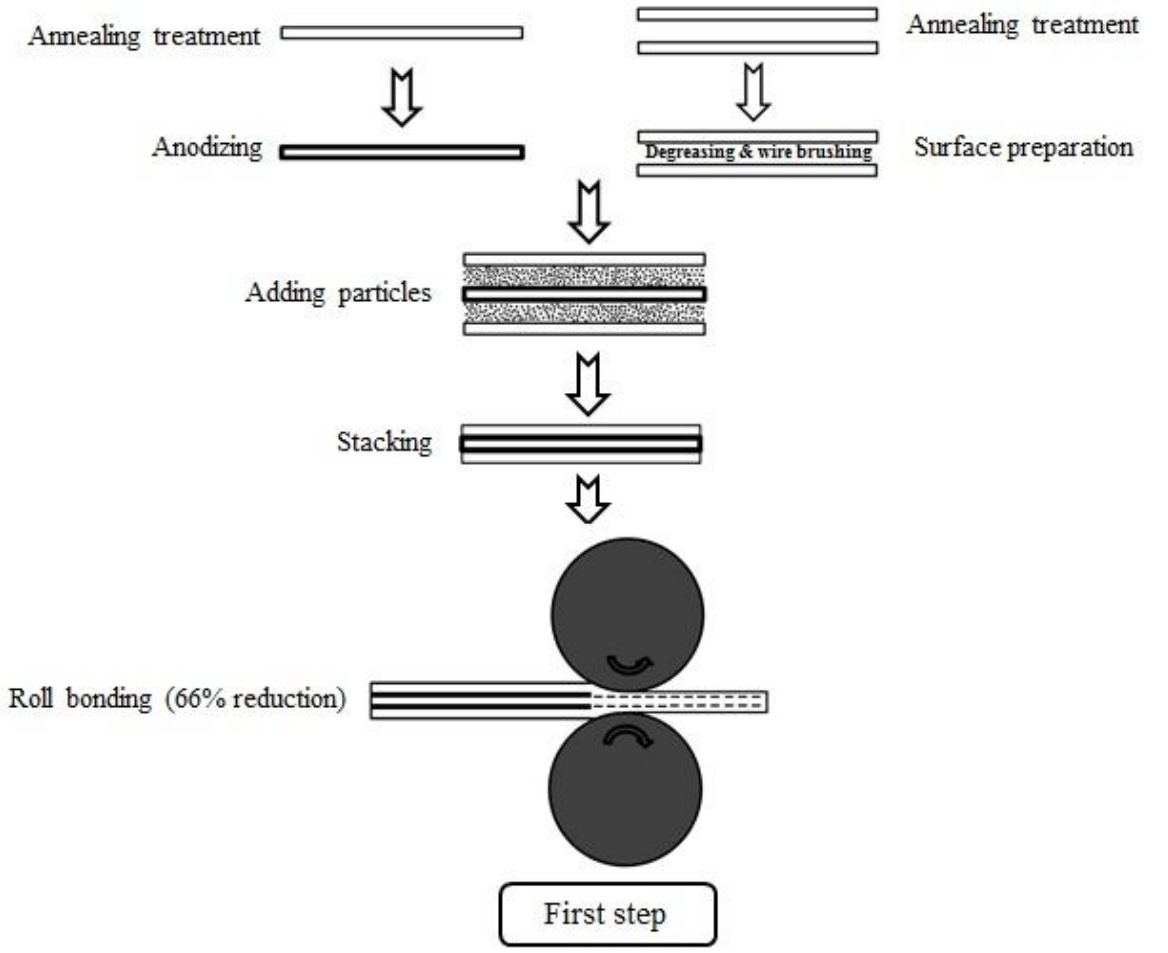
Annealing treatment
Annealing treatment
Anodizing
Degreasing & wire brushing
Surface preparation
Adding particles
Stacking
Roll bonding (66% reduction)
First step

(a)

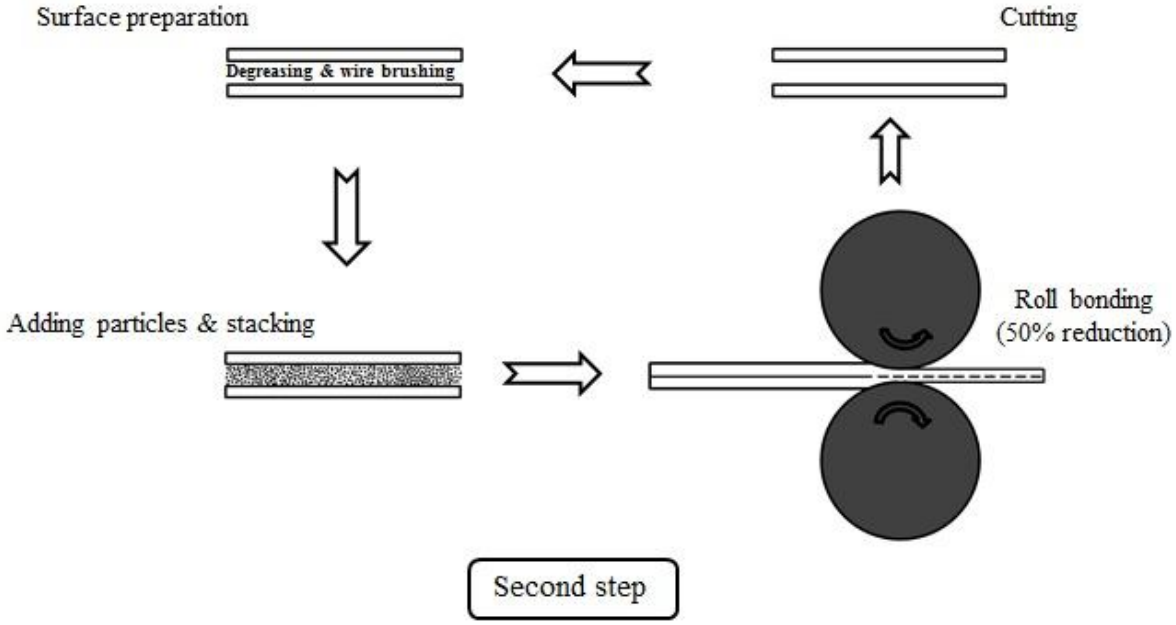
Surface preparation
Degreasing & wire brushing
Cutting
Adding particles & stacking
Roll bonding
(50% reduction)
Second step

(b)

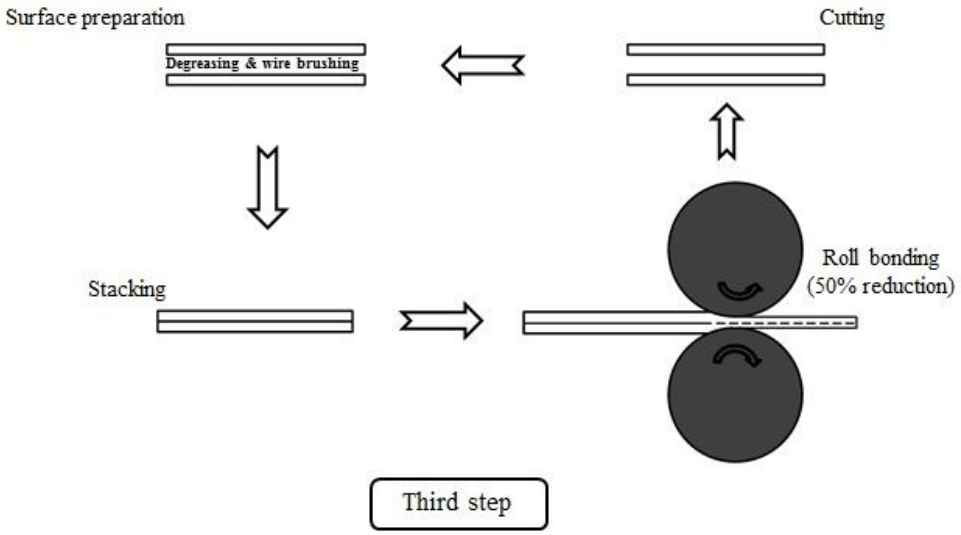

(c)

Fig 3.4: Manufacturing process of the hybrid composites by ARB.

Aluminum alloy and composite sample for in-situ dynamic loading experiments

The samples (Fig 3.5) were prepared according to ASTM E8 standard with a hole at the centre of the sample to perform in-situ tensile experiments. AA 6061 aluminum alloy specimen and hybrid composites of $Al/Al_2O_3/TiC$ produced by anodizing and accumulative roll bonding processes were used for tensile loading experiments.

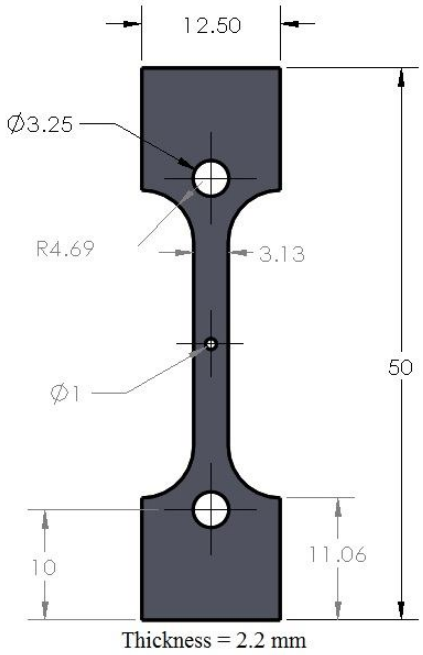

Fig 3.5: Tensile Sample.

CHAPTER 4
DESIGN OF EXPERIMENTAL STAGE FOR TENSILE LOADING

4.1 Overview of the sample stage

An automatic independent tensile and rotational sample stage was designed and fabricated for conducting the in-situ experiments. The unique feature of this experimental stage is that the sample can be rotated torsion-free for computed tomography (CT) imaging under any loading (tensile or compression) conditions. The sample stage is shown in Figure 4.1.

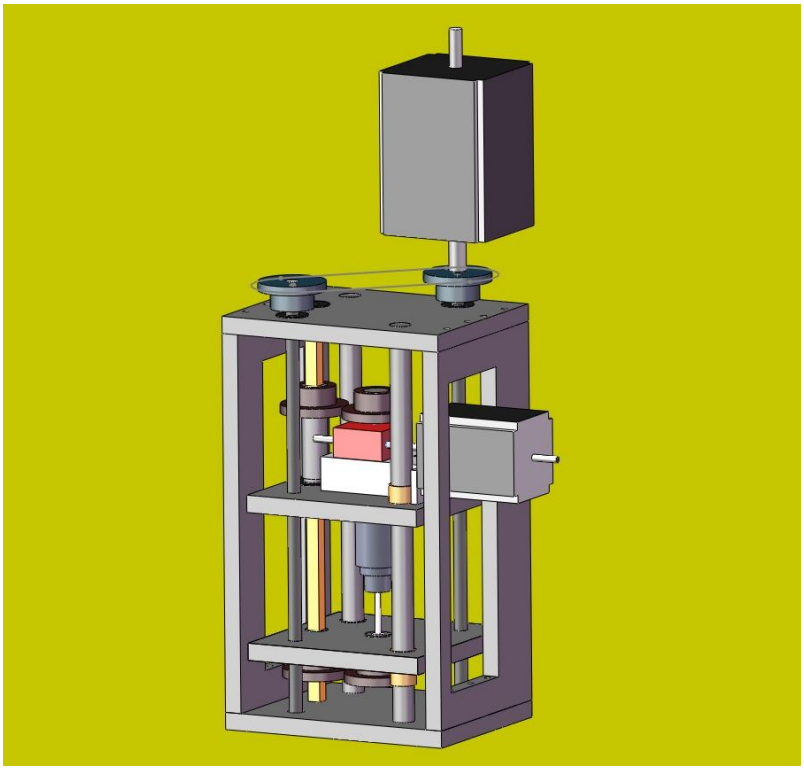

Fig 4.1: Experimental sample stage.

The specifications of the tensile and rotational sample stage are as below:

Force: 0 to 4 kN;

Elongation Rate: ~ up to 1.25 inch/sec;

Rotational step resolution: 0.003˚ per step;

Rotational Speed: ~ up to 68 rpm;

Sample size range: 1/2” (before elongation) to 3” (after elongation).

4.2 Tensile System

The tensile system is responsible for pulling the sample in a controlled manner as needed. The system has been designed in such a way that pulling does not affect the rotation of the sample (Fig 4.2).

The power to pull the sample is provided by a high torque stepper motor. Stepper motors provide very precise, extremely cost-effective motion control. Stepping action is simple to control and does not require complicated, expensive feedback devices.

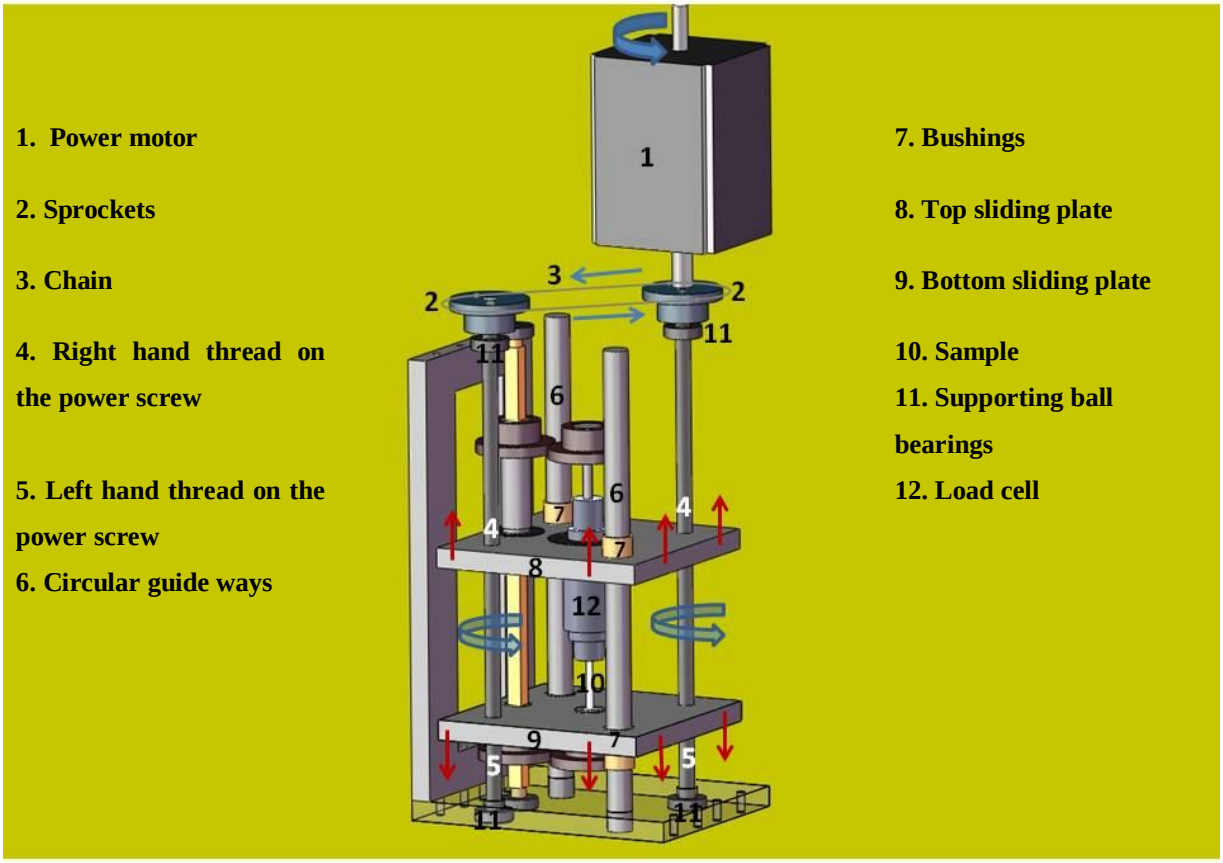

Fig 4.2: Tensile system of the sample stage.

Chain and sprockets ensure the power transmission from the stepper motor to both of the power screws so that both can rotate at the same time to pull the sample at the same rate from both sides.

These are special type of power screws made in the machine shop which have right hand side thread on top half part which is meshed with the internal thread of the top-slider plate and left hand side similar thread on bottom half part which is meshed with the internal thread of the bottom-slider plate so that the both sliding plates can move to the opposite direction at the same time. This is done for pulling the specimen from both sides to avoid any axial displacement of the center of the specimen.

Circular guide ways was used to facilitate sliding mechanism of the top and bottom slider plates. A bushing was used along with the hole of the slider to increase the surface contact area with the guide ways which decreased the tilting possibility of the slider so that slider could move smoothly on the guide ways. The material of the bushing was so chosen that it has minimum frictional co-efficient so that slider can slide smoothly on the guide ways. Both sliding plates had sample mounting facility at the very centre of the plates to avoid any bending effect on the sample.

4.3 Rotational System

The rotational system was designed to take the projection image of the sample in different angular positions compatible with the tomography set up at BMIT-BM beamline in CLS (Fig 4.3).

Sample was rotated by a stepper motor having small angular steps which helped to take the required amount of projections, at required angular intervals by rotating the sample from 0° to 180°.

The rotational stepper motor's angular step size is 0.36° i.e. motor shaft rotates 0.36° in each pulse from the controller which was not enough to get required projections around the samples. In our experiments the required intervals were in-between 0.10° to 0.20° depending on the sample size. For bigger sample step size has to be smaller to get required number of projections around the sample. A worm gear box solved this problem which has reduction capability of 120:1. Finally, the smallest achievable angular steps of the sample become 0.003° which make the rotational system more suitable for any imaging experiments.

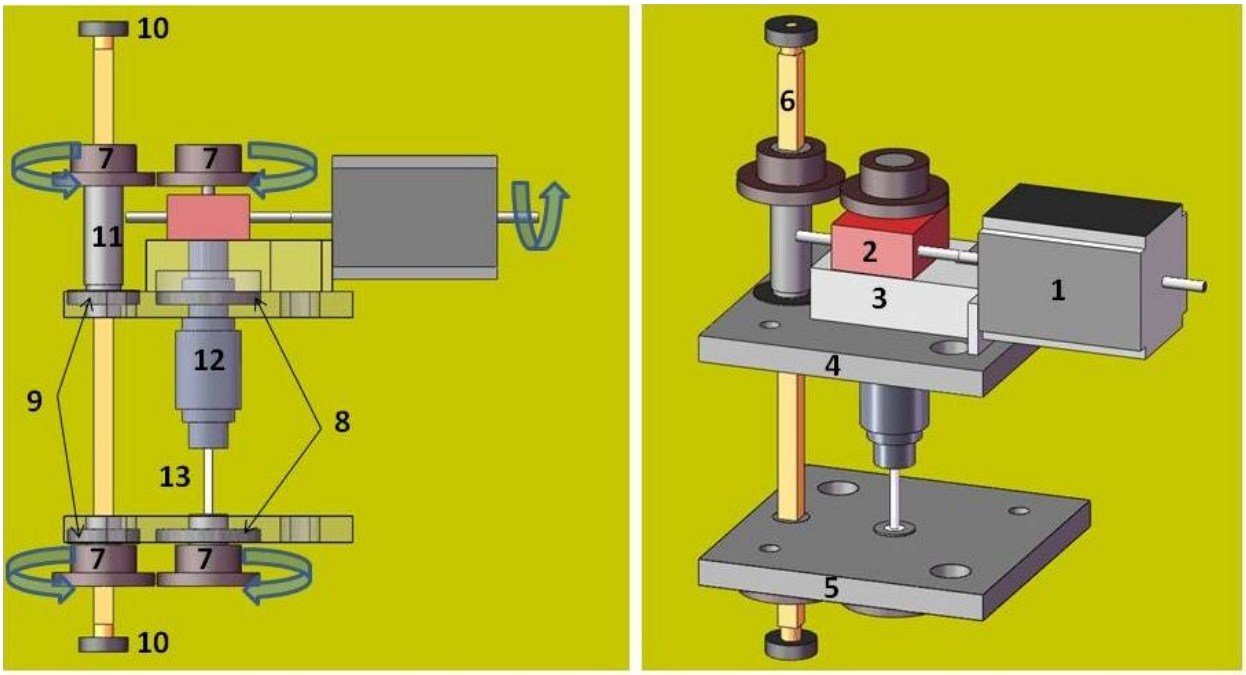

1. **Stepper motor**
2. **Worm gear box**
3. **Mountings**
4. **Top sliding plate**
5. **Bottom sliding plate**
6. **Gear transmission shaft**
7. **Transmission gears**
8. **Thrust bearings in sample mountings**
9. **Thrust bearings in gear transmission**
10. **Supporting ball bearings**
11. **Sliding shaft around the transmission shaft**
12. **Load cell**
13. **Sample**

Fig 4.3: Rotational system of the sample stage.

The main challenge in designing this experimental stage was to rotate the sample under different loading conditions. To fulfill this requirement commercially available thrust bearing were used in the sample mountings which can hold the sample during experiments and ensure the smooth rotation of the sample under loading condition.

Though thrust bearing mountings are a very efficient mechanism for rotating the sample under loading, the rotational power is transmitting from top to bottom part of the sample through the sample itself which could break the sample when the sample is vulnerable to the small

torsion load. To resolve this problem a gear transmission set-up was attached to the system which transmitted the rotational power from top to bottom part of the sample to completely eliminate the chance of torsional load in the sample. The gear transmission shaft and the sliding shafts around it were designed in such a way that the tensile loading on the sample did not affect the rotational power transmission through it.

4.4 Control System

A control system was designed and fabricated to control the tensile power stepper motor (Fig 4.4). The control system was made on a circuit board which was controlled by a micro-controller. A micro-controller is a single integrated circuit containing a processor core, memory, and programmable input/output peripherals which reduces the number of chips and the amount of wiring, and circuit board space. The controller sends the required pulses to the driver which drives the stepper motor according to the manner written in the micro-controller. The micro-controller used here is “AVR ATmega 8” from Atmel Corporation. To write the program into the micro-controller chip software from Atmel Corporation was used. The programming language used to write the codes was “C”. This micro-controller supports, in system programming which allows us to change the programs according to our requirements in service conditions. The driver used here was from National Instruments Corporation and has micro-stepping facility up to 50,000 which ensures the precise controls of the elongation of the sample. A load cell was attached to measure the tensile load on the sample and was connected to a smart indicator from which we can get the acting load directly in N or lb. To get the accurate measurement of the elongation, the rotation of the other lead screw connected though the chain sprocket has been measured by a protractor arrangement. The lead screws and the sliding plates have negligible deformation during the sliding of plates as both were made from have high strength materials compare to the materials of the measured samples, and as a result of that we can assume that the elongation measurements are reliable. But when using a displacement measuring sensor, more specifically a local strain measuring sensor, we might obtain even better accuracy of strain measurements. Such measurements can be implemented in the future. The rotational stepper motor was connected to the control system existing at CLS to make it easier to synchronize the rotation of the sample and the exposure of the detector to recording of counts.

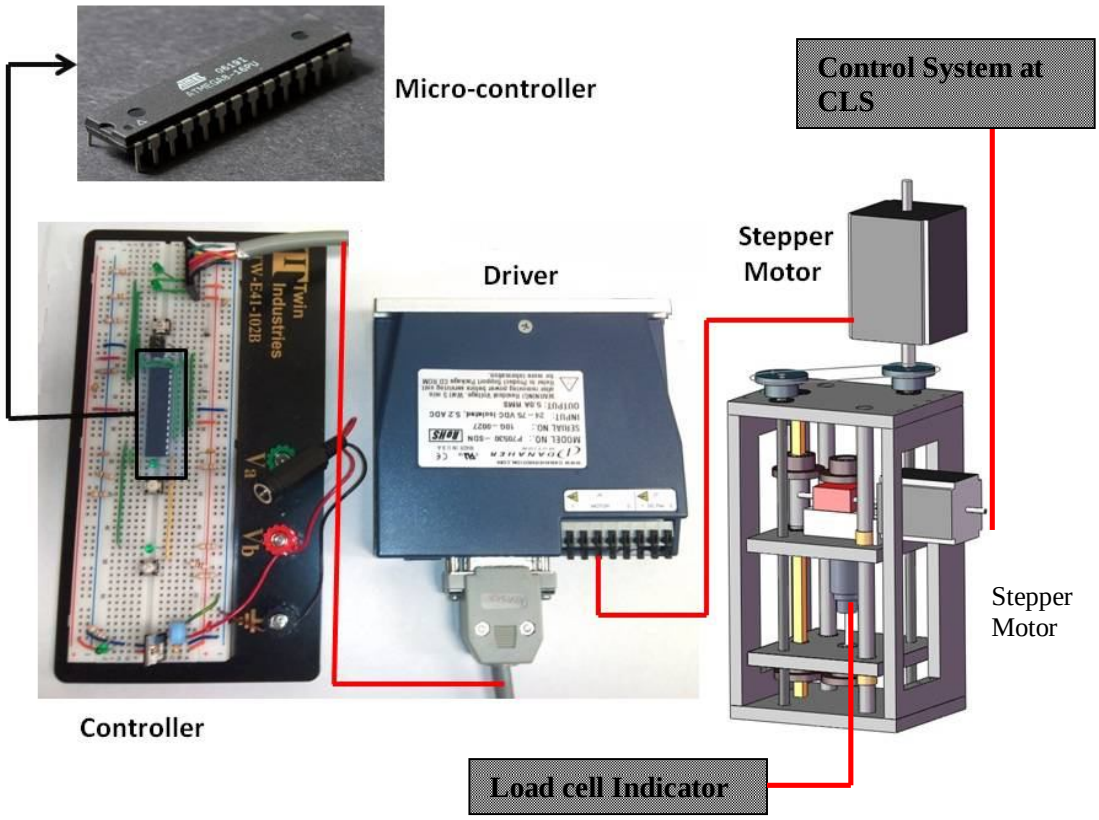

Fig 4.4: Control system of the sample stage.

4.5 Summary on Equipment Design

A novel experimental system has been designed and built for in-situ dynamic loading experiments under tensile stress at BMIT-BM at CLS. This system was used to perform dynamic testing on specimens with different structural characteristics. The system was designed in such a way that the loading and the rotation of the sample is independent so that the sample can be rotated freely under loading for taking projection images for computed tomography at CLS. The aim of designing this experimental system was to expand a platform of structural imaging at CLS for in-situ imaging under tensile load. This novel system can be used for imaging different materials including metals, MMCs and biomaterials within the limitations of specified maximum size and load of the samples. If we need higher load to pull the sample we have to mount a gear reduction in between the motor and the lead screw to increase the torque delivery to the lead screw.

CHAPTER 5
3D STRUCTURAL ANALYSIS OF POROUS ALUMINUM

3D imaging of porous aluminum has been done using synchrotron radiation tomography. The internal 3D structure of the material was clearly visible and the shape and sizes of voids inside the structure was recorded (Fig 5.2 – 5.4). The unit volume of the imaging system is voxels which depends on the pixel size of the detector. In our case the pixel size of the detector was 4.3 μm. Therefore, 1 Voxel = 4.3*4.3*4.3 μm^3 = 79.507 μm^3. In the chart (Fig 5.5) of the voids volume distribution we see that volume of voids changed from 50 voxels (3,975 μm^3) to 5,950 voxels (473,066 μm^3) with the mean volume of 343 voxels (27,270 μm^3). This means that most of the voids in the porous structure lied below the mean volume. Total volume % of the voids in this structure was 1.62% (Table 5.1). The segmentation has been done by choosing a threshold value according to the grey scales of the images. Figure 5.1 demonstrating the way of choosing the threshold value to differentiate the voids and aluminum in the porous aluminum. In all cases in this thesis threshold values were chosen in the same manner where a transition of intensity is in grey scale. We found this technique very accurate comparing the outer dimension of the sample from this technique to the dimension by using a slide calipers. We believe that the quantitative measurements are accurate (as we found accurate in bigger scale in comparing the outer physical dimension of the sample). Choosing a threshold value is a vital part of the image analysis as discussed in the literature [14] because the accuracy of the measurements depends on it.

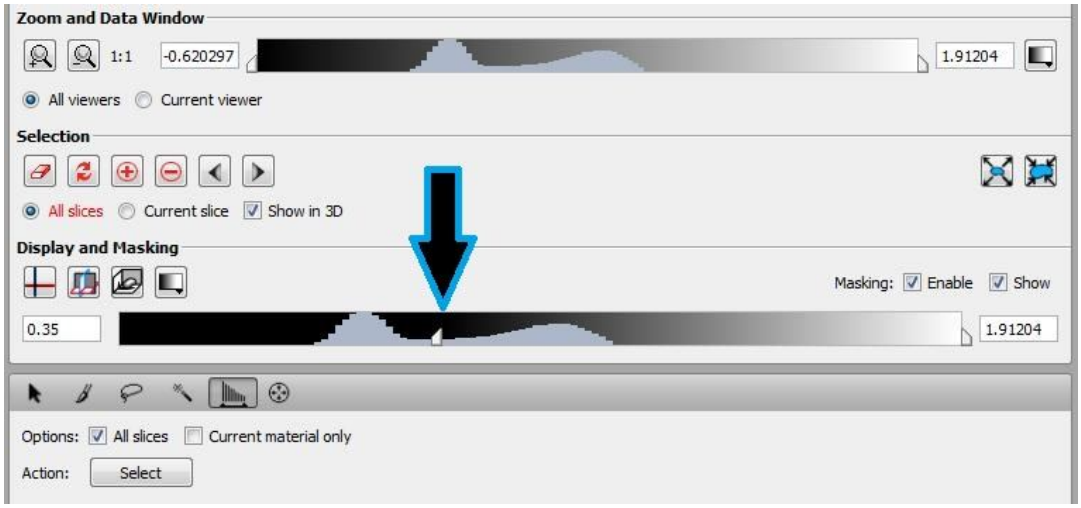

Fig 5.1: Selection of threshold value to segment the voids and aluminum

The view of the porous sintered aluminum sample is shown in fig 5.2.

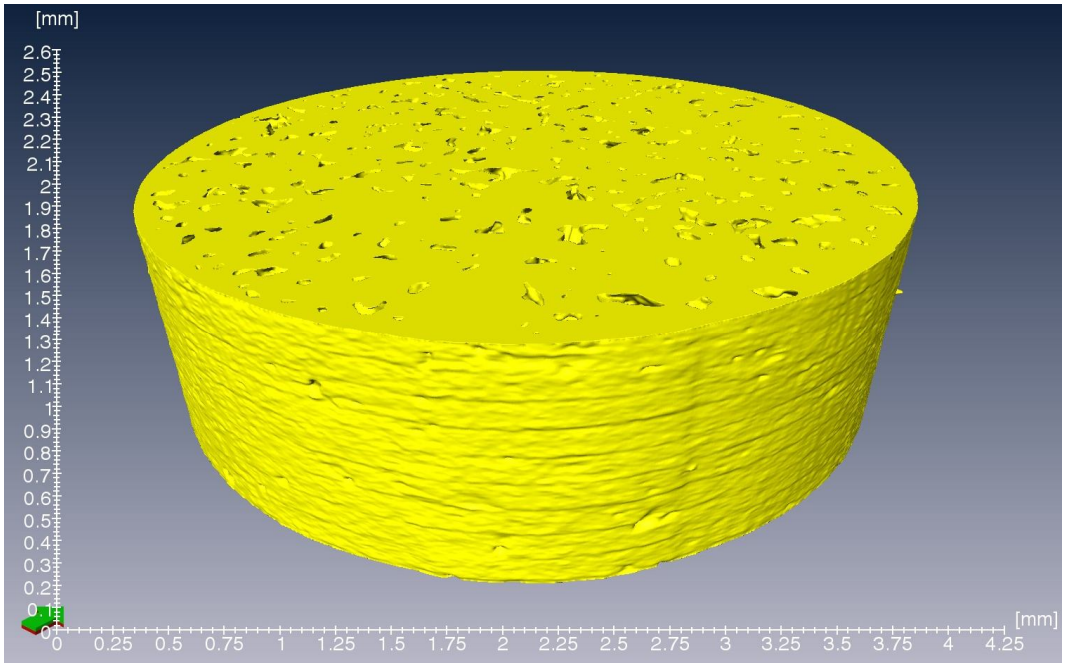

Fig 5.2: 3D view of the porous aluminum.

The internal structures are shown in Fig 5.3 and Fig 5.4, where cuts obtained from the imaging experiments are displayed (such cuts are non-destructive). The size and shape of the internal voids are imaged.

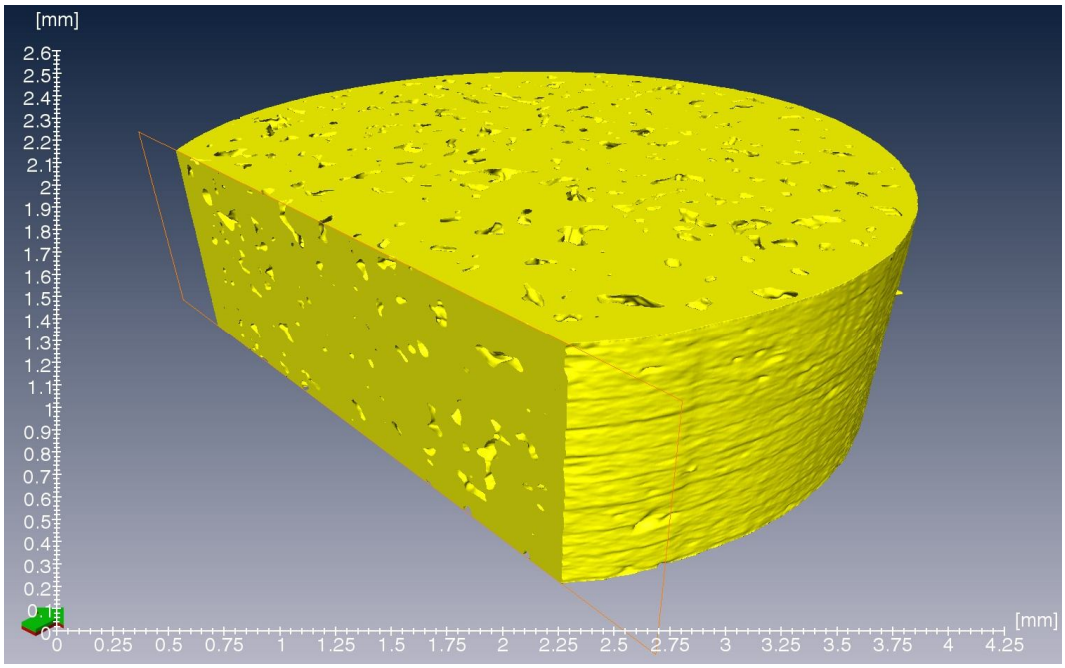

Fig 5.3: 3D view of the porous aluminum (slice cut from the left side to see inside).

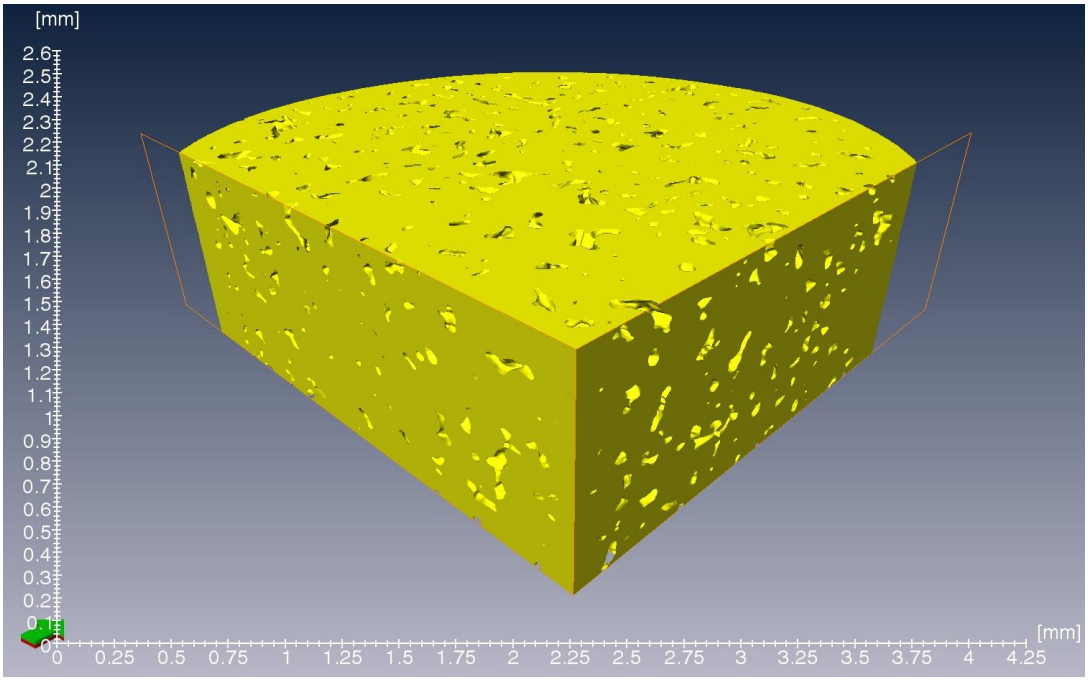

Fig 5.4: 3D view of the porous aluminum (slice cut from both sides to see inside).

Amira software is a powerful tool to measure the volume of voids which are separated from each other and it provides histogram plots showing the volume distribution of the segmented parts, in our case the number distribution of volumes of voids.

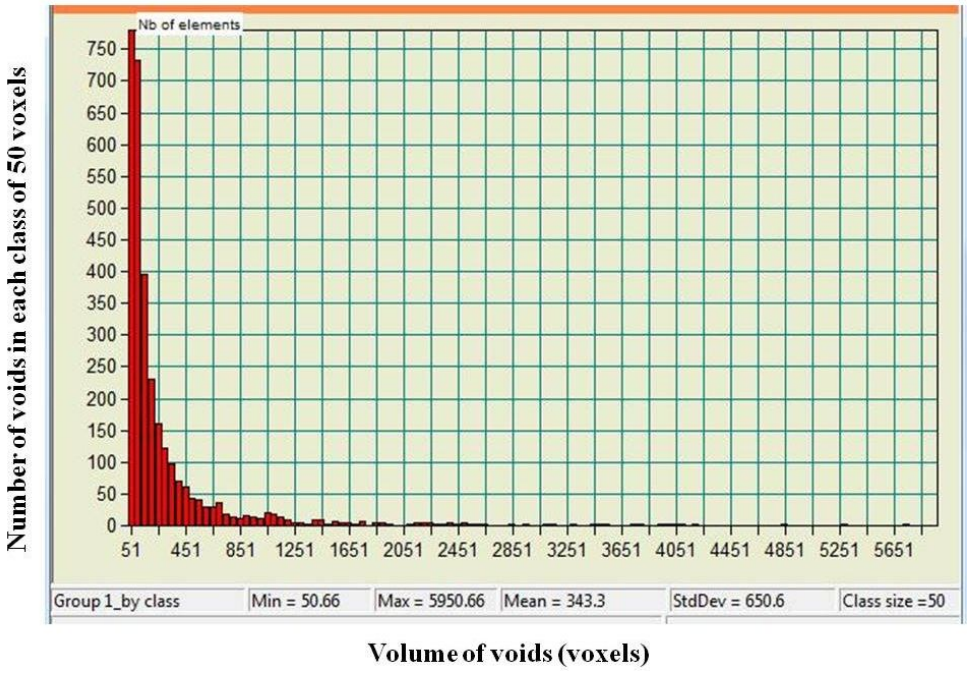

Fig 5.5: Volume distribution of voids in the porous aluminum.

Table 5.1: Volume fractions of the porous aluminum:

Total volume of the sintered aluminum μm^3*1000 (Voxels)	Volume of aluminum μm^3*1000 (Voxels)	Volume of the voids μm^3*1000 (Voxels)	% Volume of the voids
5,405,629 (67989347)	5,319,486 (66905880)	86,143 (1083467)	1.62

1 Voxel = 4.3*4.3*4.3 μm^3 = 79.507 μm^3

5.1 Summary of the findings

It has been shown that this imaging technique is a powerful technique to analyze the internal structure of porous materials i.e. porosity, differences in porosity in different parts of the sample and the size distribution of voids can be obtained from imaging experiments. Choosing the correct threshold value of the grey scale of the obtained images is very important. For example, aluminum foam which has very important industrial uses (using in car bumper as shock absorbers) can be analyzed by this technique and information obtained might be useful in improving the manufacturing process of those materials. It is not possible however to see the pores smaller than 10 μm because of the limitation of the resolution of this imaging technique.

CHAPTER 6
3D IMAGING OF ALUMINUM COMPOSITES

The manufacturing processes of Hybrid composite of $Al/Al_2O_3/TiC$ produced by anodizing and accumulative roll bonding processes are described in CHAPTER 3. As we know from the literature [16 - 19] that the material properties improve as the number of ARB cycle increases and it is important to know the structure of the materials after different ARB cycle to analyze and control the manufacturing process. 3D structural imaging can give us information on internal structure of these hybrid composites after different ARB cycles. 3D imaging of these composites has been done after the following cycles of the ARB process: (a) 4 pass (b) 8 pass and (c) 10 pass.

6.1 Al/Al2O3/TiC composite after 4 ARB passes

The composite after 4 passes consists of Alumina and TiC distributed in aluminum matrix. In the 3D images it is clear that the alumina layer has broken into particles after 4 ARB passes (Fig 6.1 and Fig 6.2). There are some voids formed inside the composite at the interface between the aluminum and alumina.

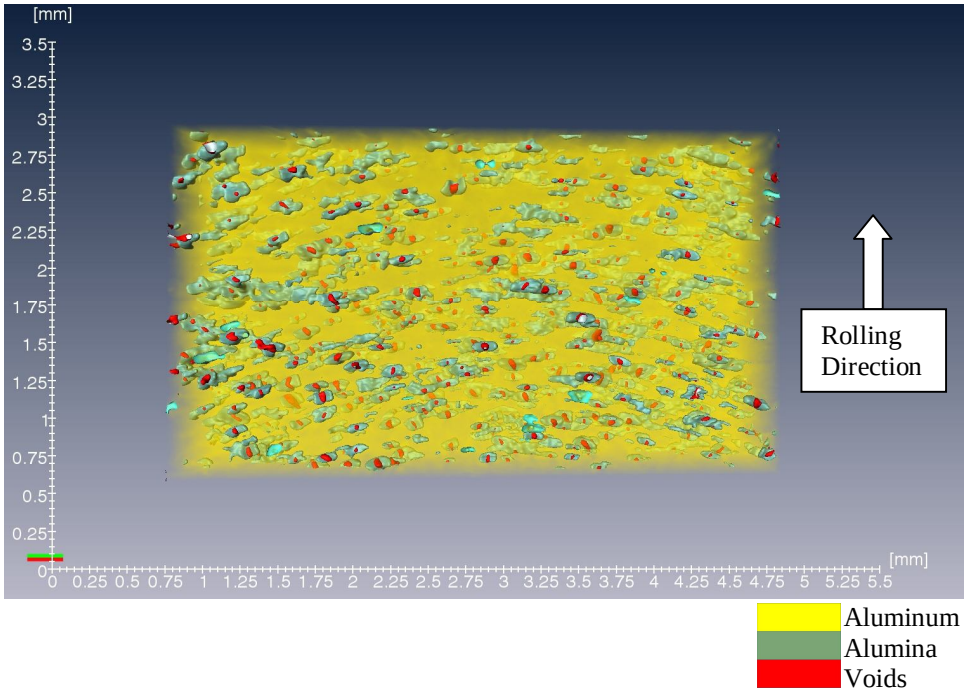

Fig 6.1: 3D view of the composite after 4 passes (front view).

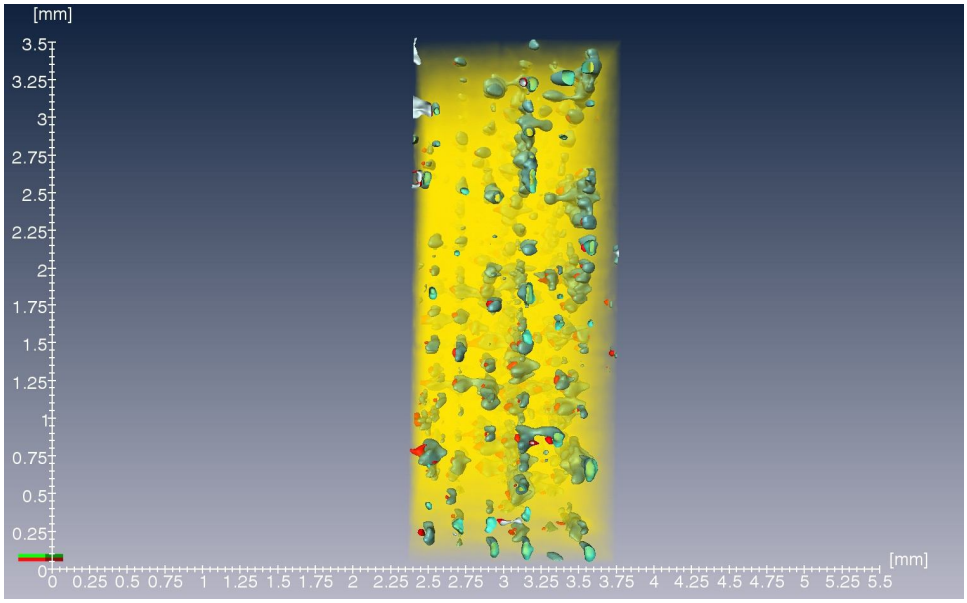

Fig 6.2: 3D view of the composite after 4 passes (side view).

3D image analyses give us the volume distribution of alumina particles (Fig 6.3 and Fig 6.4) and voids but are limited to separate TiC from the structure. We needs more detailed image analysis to quantify the presence of TiC in aluminum.

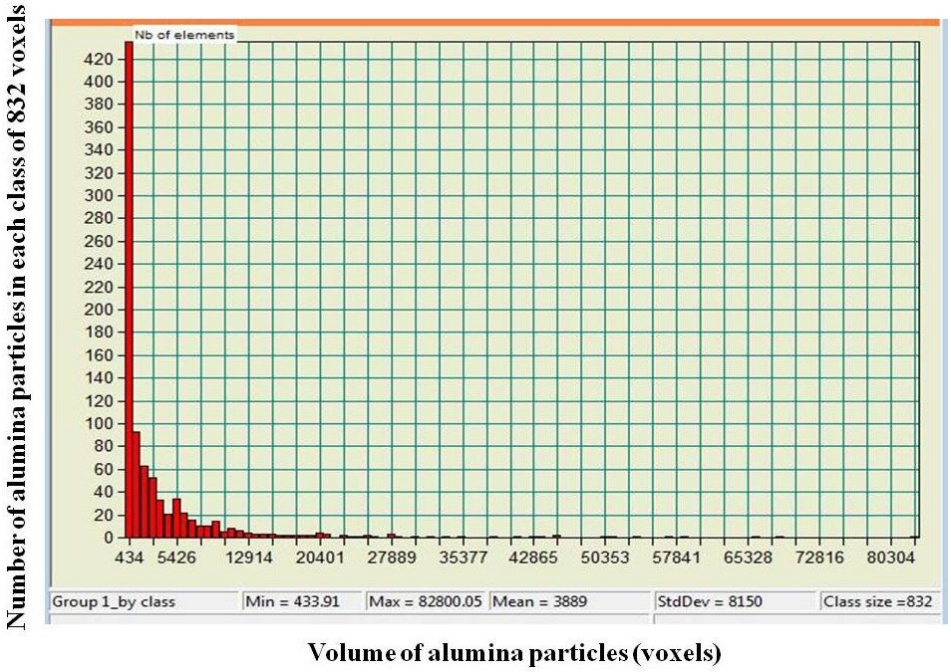

Fig 6.3: Volume of alumina particle distribution chart after 4 passes.

The volume of alumina particles lied between 434 voxels (34,506 μm^3) and 82,800 voxels (6,583,179 μm^3) with a mean of 3,889 (309,202 μm^3) voxels. That means most of alumina was broken into smaller particles and distributed in the aluminum matrix, but there were still some large alumina particles in the specimen. In the Fig 6.1 and Fig 6.2 it is clear that the distribution of alumina is not uniform.

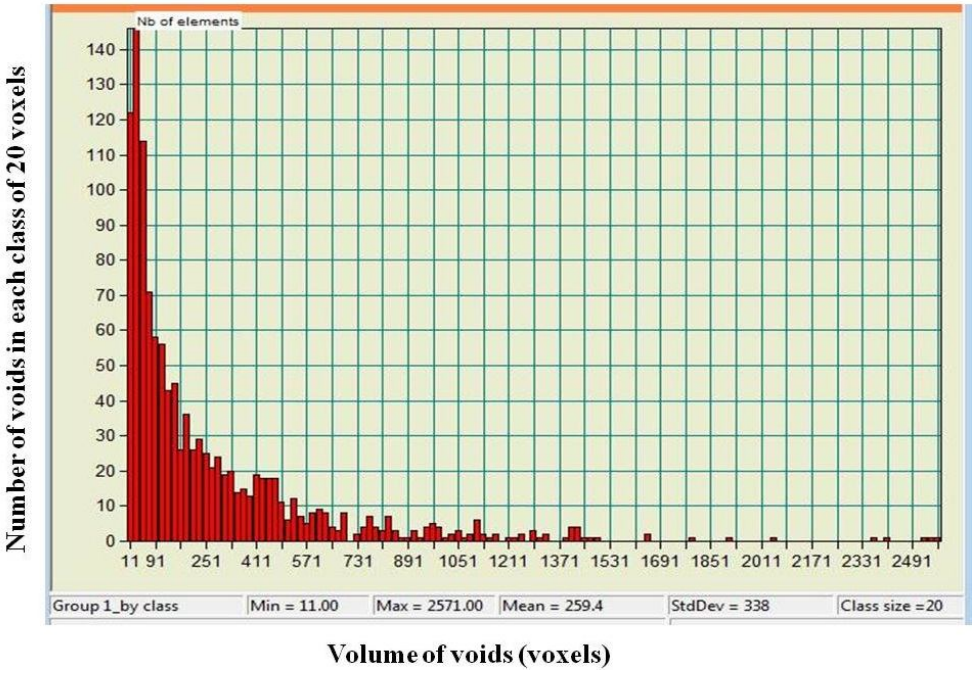

Fig 6.4: Volume of voids distribution chart after 4 passes.

The maximum volume of the observed void was 2571 voxels (204,412 μm^3) with the mean of 260 voxels (20,671 μm^3). The number of voids in the selected volume was 1178 with a volume fraction of 0.33% (Table 6.2).

6.2 Al/Al2O3/TiC composite after 8 ARB passes

The alumina particles were distributed more uniformly in this composite compare to the composite after 4 ARB passes (Fig 6.5 and Fig 6.6). The volume of alumina lied between 266 voxels (21,148 μm^3) and 49,463 voxels (3,932,654 μm^3) with a mean of 2,658 voxels (211,329 μm^3) (Fig 6.7 and Fig 6.8). That meant the largest alumina particles were broken down after 8 ARB passes because the alumina particles were smaller and distributed more uniformly as seen in the Fig 6.5 and 6.6. The maximum volume of void was 2030 voxels (161,399 μm^3) with a mean of 180 voxels (14,311 μm^3).

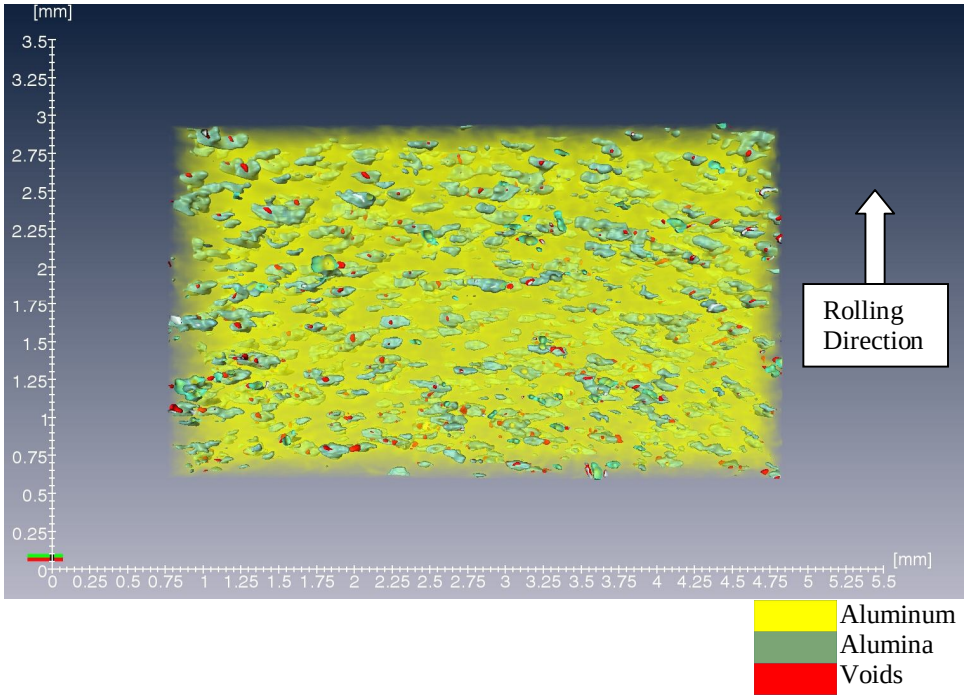

Fig 6.5: 3D view of the composite after 8 passes (front view).

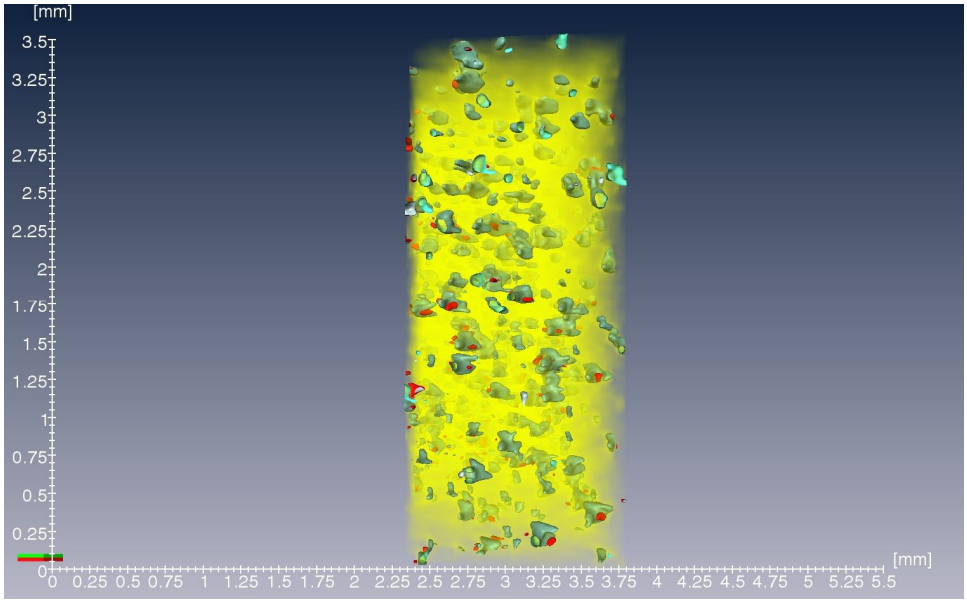

Fig 6.6: 3D view of the composite after 8 passes (side view).

The number of voids in the selected volume was 1635 with the volume fraction of 0.36% (Table 6.2). This implies that after the 8 ARB passes the average size of the voids decreased but

the number of voids and volume fraction of voids increased compare to those registered after the 4 ARB passes.

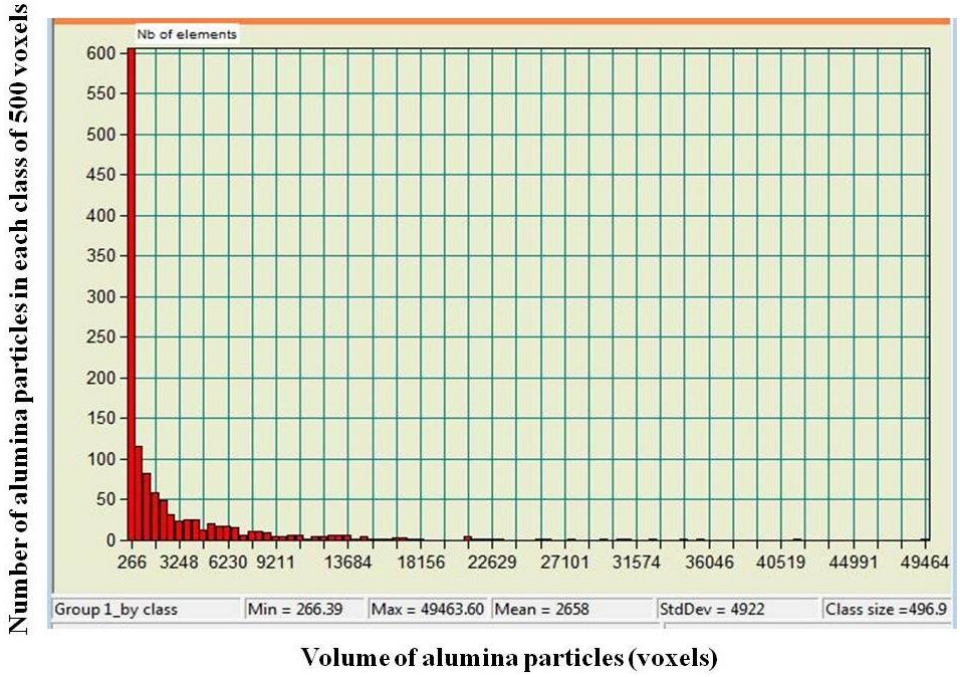

Fig 6.7: Volume of alumina particles distribution chart after 8 passes.

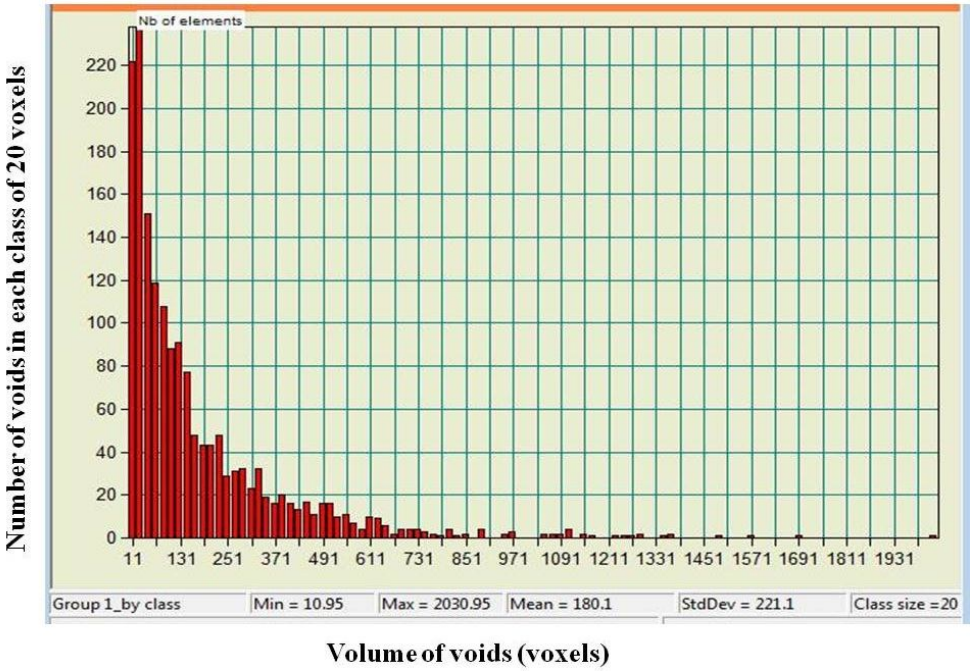

Fig 6.8: Volume of voids distribution chart after 8 passes.

6.3 Al/Al2O3/TiC composite after 10 ARB passes

The alumina particles were distributed more uniformly in the composite compare to the composite after 4 and 8 ARB passes (Fig 6.9 and Fig 6.10).

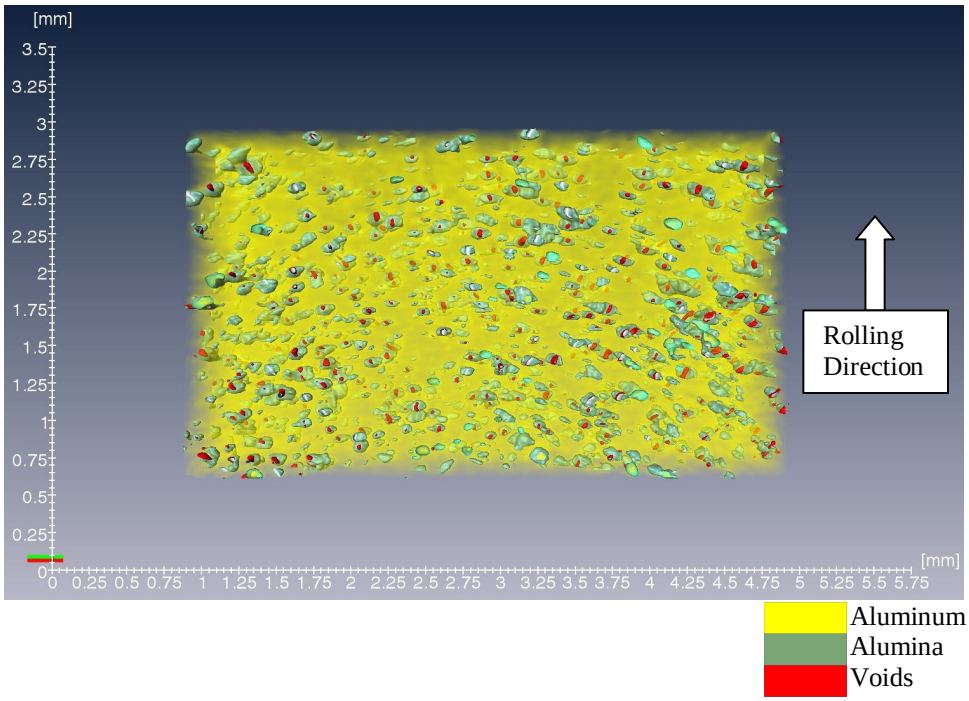

Fig 6.9: 3D view of the composite after 10 passes (front view).

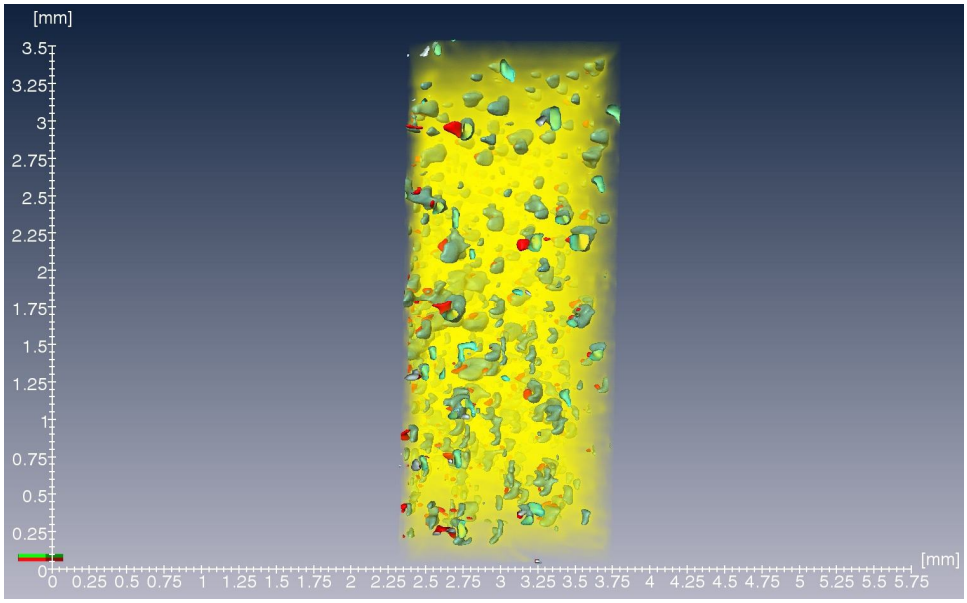

Fig 6.10: 3D view of the composite after 10 passes (side view).

The volume of alumina lied between 198 voxels (15,742 μm^3) and 35,926 voxels (2,856,368 μm^3) with a mean of 1,795 voxels (142,715 μm^3) (Fig 6.11 and Fig 6.12). That meant that the larger alumina particles left after 8 ARB passes were further broken down to smaller

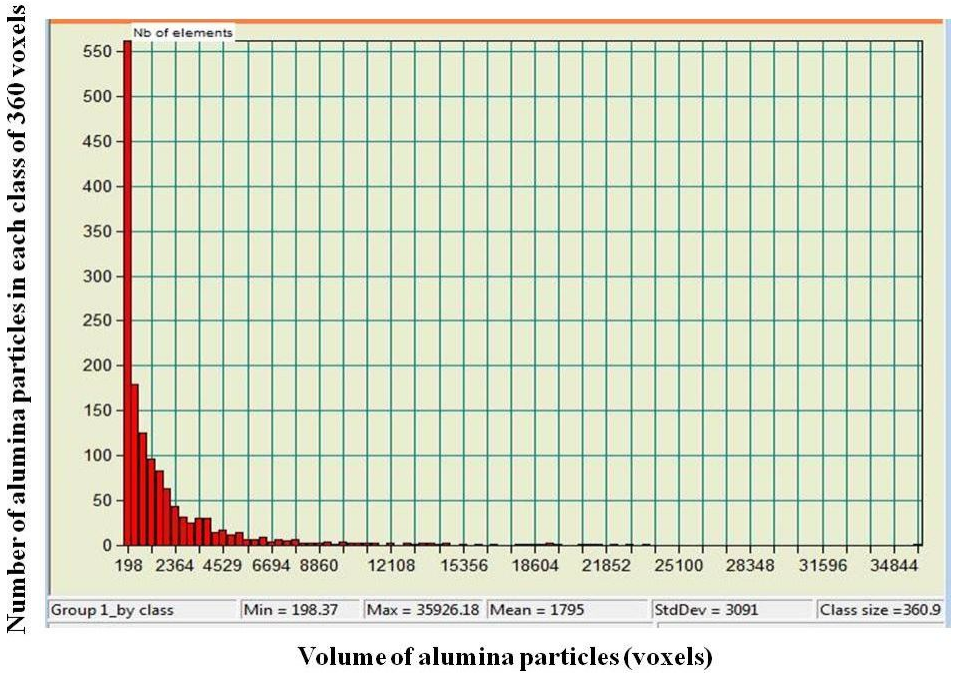

Fig 6.11: Volume of alumina particles distribution chart after 10 passes.

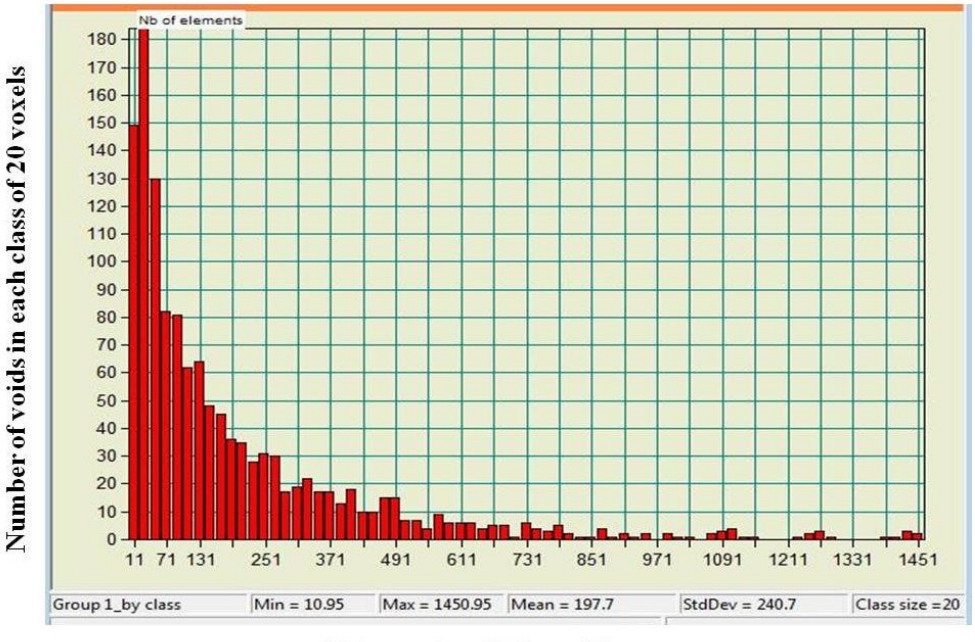

Fig 6.12: Volume of voids distribution chart after 10 ARB passes.

particles and were distributed more uniformly as seen in the Fig 6.9 and Fig 6.10. The maximum volume of voids was 1451 voxels (115,364 μm^3) with a mean value of 197 voxels (15,662 μm^3). The number of voids in the selected volume was 1305 with a volume fraction of 0.28% (Table 6.2). This implied that after 10 ARB passes the average size of the voids again increased a little but the number of voids and volume fraction of voids decreases compare to those after the 8 ARB passes. Results of measurements of alumina particles and voids in the ARB composites are given in Table 1 and Table 2.

Table 6.1: Results of measurements of alumina particles in the ARB composites:

	No. of alumina particles	**Mean volume of alumina particles** μm^3 (Voxels)	**Volume of the largest alumina particle** μm^3 (Voxels)	**Volume % of the alumina particles**
4 pass	**881**	**309k** **(3889)**	**6,583k** **(82800)**	**3.48**
8 pass	**1,235**	**211k** **(2658)**	**3,932k** **(49463)**	**3.32**
10 pass	**1,429**	**142k** **(1795)**	**2,856k** **(35926)**	**2.69**

1 Voxel = 4.3*4.3*4.3 μm^3 = 79.507 μm^3

Table 6.2: Results of measurements of voids in the ARB composites:

Voids	No. of voids	Mean volume of voids μm^3 (Voxels)	Volume of the largest void μm^3 (Voxels)	Volume % of voids
4 pass	**1,178**	**20k (260)**	**204k (2571)**	**0.33**
8 pass	**1,635**	**14k (180)**	**161k (2030)**	**0.36**
10 pass	**1,305**	**15k (197)**	**115k (1451)**	**0.28**

1 Voxel = 4.3*4.3*4.3 μm^3 = 79.507 μm^3

6.4 Comparison and discussion of the composites structure after different passes

The comparison of the composite's internal structure (Fig 6.13 – 6.20) explained the effect of ARB passes on the structure. Fig 6.13 shows that the number of alumina particle increased as the number of passes increased which ensure the uniform distribution of alumina particles throughout the aluminum matrix. Using such quantified data it would be possible, in future experiments, to co-relate the internal structure and the mechanical properties and also to determine optimum number of passes for composite manufacturing.

Fig 6.14 and Fig 6.15 show that the mean volume of the alumina particles and volume the largest alumina particle decreased as the number of ARB passes increased, which is rather obvious because increase rolling reduction breaks the larger alumina particles into smaller particles. Volume fraction of alumina decreased as ARB passes increases (Fig 6.16). The sample

was polished before the test which removed away some alumina particles near the surface. As the ARB passes increased the alumina particles were distributed more uniformly from the middle part to throughout the sample, which increased the chance of the presence of alumina particles near the surfaces. That is why volume % decreased as the number of ARB passes increased.

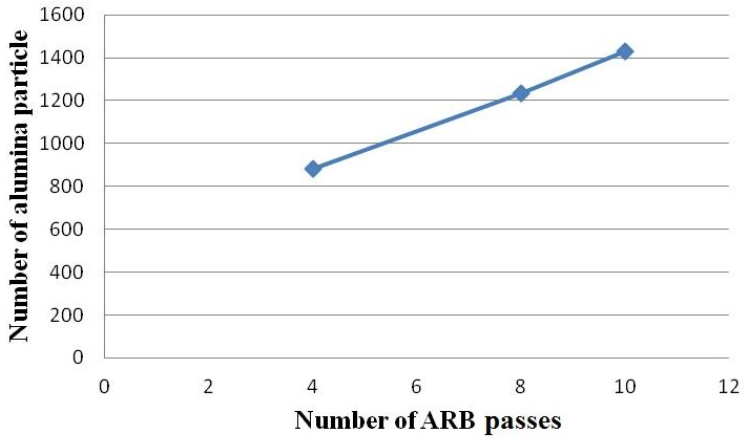

Fig 6.13: Number of alumina particle vs. number of ARB passes.

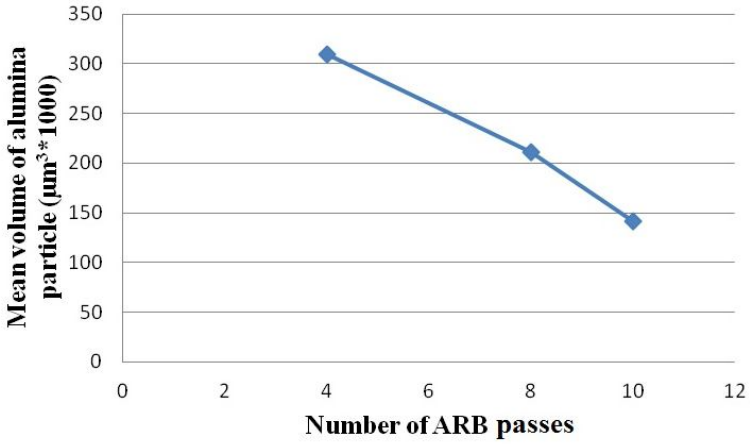

Fig 6.14: Mean volume of alumina particle vs. number of ARB passes.

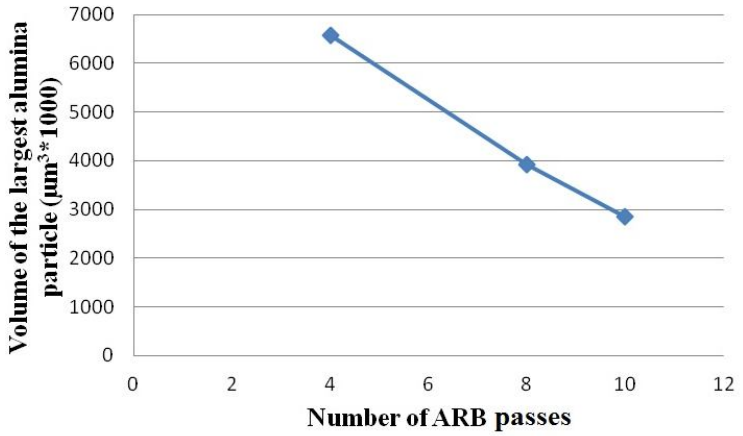

Fig 6.15: Volume of the largest alumina particle vs. number of ARB passes.

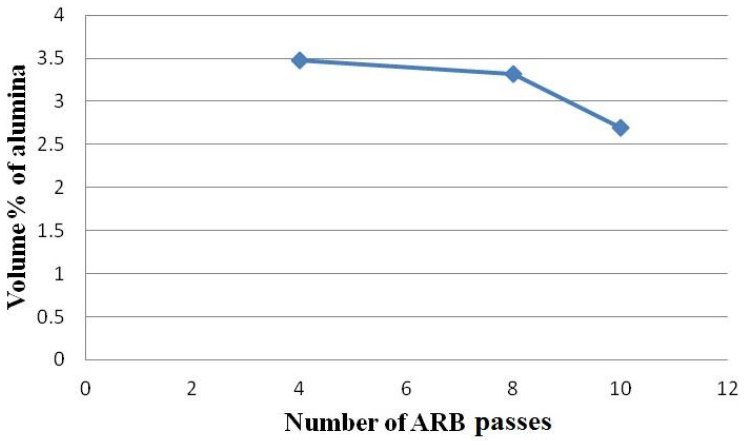

Fig 6.16: Volume % of alumina vs. number of ARB passes.

The volume distributions of the voids after different ARB passes showed some interesting results. The number of voids increased as the ARB passes increased from 4 passes to 8 passes and then decreases again after 10 ARB passes while the mean volume of voids decreased first then increased and volume of the largest void decreased as the ARB passes increased which implies that after 8 passes some new small voids are formed but bigger voids diminishes and that is why mean volume decreases (Fig 6.17 – 6.19). After 10 passes the quality of the structure improved as the number of voids and volume of the largest void decreased while mean volume increased a little.

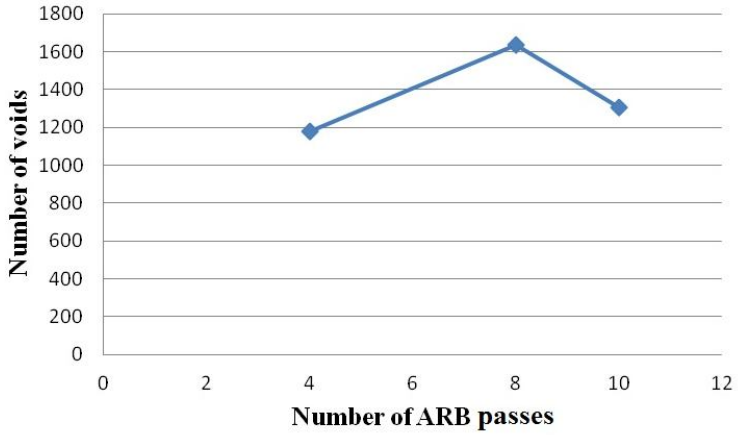

Fig 6.17: Number of voids vs. number of ARB passes.

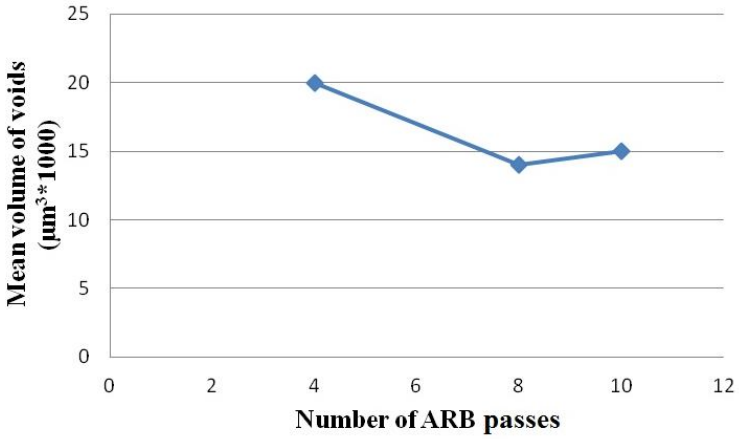

Fig 6.18: Mean volume of voids vs. number of ARB passes.

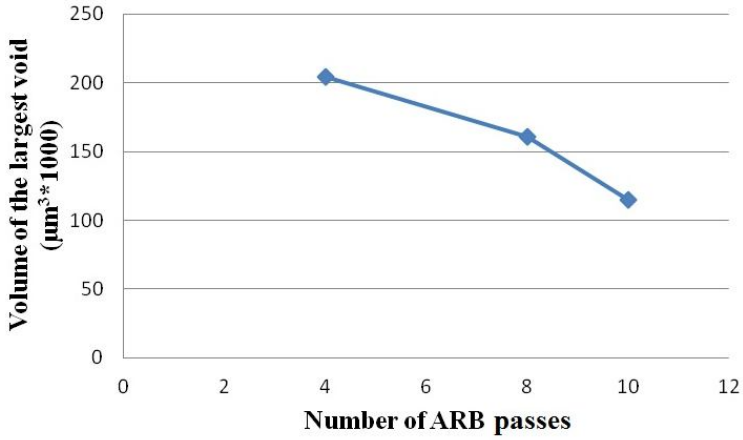

Fig 6.19: Volume of the largest void vs. number of ARB passes.

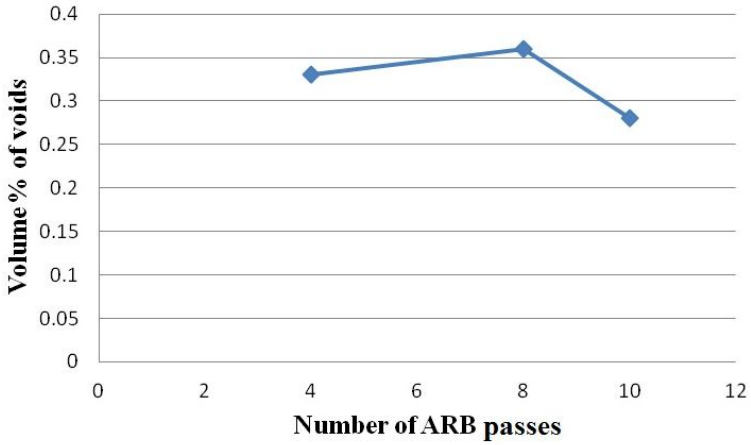

Fig 6.20: Volume % of voids vs. number of ARB passes.

6.5 Comments on the findings

The imaging technique used for absorption CT depends on the absorption characteristics of the materials; it is not difficult to segment the materials with different absorption characteristics. Unfortunately if the absorption of different materials is similar then it would be difficult to differentiate them, which has happened in our analysis. It was possible to differentiate alumina particles from the aluminum matrix but was not to identify the TiC particles. Therefore more detailed analysis to segment these particles from the matrix is needed. These composites are made by accumulated roll bonding (ARB) process. The composites after different ARB passes are studied and it was found that the number of alumina particles and voids and their shape and size distribution were different. Such information should be very useful in analysis and improvement of the manufacturing process of these types of composites.

CHAPTER 7

IN-SITU STRUCTURAL ANALYSIS OF ALUMINUM ALLOY (AA 6061) UNDER TENSILE LOADING

AA 6061 is a precipitation hardening aluminum alloy containing magnesium and silicon as its major alloying elements. It has good mechanical properties and exhibits good weldability. It is one of the most common alloys of aluminum for general purpose use. For example in:

- Construction of aircraft structures, such as wings and fuselages. AA 6061 remain resistant to corrosion even when the surface is abraded.
- Yacht construction, including small utility boats.
- Automotive parts, such as wheel spacers.
- The manufacture of aluminum cans for the packaging of foodstuffs and beverages.

7.1 In-situ 2D Experiment under Tensile Stress of AA 6061 in SEM

An in-situ tensile experiment has been done in SEM. We have in-situ tensile testing experiments module in our SEM facility. A model sample (Fig 7.1) was prepared according to ASTM E8 standard with a hole at the centre of the sample. Surface image of the sample has been captured at different strain levels (Fig 7.2). The stress strain curve (Fig 7.3) shows that the load decreases a little at the time of image taking because of the relaxation effect.

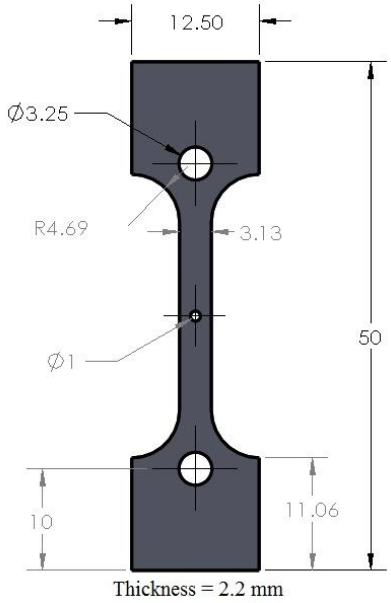

Fig 7.1: Tensile sample.

The following figure sowing the surface image of the centre part of the tensile sample in different strain levels:

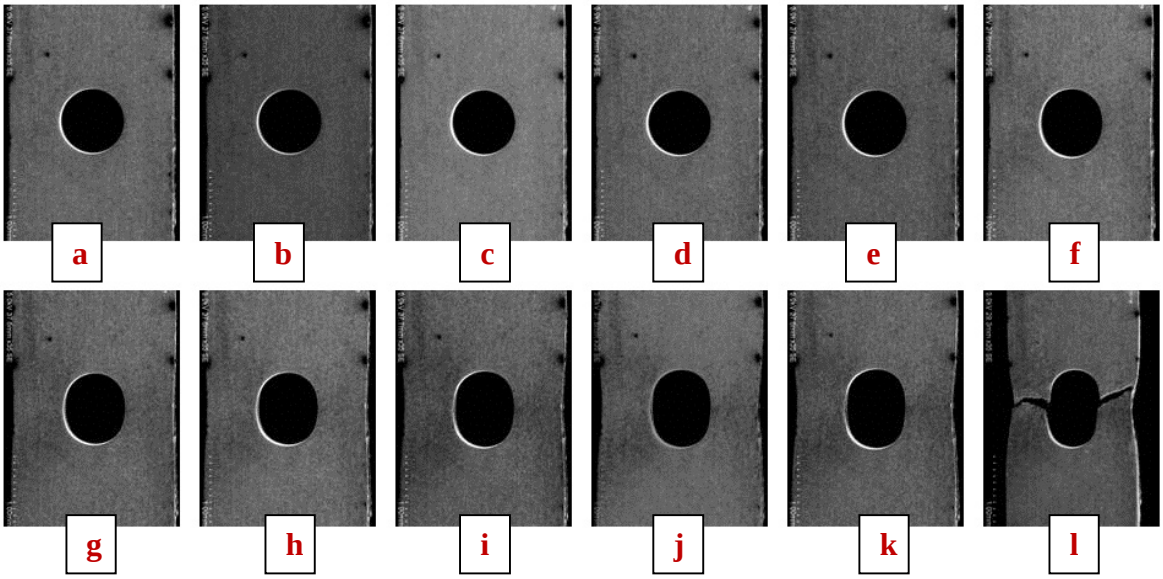

Fig 7.2: 2D surface image of AA6061 in different strain levels.

Corresponding Load vs. Elongation curve:

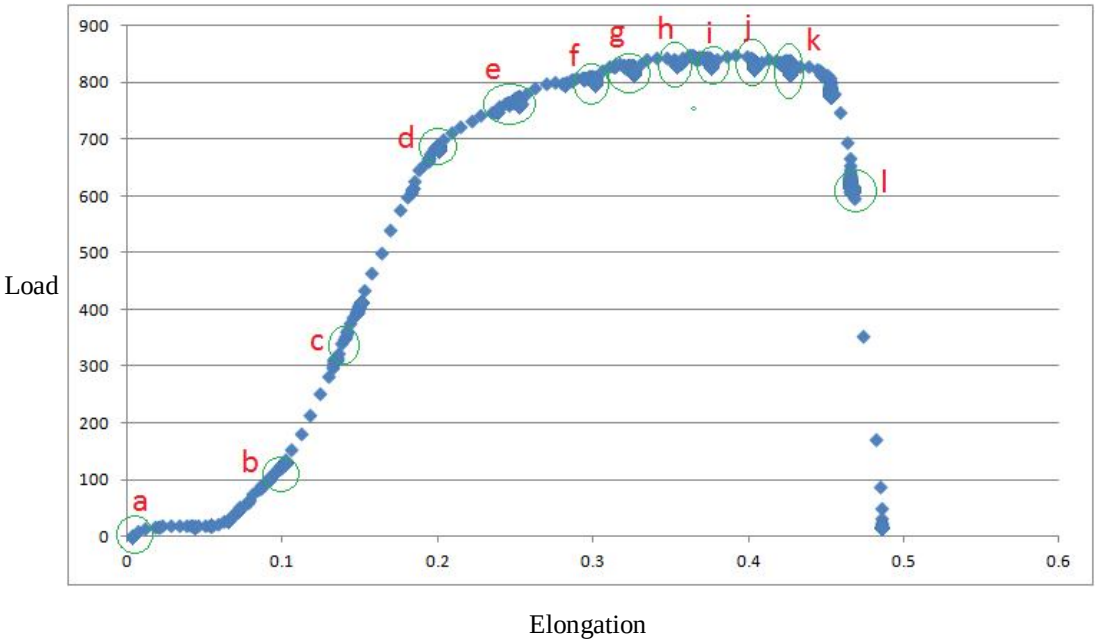

Fig 7.3: Load vs elongation curve of AA 6061 tensile test.

In the following figures (Fig 7.4) it is evident that the fracture was transgranular. The sample fractured at the time of image taking, while there was no sign of crack propagation at the surface at the time of taking the last image. We can assume that the crack started inside the specimen and fractured before showing up at the surface.

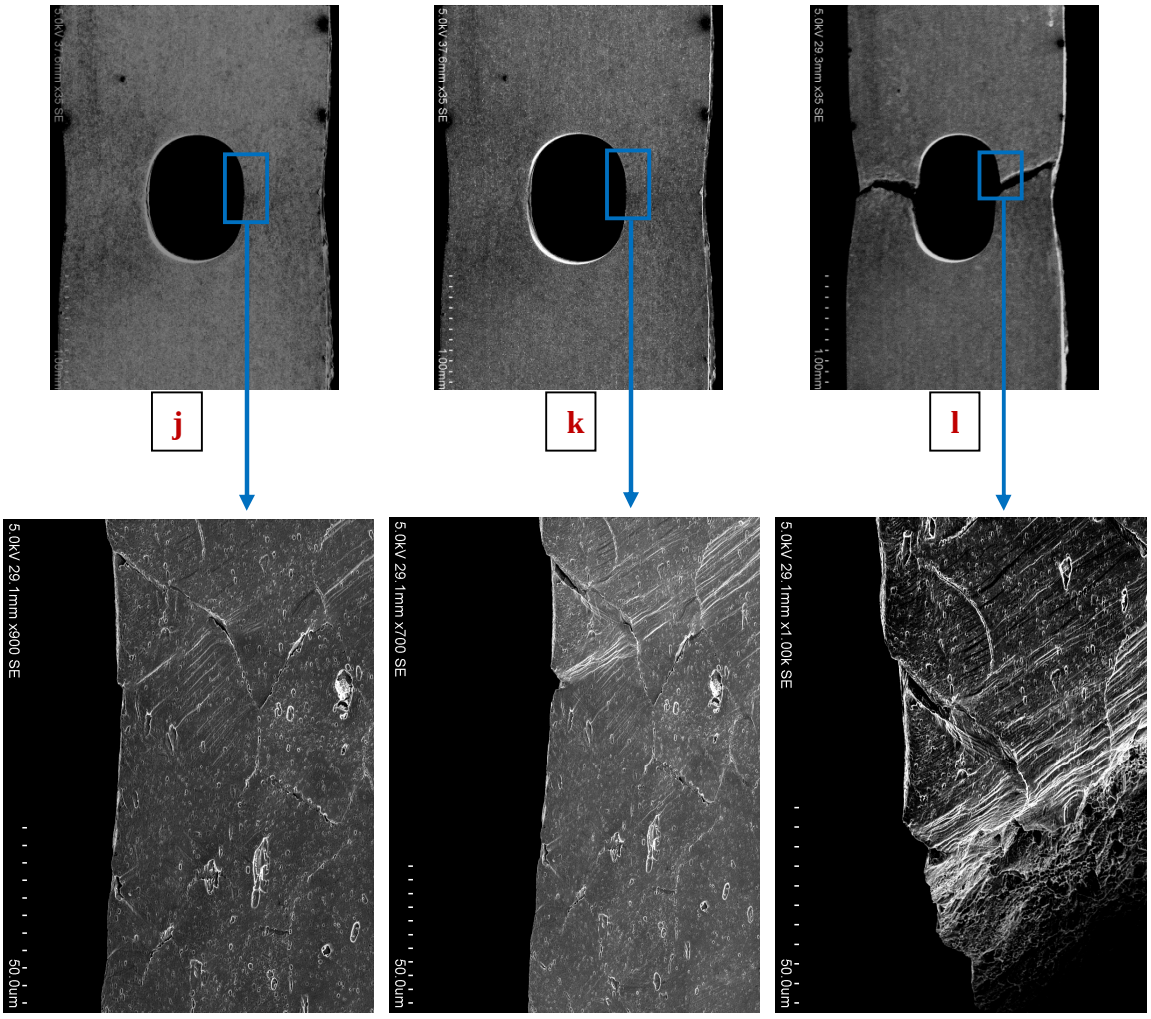

Fig 7.4: Close view of the fractured area of the AA 6061 sample.

To understand the crack initiation and propagation we will need 3D imaging. After this experiment we have done in-situ 3D imaging of the similar sample using synchrotron radiation tomography.

7.2 In-situ 3D Experiment under Tensile Stress of AA 6061 using Synchrotron Radiation Tomography

In-situ 3D imaging was done under different loading condition on AA 6061 model sample (Fig 7.5). The test was displacement control i.e. images were taken at different strain level while load was not fixed because of the relaxation effect of the pulled sample but after pulling to a specific stain level we wait till the stabilization of the load at that stain level. Unfortunately, we did not have enough time to get the 100 percent stabilization of the load but acceptable change of load which would not affect much in the imaging. It was not possible to image the whole gage length of the sample because of the limited field of view. That is why the hole in the sample was kept at the centre of the field of view and the sample was pulled from both sides in different strain levels (a) without loading, (b) after 0.30 mm elongation, (c) after 0.40 mm elongation, and after that the sample fractured.

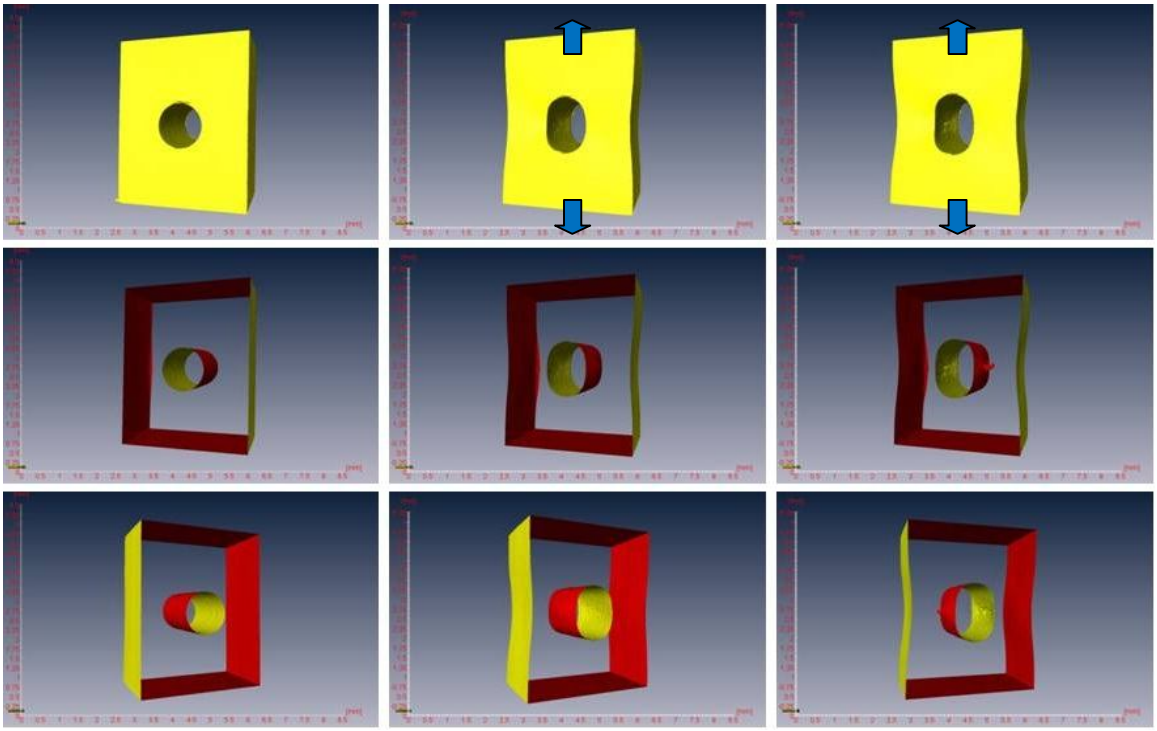

Fig 7.5: 3D images of the AA 6061 in different strain levels (a) without loading (b) after 0.30 mm elongation (c) after 0.40 mm elongation.

The 3D images presented in Fig 7.6 are after 0.40mm elongation of the sample. It is clearly visible how the cracks are propagating and connecting and changing the direction of

propagation, inside the specimen, within 3D structure. Though the resolution of this 3D imaging technique is limited and such important characteristics of structure as grain boundaries were not imaged in presented experiments, it is a very powerful tool to analyze the bulk properties of the material and failure of the materials in 3D (true volumetric). There are no indications of failure at the surface of the sample after 0.40 mm elongation whereas the cracks have been already initiated and propagated for a significant distance inside the sample before failure, see Fig 7.6 (b).

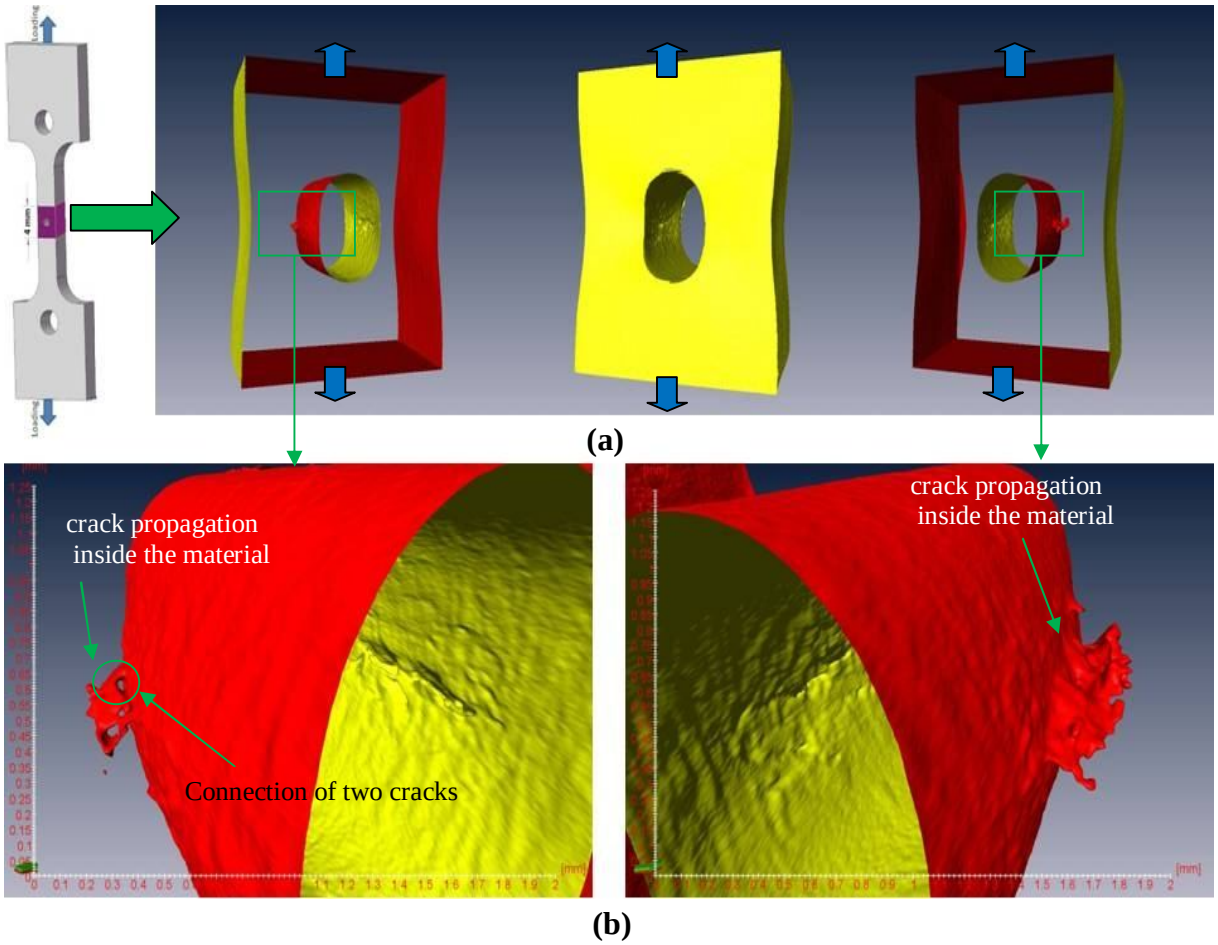

Fig 7.6: (a) 3D images of AA 6061 after 0.40 mm elongation (b) Close view of the sample showing crack propagation inside the material in 3D.

In the left figure (in Fig 7.6 (b)) we see that two cracks that are initiated from the inner surface of the hole propagate along two different directions inside the sample. After some propagation distance those two cracks merged to each other and then propagated again inside the

sample. In the right figure (in Fig 7.6 (b)) a big crack is initiated and propagated from inner surface of the sample and then changed its direction of propagation inside the sample. These crack propagation caused the fracture of the sample after a little more elongation.

7.3 Comments on the findings

In this in-situ tensile experiment of aluminum alloy (AA 6061) we see that 2D analysis cannot describe the failure of the material and 3D analysis illustrates well the processes of failure. The volumetric analysis is however limited by low resolution; therefore, 2D SEM methods will be used as complementary method to explain the scenario of failure. It would be ideal if we could image the 3D grain boundaries and relate these observations to crack propagation. In the literature [20] it was demonstrated that the grain boundaries could be made visible by decorating them by diffusion of gallium into the sample which, however, make the sample brittle and such additions may change the mode of failure.

CHAPTER 8
IN-SITU 3D STRUCTURAL ANALYSIS OF ALUMINUM COMPOSITE UNDER TENSILE LOADING

The manufacturing process of hybrid composite of $Al/Al_2O_3/TiC$ produced by anodizing and accumulative roll bonding processes is described in Chapter 3. One of these composites was investigated by in-situ 3D imaging at different strain levels with hole at the centre. The composite after 8 passes were investigated.

8.1 3D view of the composite in different strain using synchrotron radiation tomography

It was not possible to image the whole gage length of the sample because of the limited field of view. That is why the hole in the sample was kept at the centre of the field of view and then the sample was pulled from both sides. The projections were taken at different strain levels (a) without loading (b) after 0.30 mm elongation (c) after 0.40 mm elongation (d) after 0.45 mm elongation, and after that the sample fractured.

The 3D view of the composite in different strain levels showed that the alumina along with aluminum were deforming and some were moving out of the field of view as elongation increased (Fig 8.1 – 8.12). Most of the voids were at the interfaces between the aluminum and alumina.

The figures (Fig 8.2, 8.5, 8.8 and 8.11) show that the alumina particles moved a little amount because the loading increased the distance between the particles along the loading direction. It can be speculated from those figures that most of the voids were created because the loading stress must have concentrated near the alumina particles or perhaps at the interfaces between the alumina particles and aluminum matrix. Crack starts from the inner surface of the hole as the stress is maximum there because of the lowest cross sectional area of the specimen and stress raiser effect because of the hole and continues to propagate inside the composite and finally causes the fracture of the sample as load increases.

The figures (Fig 8.3, 8.6, 8.9 and 8.12) show that the volume and number of voids increases as the elongation increases but there is no significant increase in size and the number of voids up to 0.30 mm elongation. After more elongation new voids were created and some voids coalesced and, as a result, the number and size of the voids increased.

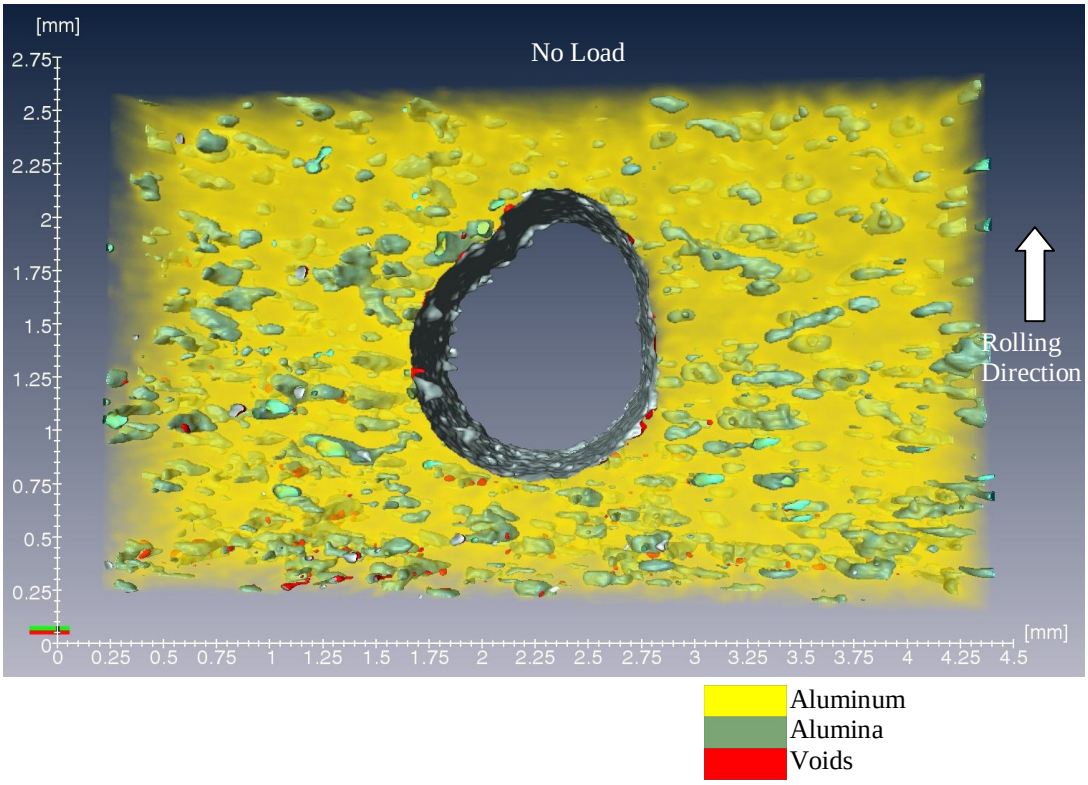

Fig 8.1: 3D view of the composite without loading.

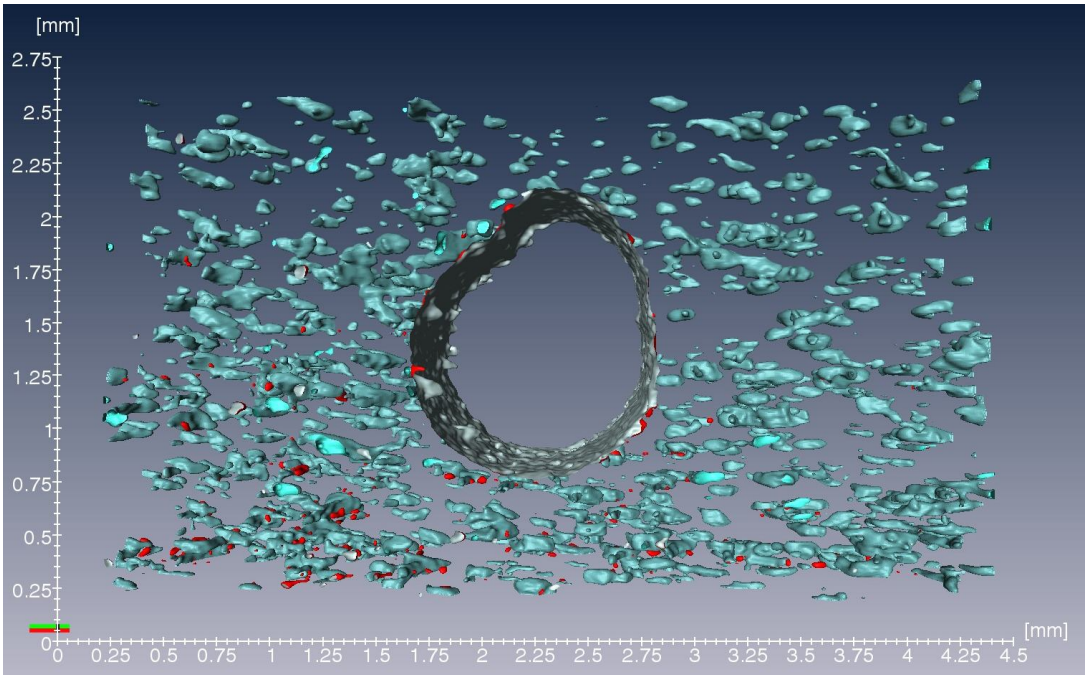

Fig 8.2: 3D view of the composite without loading (without aluminum matrix).

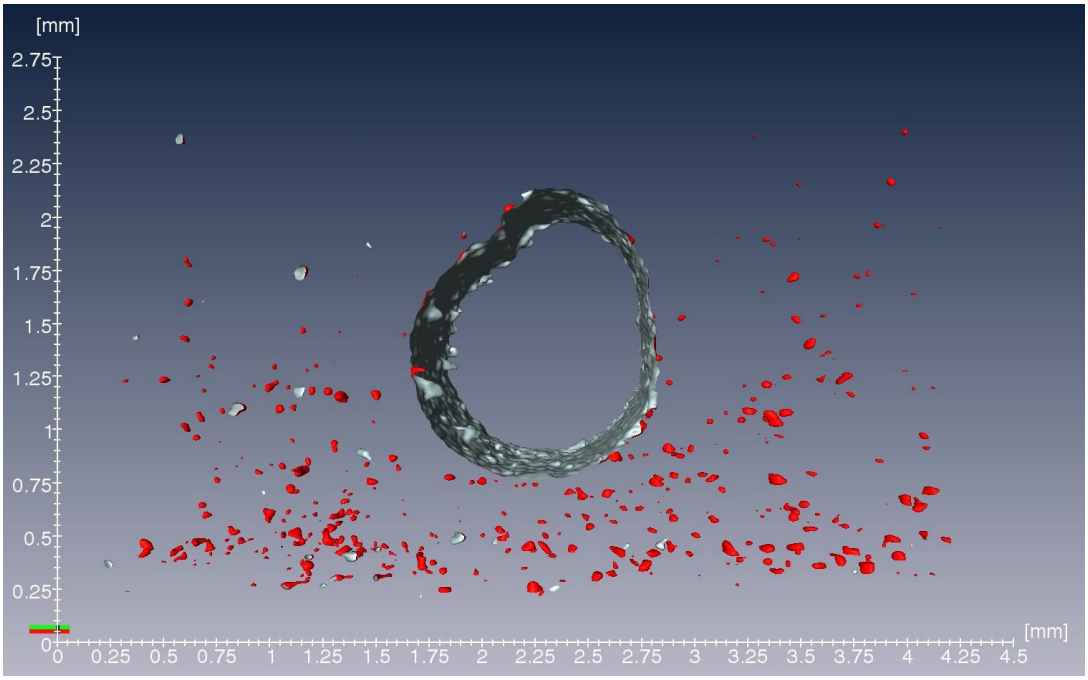

Fig 8.3: 3D view of voids in the composite without loading.

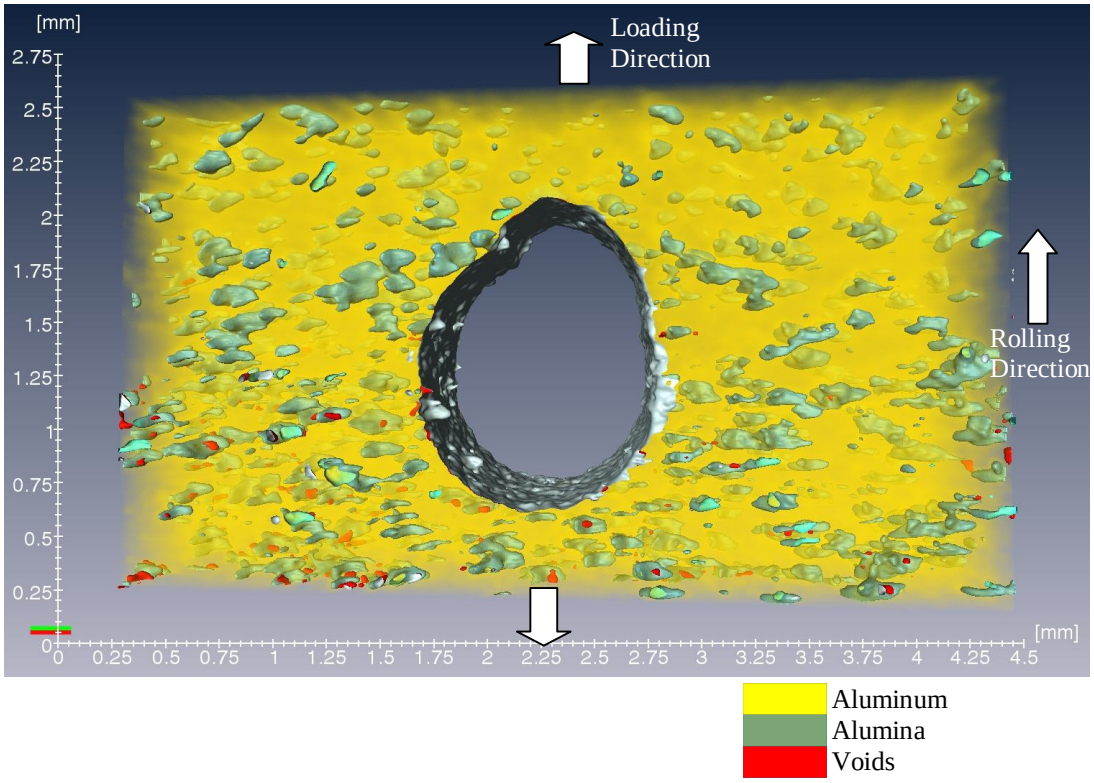

Fig 8.4: 3D view of the composite after 0.30 mm elongation.

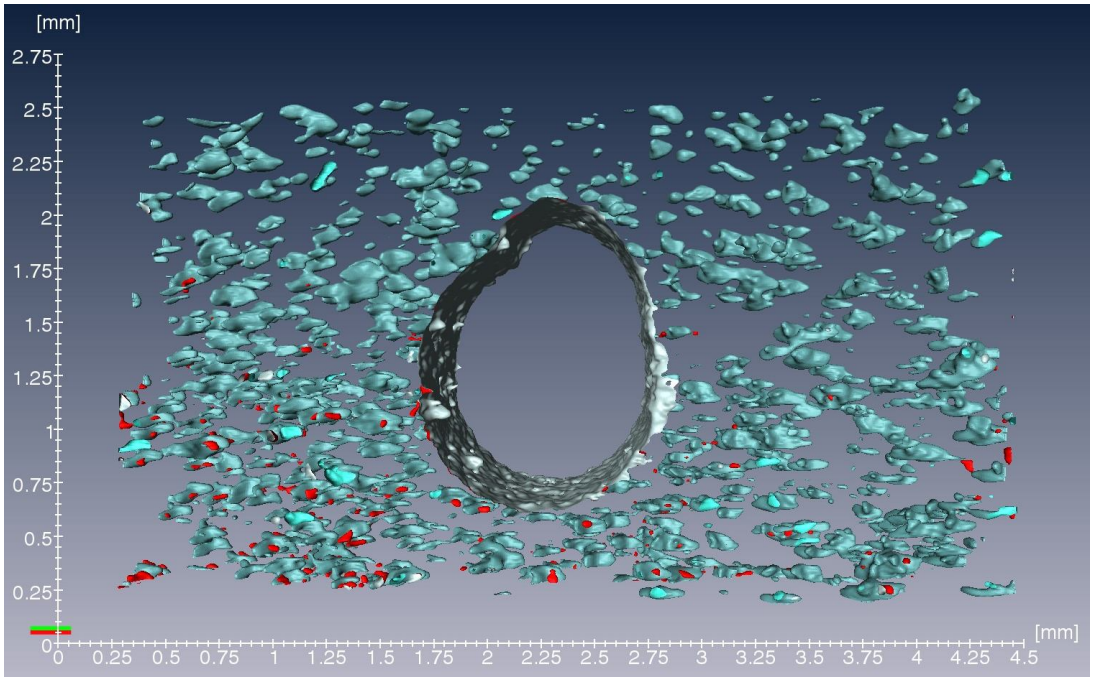

Fig 8.5: 3D view of the composite after 0.30 mm elongation (without aluminum matrix).

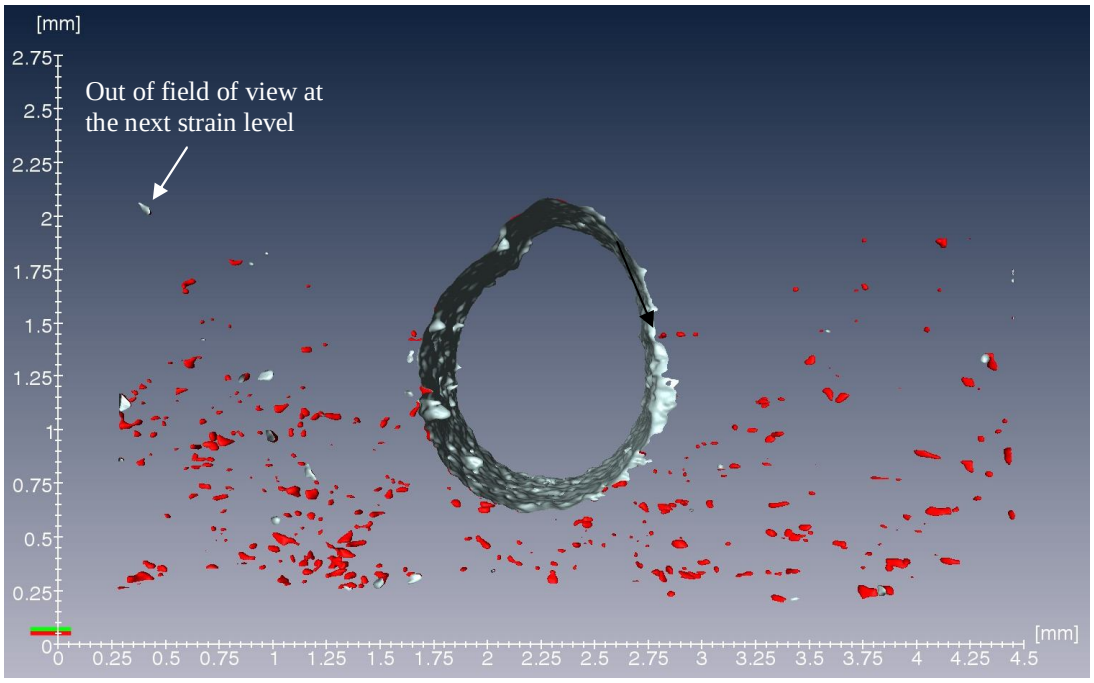

Fig 8.6: 3D view of voids in the composite after 0.30 mm elongation.

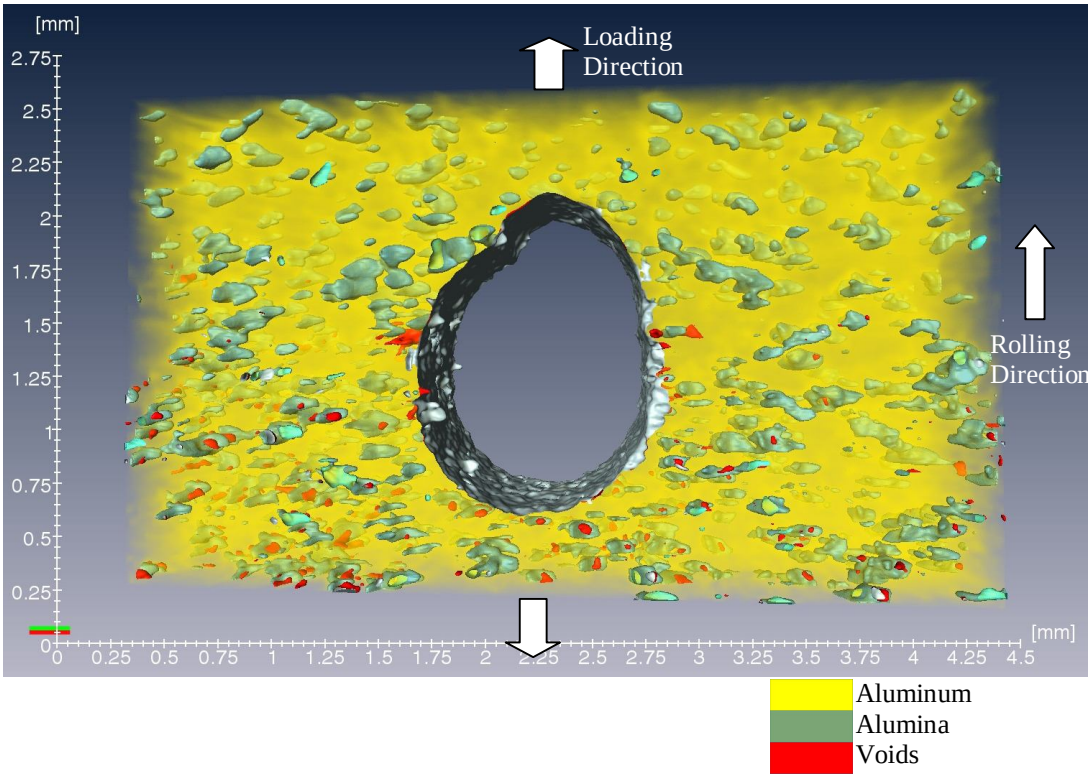

Fig 8.7: 3D view of the composite after 0.40mm elongation.

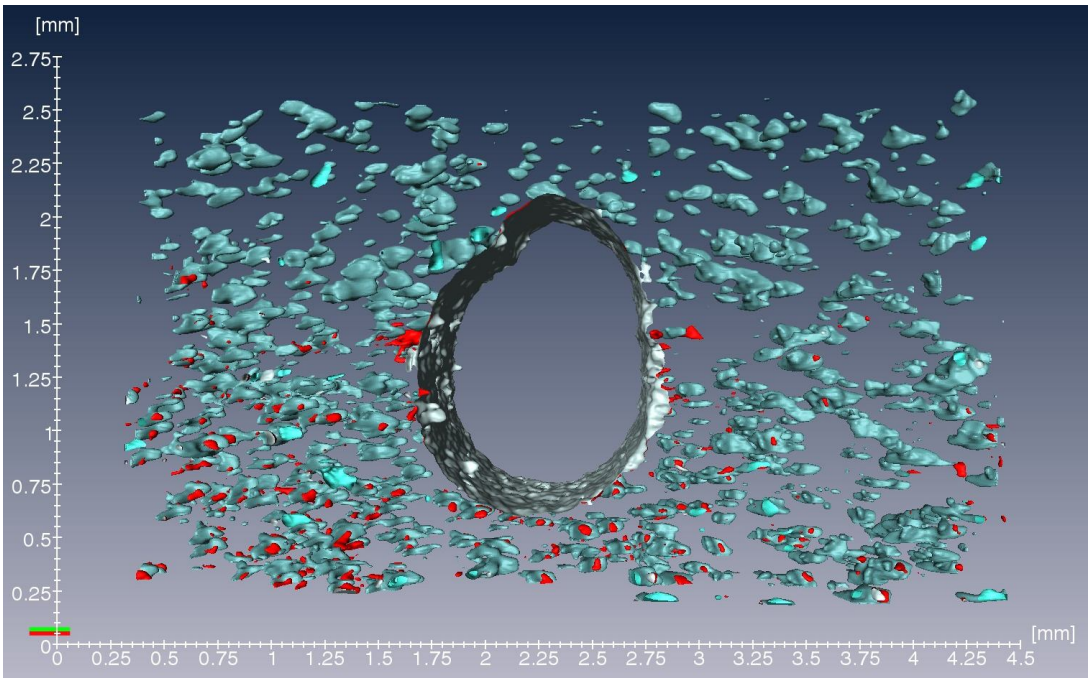

Fig 8.8: 3D view of the composite after 0.40mm elongation (without aluminum matrix).

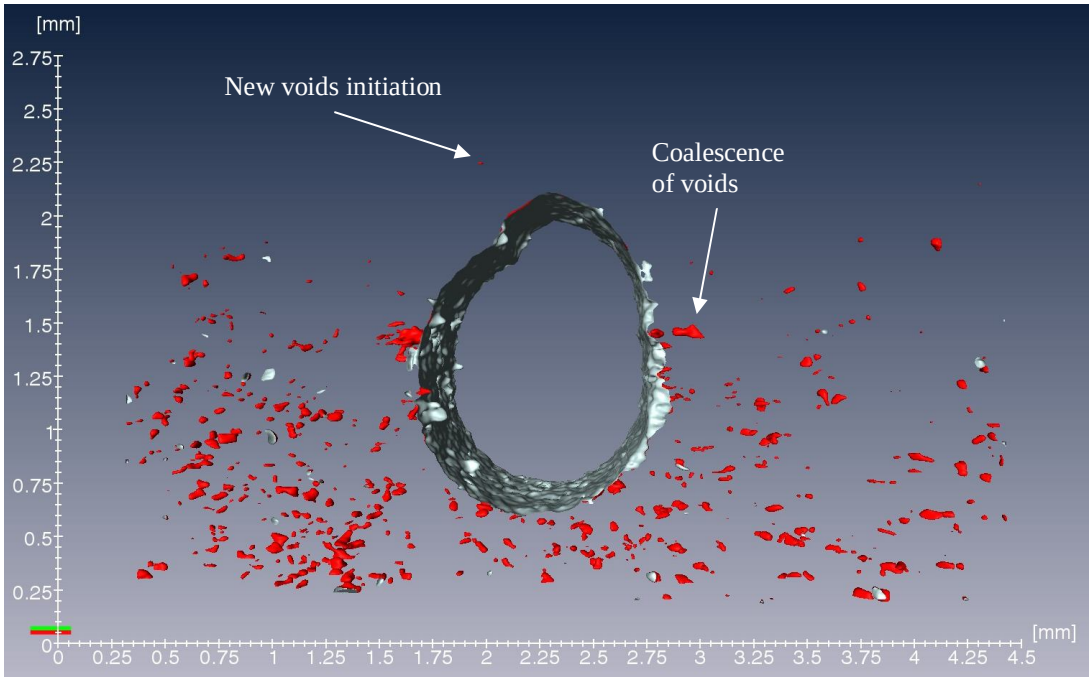

Fig 8.9: 3D view of voids in the composite after 0.40 mm elongation.

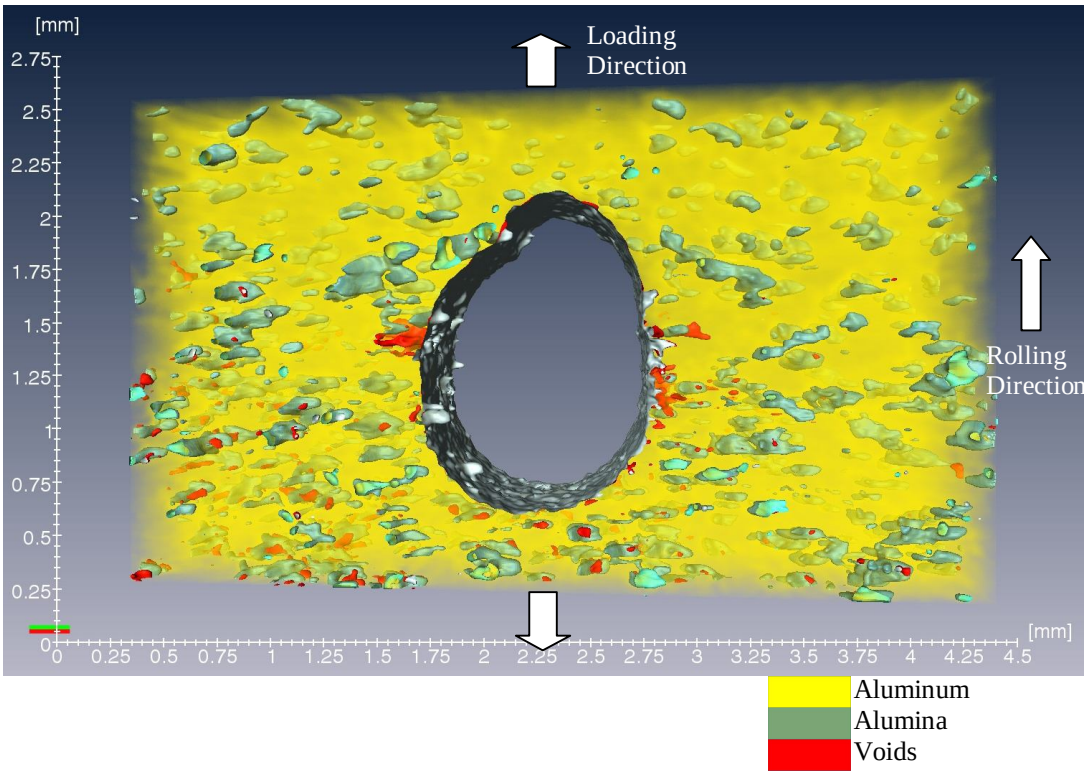

Fig 8.10: 3D view of the composite after 0.45mm elongation.

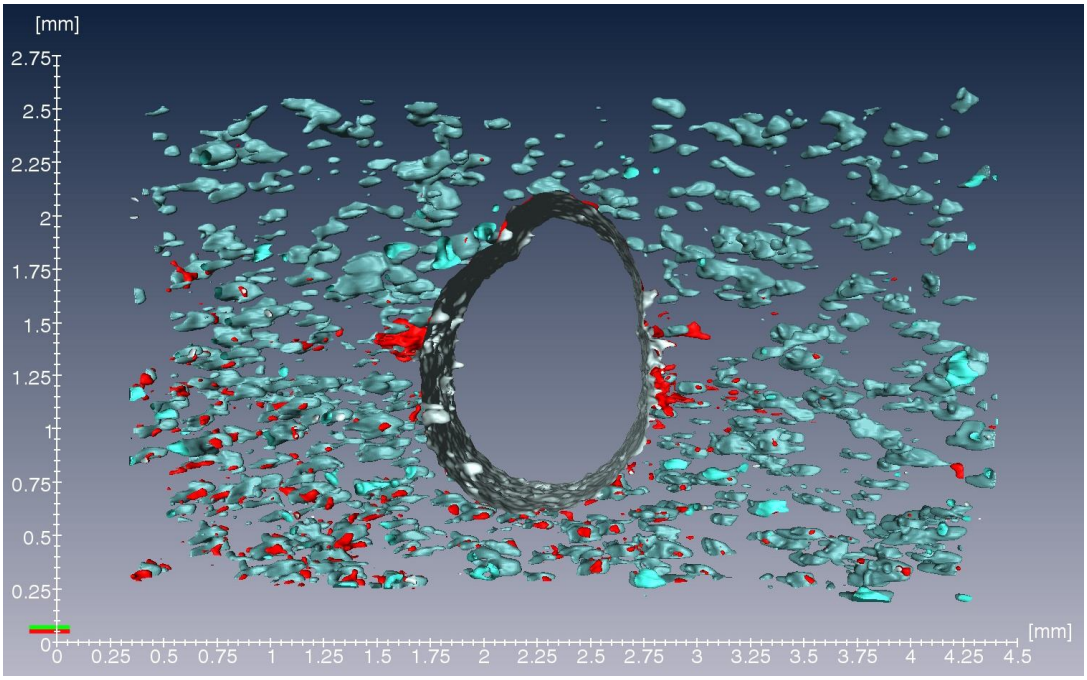

Fig 8.11: 3D view of the composite after 0.45mm elongation (without aluminum matrix).

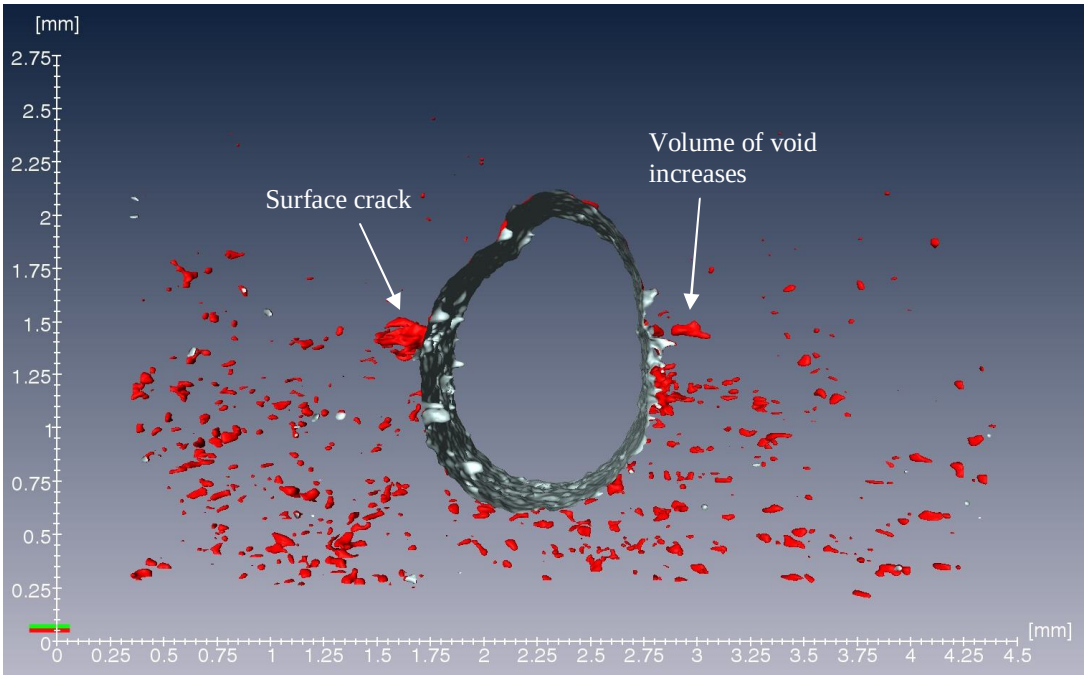

Fig 8.12: 3D view of voids in the composite after 0.45 mm elongation.

In the Fig 8.12 we can see that though volume of voids increased, the crack initiated at the surface propagated though the material and caused fracture. The voids acted as a favorable path for the failure crack to propagate.

8.2 Size distribution of voids in the composite at different strain levels

The following charts (Fig 8.13 - 8.16) show the volume of the voids distribution in the composite at different strain levels and results of measurements of size of voids in different stain levels in the composite are presented in Table 8.1. In all the volume distribution charts the columns represent the number of voids present in the investigated volume of the sample, where volume of each 50 voxels = 3,975 μm^3. Again, the accuracy in measuring the number of voids and the volume of each void strongly depended upon the accuracy of choosing the threshold value of the grey scale images. In Fig 8.13 the volume distribution of voids without loading of the sample is shown. In the figure it is clear that most of the voids in the composite are small. The total number of voids was 1,020 (Table 8.1) where around 700 voids lied below the mean volume of total voids of 154 voxles (12,244 μm^3). The volume of the largest void is 2201 voxels (174,994 μm^3).

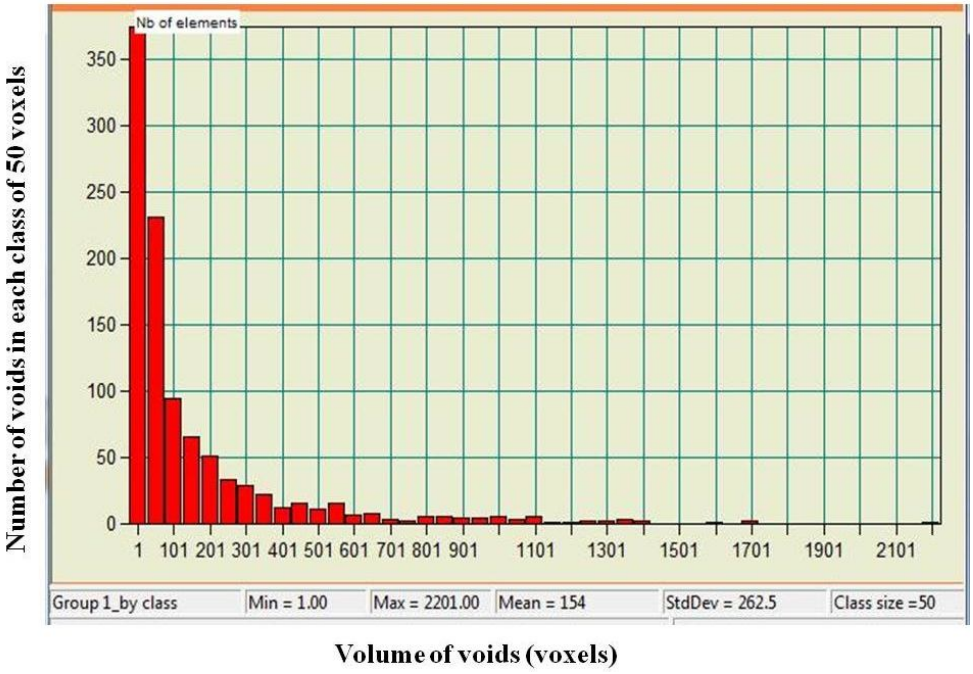

Fig 8.13: Volume of voids distribution chart without loading.

In Fig 8.14 the volume distribution of voids after 0.30 mm elongation of the sample is shown. The total number of voids was 1,026 (Table 8.1) where around 700 voids have a dimension below the mean volume which was 150 voxels (11,926 μm^3). The size distribution of voids was very similar to the distribution of volume of voids without loading. The volume of the largest void was 3201 voxels (254,501 μm^3).

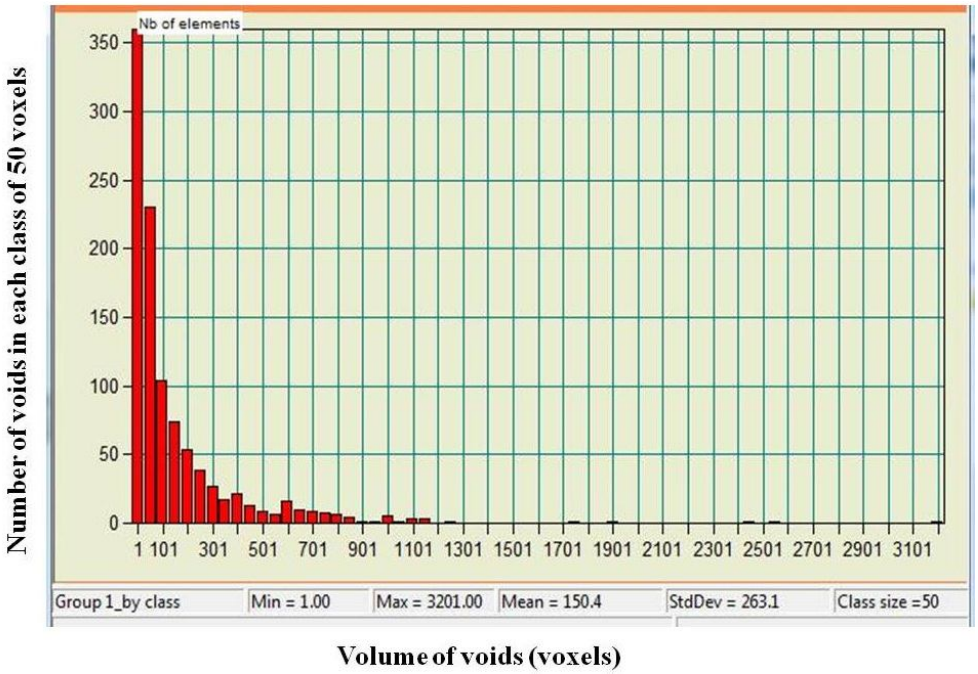

Fig 8.14: Volume of voids distribution chart after 0.30 mm elongation.

In Fig 8.15 the volume distribution of voids after 0.40 mm elongation of the sample is shown. At this strain level the total number of voids and the size of the voids increased but the distribution pattern remained the same i.e. more than 60% of the voids lied below the mean volume of the voids and this number was reduced as volume of voids increased. In the present case the total number of voids was 1,384 (Table 8.1) and around 900 voids lied below the mean volume which was 169.9 voxels (13,508 μm^3). The volume of the largest void was 3551 voxels (282,329 μm^3).

In Fig 8.16 the volume distribution of voids after 0.45 mm elongation of the sample was shown. At this strain level, the total number of voids and the size of the voids increased more and the distribution pattern remained the same again i.e. more than 70% of the voids lied below the mean volume of the voids, and this percentage was reduced when the volume of voids increased. In this case the total number of voids was 1,590 (Table 8.1) where around 1150 voids lied below

the mean volume which was 169.6 voxles (13,484 μm^3). The volume of the largest void was 4751 voxels (377,737 μm^3) whereas the volume of largest void without loading was 2201 voxels (174,994 μm^3) i.e. loading increased the volume of voids in significant amount which might be main responsible cause of failure of the material.

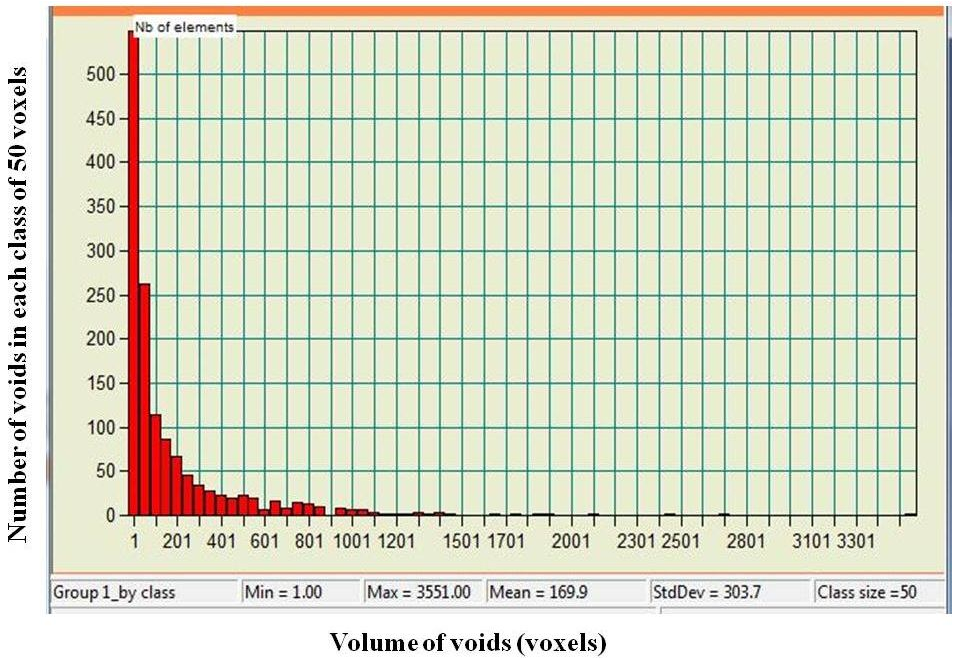

Fig 8.15: Volume of voids distribution chart after 0.40 mm elongation.

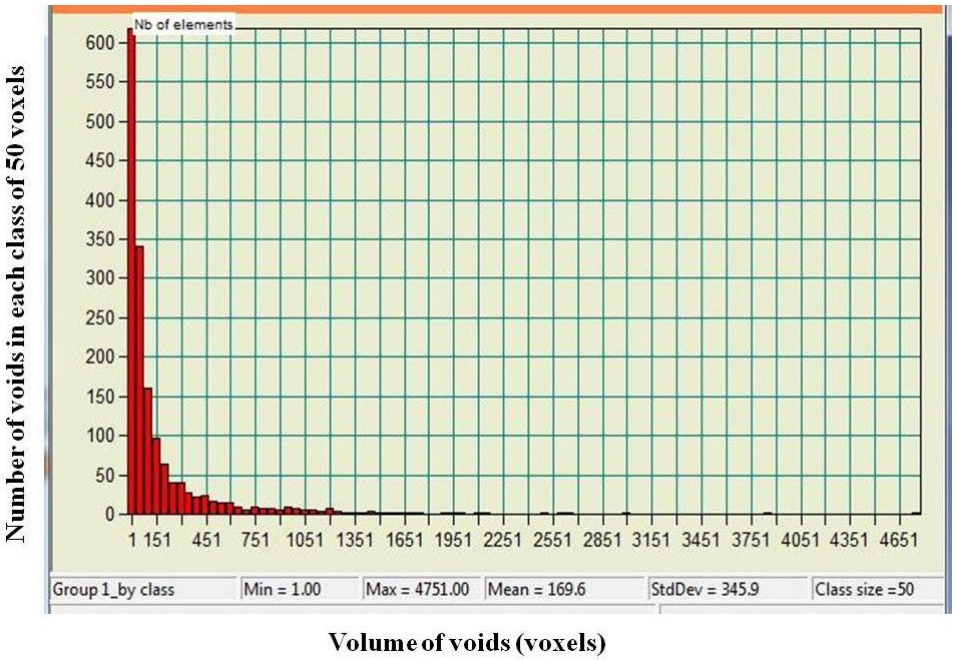

Fig 8.16: Volume of voids distribution chart after 0.45mm elongation.

Table 8.1: Results of measurements of size of voids in different stain levels in the composite:

	Total no. of Voids	**Total volume of voids μm^3 (voxels)**	**Mean volume of voids μm^3 (voxels)**	**Volume of the largest void μm^3 (voxels)**
Without loading	**1,020**	**12,638k (158955)**	**12.25k (154)**	**175k (2201)**
After 0.30mm elongation	**1,026**	**12,391k (155856)**	**12.00k (150)**	**254k (3201)**
After 0.40mm elongation	**1,384**	**18,889k (237579)**	**13.5k (170)**	**282k (3551)**
After 0.45mm elongation	**1,590**	**21,751k (273581)**	**13.4k (169)**	**377k (4751)**

1 voxel = 4.3*4.3*4.3 μm^3 = 79.507 μm^3

From the void size distributions it is obvious that most of the voids lied below the median volume of the voids. Figs 8.17- 8.20 are showing the number and volume of voids at different strain levels. There is almost no change in the number of voids between the specimen without loading and the specimen after 0.30 mm elongation, but an increase of size of some voids is observed. However there is a significant difference in number of voids and average size of the voids between the sample after 0.30 mm elongation and 0.40 mm elongation. Again, at the next strain level (after 0.45 mm elongation) the average size of the voids remained the same but the number of voids increase which mean that new smaller voids are formed. Volume of the largest void (Fig 8.20) increased dramatically after 0.45 mm elongation and this increment favored the fracture of the sample.

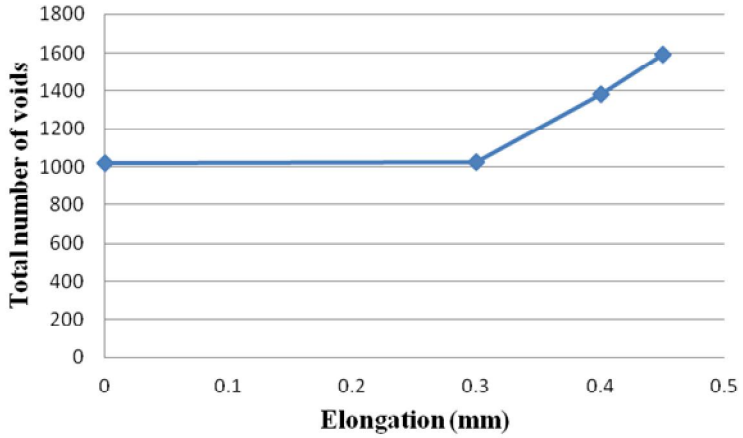

Fig 8.17: Total number voids vs. the elongation.

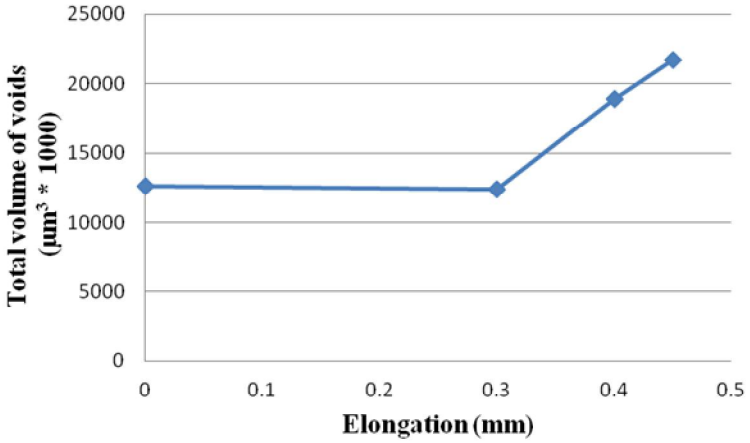

Fig 8.18: Total volume of void vs. elongation.

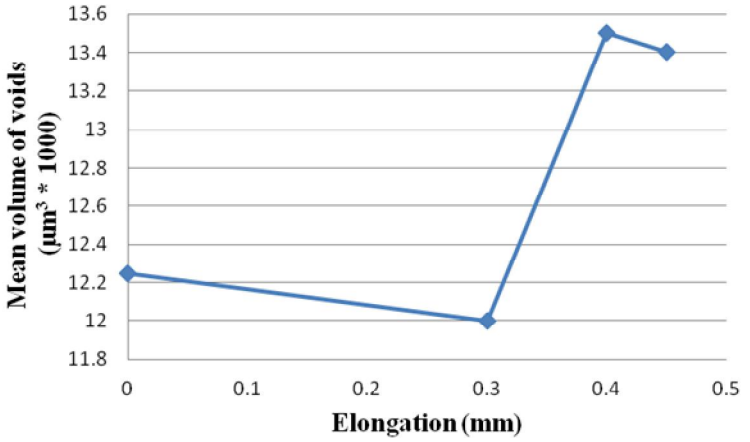

Fig 8.19: Mean volume of voids vs. elongation.

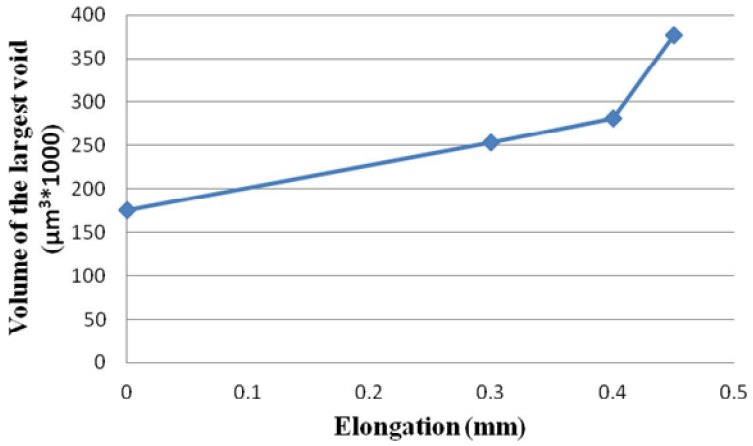

Fig 8.20: Volume of the largest void vs. elongation.

8.3 Discussion on findings

In the in-situ 3D imaging of $Al/Al_2O_3/TiC$ hybrid composite it has been found that the number and size of voids increased and then the voids coalesced with each other as load increased which is rather obvious. However, the failure occurred because of the crack initiation at the inner surface of the hole where the stress was maximum because of the smaller cross-sectional area and stress raiser effect at the hole, and then crack propagated inside the material causing failure. This technique makes it possible to visualize how the internal structure (size, shape and distribution) of voids changes with the increment of the load and to observe the initiation of failure in the sample under the tensile load.

CHAPTER 9
CONCLUSION

High-resolution industrial computed tomography (micro CT and nano CT) was used for imaging and inspecting structure of metallic materials, composites and porous metals. Different phases of materials as well as voids and cracks were visualized in 3D with microscopic resolution.

A novel experimental system has been designed and built for in-situ experiments under tensile loading at BMIT-BM at CLS. This system was used to perform dynamic testing on specimens with different structural characteristics. The system was designed in such a way that the loading and the rotation of the sample was independent so that the sample can be rotated freely under loading for taking projection images for synchrotron-based computed tomography at the CLS. The aim of designing this experimental system was to make a platform at CLS for doing in-situ experiment under loading of different materials including metals, MMCs and biomaterials within the limitations of specified maximum size and load of the samples.

The system has been used to image the structure of porous aluminum and analyze the size and distribution of voids. It has been shown that this technique is a powerful technique to analyze the internal structure of porous materials i.e. porosity, differences in porosity in different parts of the sample, size distribution of voids if we can segment the structure properly by choosing correct threshold value of the grey scale of the images.

The system was also used to image the structure of $Al/Al_2O_3/TiC$ hybrid composites to analyze the size distribution of reinforcing particles and voids. As the technique we used is absorption CT which depends on the density and absorption characteristics of the materials, it is easier to segment the materials with different densities in the samples. Unfortunately, if the absorption of different materials is close then it would be difficult to differentiate them which happened in our analysis. It was possible to differentiate alumina particles from the aluminum matrix but not the TiC particles in our present study because the density of TiC particles was close to the aluminum matrix which needs more detailed analysis to segment these particles from the matrix. These composites were made by accumulated roll bonding (ARB) process. The

composites after different ARB passes are studied and it was found that the number of alumina particles and voids and their shape and size distribution are different.

It was demonstrated that in-situ system could be used to image consecutive stages of structural transformation in aluminum alloy and aluminum composites during tensile deformation and to illustrate the nucleation of failure. In the case of in-situ tensile experiment of aluminum alloy (AA 6061), we see that 2D SEM analysis is not enough to describe the failure of the material and 3D analysis is true volumetric but limited to low resolution i.e. both techniques work as complementary for each other to explain the whole scenario. In case of in-situ 3D imaging of $Al/Al_2O_3/TiC$ hybrid composite, it has been found that the number and size of voids increased and then coalesced with each other as load increased which is obvious but failure occurred because of the initiation of crack at inner surface of the hole as the stress was maximum there which propagate inside the material cause facture.

The novel experimental system of dynamic testing, used for imaging at BMIT-BM at CLS, can help in better description of structural transformation associated with the application of load and will contribute to better understanding of the failure mechanisms of different types of materials during straining.

CHAPTER 10
FUTURE WORK

The developed 3D in-situ dynamic experimental technique can be used to study of failure in technologically important light weight materials like:

- Aeronautic Aluminum Alloy with Precipitates
- Porous Aluminum/ Aluminum Foam
- Aluminum-Alumina Composites
- Aluminum-Alumina-SiC hybrid Composites

In our present study (in imaging of $Al/Al_2O_3/TiC$ hybrid composite) we were unable to separate TiC from structure. We need more details study to quantify the presence of TiC in the composites.

We believe that the quantitative measurements are accurate (as we found accurate in bigger scale in comparing the outer physical dimension of the sample) but for the smaller structural components (voids, reinforcing particles) inside the material it may need concrete proof of the accuracy of measurements.

In the literature [12, 13] it is evident that the heavy weight material can be inspected by using higher energy synchrotron radiation. This technique would be useful to investigate failure mechanisms of technologically important pipeline steel when BMIT-ID beamline (energy level is 20 KeV to 100 KeV) is available.

We know from the literature [21] that the available software can produce 3D volume data for the simulation software i.e. COMSOL. The 3D image data obtained from CT measurements can be used also for modeling of the failure processes of the investigated materials.

CHAPTER 11
REFERENCES

1. L. Salvo et al. / Nucl. Instr. and Meth. in Phys. Res. B 200 (2003) 273–286
2. R.T. DeHoff, F.N. Rhines, dans ‘‘Microscopie Quantitative’’, Eds Masson, 1972.
3. J.H. Han, D.Y. Kim, Acta Mater. 43 (1995) 3185.
4. J.H. Han, D.Y. Kim, Acta Mater. 46 (1998) 2021.
5. J-Y. Buffi_ere, E. Maire, P. Cloetens, G. Lormand, R. Foug_eres, Acta Metall. 47 (1999) 1613.
6. G.T. Herman, Image Reconstruction from Projections, Academic Press, New York, 1980.
7. Felix Beckmann, Rainer Grupp, Astrid Haibel, Michael Huppmann, Michael Nöthe, Anke Pyzalla, Walter Reimers, Andreas Schreyer and Rudolf Zettler. ADVANCED ENGINEERING MATERIALS 2007, *9*, No. 11.
8. W. Reimers, A. R. Pyzalla, A. K. Schreyer, H. Clemens, Neutrons and Synchrotron Radiation in Eng. Mater. Sci. Wiley-VCH Verlag, Weinheim, 2007.
9. E. Maire et al. / Engineering Fracture Mechanics 78 (2011) 2679–2690.
10. J.J. Williams et al. / Acta Materialia 58 (2010) 6194–6205.
11. T. OHGAKI, H. TODA, M. KOBAYASHI, K. UESUGI, M. NIINOMI, T. AKAHORI, T. KOBAYASH, K. MAKII and Y. ARUGA. Philosophical Magazine, Vol. 86, No. 28, 1 October 2006, 4417–4438
12. E. Maire et al. / Acta Materialia 56 (2008) 4954–4964.
13. A. Bareggi · E. Maire · O. Bouaziz · M. Di Michiel. Int J Fract (2012) 174:217–227.
14. Brian M. Patterson and Christopher E. Hamilton. Analytical Chemistry, Vol. 82, No. 20, October 15, 2010.
15. The Scientist and Engineer's Guide to Digital Signal Processing By Steven W. Smith, Ph.D.
16. Y. SAITO, H. UTSUNOMIYA, N. TSUJI and T. SAKAI. Acta mater. Vol. 47, No. 2, pp. 579±583, 1999.
17. Mohammad Raei, Mohammad Reza Toroghinejad, and Roohollah Jamaati. Materials and Manufacturing Processes, 26: 1352–1356, 2011.

18. R. Jamaati, M.R. Toroghinejad / Materials Science and Engineering A 527 (2010) 4146–4151.
19. R. Jamaati et al. / Materials and Design 35 (2012) 37–42
20. T. Ohgaki et al. / Materials Science and Engineering A 406 (2005) 261–267.
21. Y. Haba, W. Kröger, H. Ewald, R. Souffrant, E. Otterstein, W. Mittelmeier and R. Bader. Numerical Simulation of the Functional Electromagnetic Stimulation of the Human Femoral Bone using COMSOL. Proceedings of the COMSOL Conference 2009 Milan.

APPENDIX

The appendix contains the permission of the figures to reprint from the publisher in the following order:

1. Figure 2.1
2. Figure 2.2
3. Figure 2.3
4. Figure 2.4a
5. Figure 2.4b
6. Figure 2.5, 2.6 and 2.7

ELSEVIER LICENSE
TERMS AND CONDITIONS

Apr 04, 2013

This is a License Agreement between K M Mostafijur Rahman ("You") and Elsevier ("Elsevier") provided by Copyright Clearance Center ("CCC"). The license consists of your order details, the terms and conditions provided by Elsevier, and the payment terms and conditions.

All payments must be made in full to CCC. For payment instructions, please see information listed at the bottom of this form.

Supplier	Elsevier Limited The Boulevard,Langford Lane Kidlington,Oxford,OX5 1GB,UK
Registered Company Number	1982084
Customer name	K M Mostafijur Rahman
Customer address	414A, 108th Street Saskatoon, SK S7N1P9
License number	3120640165075
License date	Apr 02, 2013
Licensed content publisher	Elsevier
Licensed content publication	Engineering Fracture Mechanics
Licensed content title	Damage quantification in aluminium alloys using in situ tensile tests in X-ray tomography
Licensed content author	Eric Maire,Suxia Zhou,Jerome Adrien,Marco Dimichiel
Licensed content date	October 2011
Licensed content volume number	78
Licensed content issue number	15
Number of pages	12
Start Page	2679
End Page	2690
Type of Use	reuse in a thesis/dissertation
Intended publisher of new work	other
Portion	figures/tables/illustrations
Number of figures/tables /illustrations	2
Format	both print and electronic
Are you the author of this Elsevier article?	No
Will you be translating?	No

Order reference number	
Title of your thesis/dissertation	IN-SITU 3D IMAGING OF STRUCTURE AND FAILURE OF MATERIALS USING SYNCHROTRON RADIATION TOMOGRAPHY
Expected completion date	Apr 2013
Estimated size (number of pages)	80
Elsevier VAT number	GB 494 6272 12
Permissions price	0.00 USD
VAT/Local Sales Tax	0.0 USD / 0.0 GBP
Total	0.00 USD
Terms and Conditions	

INTRODUCTION

1. The publisher for this copyrighted material is Elsevier. By clicking "accept" in connection with completing this licensing transaction, you agree that the following terms and conditions apply to this transaction (along with the Billing and Payment terms and conditions established by Copyright Clearance Center, Inc. ("CCC"), at the time that you opened your Rightslink account and that are available at any time at http://myaccount.copyright.com).

GENERAL TERMS

2. Elsevier hereby grants you permission to reproduce the aforementioned material subject to the terms and conditions indicated.

3. Acknowledgement: If any part of the material to be used (for example, figures) has appeared in our publication with credit or acknowledgement to another source, permission must also be sought from that source. If such permission is not obtained then that material may not be included in your publication/copies. Suitable acknowledgement to the source must be made, either as a footnote or in a reference list at the end of your publication, as follows:

"Reprinted from Publication title, Vol /edition number, Author(s), Title of article / title of chapter, Pages No., Copyright (Year), with permission from Elsevier [OR APPLICABLE SOCIETY COPYRIGHT OWNER]." Also Lancet special credit - "Reprinted from The Lancet, Vol. number, Author(s), Title of article, Pages No., Copyright (Year), with permission from Elsevier."

4. Reproduction of this material is confined to the purpose and/or media for which permission is hereby given.

5. Altering/Modifying Material: Not Permitted. However figures and illustrations may be altered/adapted minimally to serve your work. Any other abbreviations, additions, deletions and/or any other alterations shall be made only with prior written authorization of Elsevier Ltd. (Please contact Elsevier at permissions@elsevier.com)

6. If the permission fee for the requested use of our material is waived in this instance, please be advised that your future requests for Elsevier materials may attract a fee.

7. Reservation of Rights: Publisher reserves all rights not specifically granted in the

combination of (i) the license details provided by you and accepted in the course of this licensing transaction, (ii) these terms and conditions and (iii) CCC's Billing and Payment terms and conditions.

8. License Contingent Upon Payment: While you may exercise the rights licensed immediately upon issuance of the license at the end of the licensing process for the transaction, provided that you have disclosed complete and accurate details of your proposed use, no license is finally effective unless and until full payment is received from you (either by publisher or by CCC) as provided in CCC's Billing and Payment terms and conditions. If full payment is not received on a timely basis, then any license preliminarily granted shall be deemed automatically revoked and shall be void as if never granted. Further, in the event that you breach any of these terms and conditions or any of CCC's Billing and Payment terms and conditions, the license is automatically revoked and shall be void as if never granted. Use of materials as described in a revoked license, as well as any use of the materials beyond the scope of an unrevoked license, may constitute copyright infringement and publisher reserves the right to take any and all action to protect its copyright in the materials.

9. Warranties: Publisher makes no representations or warranties with respect to the licensed material.

10. Indemnity: You hereby indemnify and agree to hold harmless publisher and CCC, and their respective officers, directors, employees and agents, from and against any and all claims arising out of your use of the licensed material other than as specifically authorized pursuant to this license.

11. No Transfer of License: This license is personal to you and may not be sublicensed, assigned, or transferred by you to any other person without publisher's written permission.

12. No Amendment Except in Writing: This license may not be amended except in a writing signed by both parties (or, in the case of publisher, by CCC on publisher's behalf).

13. Objection to Contrary Terms: Publisher hereby objects to any terms contained in any purchase order, acknowledgment, check endorsement or other writing prepared by you, which terms are inconsistent with these terms and conditions or CCC's Billing and Payment terms and conditions. These terms and conditions, together with CCC's Billing and Payment terms and conditions (which are incorporated herein), comprise the entire agreement between you and publisher (and CCC) concerning this licensing transaction. In the event of any conflict between your obligations established by these terms and conditions and those established by CCC's Billing and Payment terms and conditions, these terms and conditions shall control.

14. Revocation: Elsevier or Copyright Clearance Center may deny the permissions described in this License at their sole discretion, for any reason or no reason, with a full refund payable to you. Notice of such denial will be made using the contact information provided by you. Failure to receive such notice will not alter or invalidate the denial. In no event will Elsevier or Copyright Clearance Center be responsible or liable for any costs, expenses or damage incurred by you as a result of a denial of your permission request, other than a refund of the amount(s) paid by you to Elsevier and/or Copyright Clearance Center for denied permissions.

LIMITED LICENSE

The following terms and conditions apply only to specific license types:

15. **Translation**: This permission is granted for non-exclusive world **English** rights only unless your license was granted for translation rights. If you licensed translation rights you may only translate this content into the languages you requested. A professional translator must perform all translations and reproduce the content word for word preserving the integrity of the article. If this license is to re-use 1 or 2 figures then permission is granted for non-exclusive world rights in all languages.

16. **Website**: The following terms and conditions apply to electronic reserve and author websites:
Electronic reserve: If licensed material is to be posted to website, the web site is to be password-protected and made available only to bona fide students registered on a relevant course if:
This license was made in connection with a course,
This permission is granted for 1 year only. You may obtain a license for future website posting,
All content posted to the web site must maintain the copyright information line on the bottom of each image,
A hyper-text must be included to the Homepage of the journal from which you are licensing at http://www.sciencedirect.com/science/journal/xxxxx or the Elsevier homepage for books at http://www.elsevier.com , and
Central Storage: This license does not include permission for a scanned version of the material to be stored in a central repository such as that provided by Heron/XanEdu.

17. **Author website** for journals with the following additional clauses:

All content posted to the web site must maintain the copyright information line on the bottom of each image, and the permission granted is limited to the personal version of your paper. You are not allowed to download and post the published electronic version of your article (whether PDF or HTML, proof or final version), nor may you scan the printed edition to create an electronic version. A hyper-text must be included to the Homepage of the journal from which you are licensing at http://www.sciencedirect.com/science/journal/xxxxx . As part of our normal production process, you will receive an e-mail notice when your article appears on Elsevier's online service ScienceDirect (www.sciencedirect.com). That e-mail will include the article's Digital Object Identifier (DOI). This number provides the electronic link to the published article and should be included in the posting of your personal version. We ask that you wait until you receive this e-mail and have the DOI to do any posting.

Central Storage: This license does not include permission for a scanned version of the material to be stored in a central repository such as that provided by Heron/XanEdu.

18. **Author website** for books with the following additional clauses:
Authors are permitted to place a brief summary of their work online only.
A hyper-text must be included to the Elsevier homepage at http://www.elsevier.com . All content posted to the web site must maintain the copyright information line on the bottom of each image. You are not allowed to download and post the published electronic version of your chapter, nor may you scan the printed edition to create an electronic version.

Central Storage: This license does not include permission for a scanned version of the

material to be stored in a central repository such as that provided by Heron/XanEdu.

19. **Website** (regular and for author): A hyper-text must be included to the Homepage of the journal from which you are licensing at http://www.sciencedirect.com/science/journal/xxxxx. or for books to the Elsevier homepage at http://www.elsevier.com

20. **Thesis/Dissertation**: If your license is for use in a thesis/dissertation your thesis may be submitted to your institution in either print or electronic form. Should your thesis be published commercially, please reapply for permission. These requirements include permission for the Library and Archives of Canada to supply single copies, on demand, of the complete thesis and include permission for UMI to supply single copies, on demand, of the complete thesis. Should your thesis be published commercially, please reapply for permission.

21. **Other Conditions**:

v1.6

If you would like to pay for this license now, please remit this license along with your payment made payable to "COPYRIGHT CLEARANCE CENTER" otherwise you will be invoiced within 48 hours of the license date. Payment should be in the form of a check or money order referencing your account number and this invoice number RLNK500990097.
Once you receive your invoice for this order, you may pay your invoice by credit card. Please follow instructions provided at that time.

Make Payment To:
Copyright Clearance Center
Dept 001
P.O. Box 843006
Boston, MA 02284-3006

For suggestions or comments regarding this order, contact RightsLink Customer Support: customercare@copyright.com or +1-877-622-5543 (toll free in the US) or +1-978-646-2777.

Gratis licenses (referencing $0 in the Total field) are free. Please retain this printable license for your reference. No payment is required.

ELSEVIER LICENSE
TERMS AND CONDITIONS

Apr 04, 2013

This is a License Agreement between K M Mostafijur Rahman ("You") and Elsevier ("Elsevier") provided by Copyright Clearance Center ("CCC"). The license consists of your order details, the terms and conditions provided by Elsevier, and the payment terms and conditions.

All payments must be made in full to CCC. For payment instructions, please see information listed at the bottom of this form.

Supplier	Elsevier Limited The Boulevard,Langford Lane Kidlington,Oxford,OX5 1GB,UK
Registered Company Number	1982084
Customer name	K M Mostafijur Rahman
Customer address	414A, 108th Street Saskatoon, SK S7N1P9
License number	3120640221929
License date	Apr 02, 2013
Licensed content publisher	Elsevier
Licensed content publication	Engineering Fracture Mechanics
Licensed content title	Damage quantification in aluminium alloys using in situ tensile tests in X-ray tomography
Licensed content author	Eric Maire,Suxia Zhou,Jerome Adrien,Marco Dimichiel
Licensed content date	October 2011
Licensed content volume number	78
Licensed content issue number	15
Number of pages	12
Start Page	2679
End Page	2690
Type of Use	reuse in a thesis/dissertation
Intended publisher of new work	other
Portion	figures/tables/illustrations
Number of figures/tables /illustrations	3
Format	both print and electronic
Are you the author of this Elsevier article?	No
Will you be translating?	No

Order reference number	
Title of your thesis/dissertation	IN-SITU 3D IMAGING OF STRUCTURE AND FAILURE OF MATERIALS USING SYNCHROTRON RADIATION TOMOGRAPHY
Expected completion date	Apr 2013
Estimated size (number of pages)	80
Elsevier VAT number	GB 494 6272 12
Permissions price	0.00 USD
VAT/Local Sales Tax	0.0 USD / 0.0 GBP
Total	0.00 USD
Terms and Conditions	

INTRODUCTION

1. The publisher for this copyrighted material is Elsevier. By clicking "accept" in connection with completing this licensing transaction, you agree that the following terms and conditions apply to this transaction (along with the Billing and Payment terms and conditions established by Copyright Clearance Center, Inc. ("CCC"), at the time that you opened your Rightslink account and that are available at any time at http://myaccount.copyright.com).

GENERAL TERMS

2. Elsevier hereby grants you permission to reproduce the aforementioned material subject to the terms and conditions indicated.

3. Acknowledgement: If any part of the material to be used (for example, figures) has appeared in our publication with credit or acknowledgement to another source, permission must also be sought from that source. If such permission is not obtained then that material may not be included in your publication/copies. Suitable acknowledgement to the source must be made, either as a footnote or in a reference list at the end of your publication, as follows:

"Reprinted from Publication title, Vol /edition number, Author(s), Title of article / title of chapter, Pages No., Copyright (Year), with permission from Elsevier [OR APPLICABLE SOCIETY COPYRIGHT OWNER]." Also Lancet special credit - "Reprinted from The Lancet, Vol. number, Author(s), Title of article, Pages No., Copyright (Year), with permission from Elsevier."

4. Reproduction of this material is confined to the purpose and/or media for which permission is hereby given.

5. Altering/Modifying Material: Not Permitted. However figures and illustrations may be altered/adapted minimally to serve your work. Any other abbreviations, additions, deletions and/or any other alterations shall be made only with prior written authorization of Elsevier Ltd. (Please contact Elsevier at permissions@elsevier.com)

6. If the permission fee for the requested use of our material is waived in this instance, please be advised that your future requests for Elsevier materials may attract a fee.

7. Reservation of Rights: Publisher reserves all rights not specifically granted in the

combination of (i) the license details provided by you and accepted in the course of this licensing transaction, (ii) these terms and conditions and (iii) CCC's Billing and Payment terms and conditions.

8. License Contingent Upon Payment: While you may exercise the rights licensed immediately upon issuance of the license at the end of the licensing process for the transaction, provided that you have disclosed complete and accurate details of your proposed use, no license is finally effective unless and until full payment is received from you (either by publisher or by CCC) as provided in CCC's Billing and Payment terms and conditions. If full payment is not received on a timely basis, then any license preliminarily granted shall be deemed automatically revoked and shall be void as if never granted. Further, in the event that you breach any of these terms and conditions or any of CCC's Billing and Payment terms and conditions, the license is automatically revoked and shall be void as if never granted. Use of materials as described in a revoked license, as well as any use of the materials beyond the scope of an unrevoked license, may constitute copyright infringement and publisher reserves the right to take any and all action to protect its copyright in the materials.

9. Warranties: Publisher makes no representations or warranties with respect to the licensed material.

10. Indemnity: You hereby indemnify and agree to hold harmless publisher and CCC, and their respective officers, directors, employees and agents, from and against any and all claims arising out of your use of the licensed material other than as specifically authorized pursuant to this license.

11. No Transfer of License: This license is personal to you and may not be sublicensed, assigned, or transferred by you to any other person without publisher's written permission.

12. No Amendment Except in Writing: This license may not be amended except in a writing signed by both parties (or, in the case of publisher, by CCC on publisher's behalf).

13. Objection to Contrary Terms: Publisher hereby objects to any terms contained in any purchase order, acknowledgment, check endorsement or other writing prepared by you, which terms are inconsistent with these terms and conditions or CCC's Billing and Payment terms and conditions. These terms and conditions, together with CCC's Billing and Payment terms and conditions (which are incorporated herein), comprise the entire agreement between you and publisher (and CCC) concerning this licensing transaction. In the event of any conflict between your obligations established by these terms and conditions and those established by CCC's Billing and Payment terms and conditions, these terms and conditions shall control.

14. Revocation: Elsevier or Copyright Clearance Center may deny the permissions described in this License at their sole discretion, for any reason or no reason, with a full refund payable to you. Notice of such denial will be made using the contact information provided by you. Failure to receive such notice will not alter or invalidate the denial. In no event will Elsevier or Copyright Clearance Center be responsible or liable for any costs, expenses or damage incurred by you as a result of a denial of your permission request, other than a refund of the amount(s) paid by you to Elsevier and/or Copyright Clearance Center for denied permissions.

LIMITED LICENSE

The following terms and conditions apply only to specific license types:

15. **Translation**: This permission is granted for non-exclusive world **English** rights only unless your license was granted for translation rights. If you licensed translation rights you may only translate this content into the languages you requested. A professional translator must perform all translations and reproduce the content word for word preserving the integrity of the article. If this license is to re-use 1 or 2 figures then permission is granted for non-exclusive world rights in all languages.

16. **Website**: The following terms and conditions apply to electronic reserve and author websites:
Electronic reserve: If licensed material is to be posted to website, the web site is to be password-protected and made available only to bona fide students registered on a relevant course if:
This license was made in connection with a course,
This permission is granted for 1 year only. You may obtain a license for future website posting,
All content posted to the web site must maintain the copyright information line on the bottom of each image,
A hyper-text must be included to the Homepage of the journal from which you are licensing at http://www.sciencedirect.com/science/journal/xxxxx or the Elsevier homepage for books at http://www.elsevier.com , and
Central Storage: This license does not include permission for a scanned version of the material to be stored in a central repository such as that provided by Heron/XanEdu.

17. **Author website** for journals with the following additional clauses:

All content posted to the web site must maintain the copyright information line on the bottom of each image, and the permission granted is limited to the personal version of your paper. You are not allowed to download and post the published electronic version of your article (whether PDF or HTML, proof or final version), nor may you scan the printed edition to create an electronic version. A hyper-text must be included to the Homepage of the journal from which you are licensing at http://www.sciencedirect.com/science/journal/xxxxx . As part of our normal production process, you will receive an e-mail notice when your article appears on Elsevier's online service ScienceDirect (www.sciencedirect.com). That e-mail will include the article's Digital Object Identifier (DOI). This number provides the electronic link to the published article and should be included in the posting of your personal version. We ask that you wait until you receive this e-mail and have the DOI to do any posting.

Central Storage: This license does not include permission for a scanned version of the material to be stored in a central repository such as that provided by Heron/XanEdu.

18. **Author website** for books with the following additional clauses:
Authors are permitted to place a brief summary of their work online only.
A hyper-text must be included to the Elsevier homepage at http://www.elsevier.com . All content posted to the web site must maintain the copyright information line on the bottom of each image. You are not allowed to download and post the published electronic version of your chapter, nor may you scan the printed edition to create an electronic version.

Central Storage: This license does not include permission for a scanned version of the

material to be stored in a central repository such as that provided by Heron/XanEdu.

19. **Website** (regular and for author): A hyper-text must be included to the Homepage of the journal from which you are licensing at http://www.sciencedirect.com/science/journal/xxxxx. or for books to the Elsevier homepage at http://www.elsevier.com

20. **Thesis/Dissertation**: If your license is for use in a thesis/dissertation your thesis may be submitted to your institution in either print or electronic form. Should your thesis be published commercially, please reapply for permission. These requirements include permission for the Library and Archives of Canada to supply single copies, on demand, of the complete thesis and include permission for UMI to supply single copies, on demand, of the complete thesis. Should your thesis be published commercially, please reapply for permission.

21. **Other Conditions**:

v1.6

If you would like to pay for this license now, please remit this license along with your payment made payable to "COPYRIGHT CLEARANCE CENTER" otherwise you will be invoiced within 48 hours of the license date. Payment should be in the form of a check or money order referencing your account number and this invoice number RLNK500990100.
Once you receive your invoice for this order, you may pay your invoice by credit card. Please follow instructions provided at that time.

Make Payment To:
Copyright Clearance Center
Dept 001
P.O. Box 843006
Boston, MA 02284-3006

For suggestions or comments regarding this order, contact RightsLink Customer Support: customercare@copyright.com or +1-877-622-5543 (toll free in the US) or +1-978-646-2777.

Gratis licenses (referencing $0 in the Total field) are free. Please retain this printable license for your reference. No payment is required.

ELSEVIER LICENSE
TERMS AND CONDITIONS

Apr 04, 2013

This is a License Agreement between K M Mostafijur Rahman ("You") and Elsevier ("Elsevier") provided by Copyright Clearance Center ("CCC"). The license consists of your order details, the terms and conditions provided by Elsevier, and the payment terms and conditions.

All payments must be made in full to CCC. For payment instructions, please see information listed at the bottom of this form.

Supplier	Elsevier Limited The Boulevard,Langford Lane Kidlington,Oxford,OX5 1GB,UK
Registered Company Number	1982084
Customer name	K M Mostafijur Rahman
Customer address	414A, 108th Street Saskatoon, SK S7N1P9
License number	3120631120285
License date	Apr 02, 2013
Licensed content publisher	Elsevier
Licensed content publication	Acta Materialia
Licensed content title	Damage evolution in SiC particle reinforced Al alloy matrix composites by X-ray synchrotron tomography
Licensed content author	J.J. Williams,Z. Flom,A.A. Amell,N. Chawla,X. Xiao,F. De Carlo
Licensed content date	October 2010
Licensed content volume number	58
Licensed content issue number	18
Number of pages	12
Start Page	6194
End Page	6205
Type of Use	reuse in a thesis/dissertation
Portion	figures/tables/illustrations
Number of figures/tables /illustrations	8
Format	both print and electronic
Are you the author of this Elsevier article?	No
Will you be translating?	No
Order reference number	

Title of your thesis/dissertation	IN-SITU 3D IMAGING OF STRUCTURE AND FAILURE OF MATERIALS USING SYNCHROTRON RADIATION TOMOGRAPHY
Expected completion date	Apr 2013
Estimated size (number of pages)	80
Elsevier VAT number	GB 494 6272 12
Permissions price	0.00 USD
VAT/Local Sales Tax	0.0 USD / 0.0 GBP
Total	0.00 USD
Terms and Conditions	

INTRODUCTION

1. The publisher for this copyrighted material is Elsevier. By clicking "accept" in connection with completing this licensing transaction, you agree that the following terms and conditions apply to this transaction (along with the Billing and Payment terms and conditions established by Copyright Clearance Center, Inc. ("CCC"), at the time that you opened your Rightslink account and that are available at any time at http://myaccount.copyright.com).

GENERAL TERMS

2. Elsevier hereby grants you permission to reproduce the aforementioned material subject to the terms and conditions indicated.

3. Acknowledgement: If any part of the material to be used (for example, figures) has appeared in our publication with credit or acknowledgement to another source, permission must also be sought from that source. If such permission is not obtained then that material may not be included in your publication/copies. Suitable acknowledgement to the source must be made, either as a footnote or in a reference list at the end of your publication, as follows:

“Reprinted from Publication title, Vol /edition number, Author(s), Title of article / title of chapter, Pages No., Copyright (Year), with permission from Elsevier [OR APPLICABLE SOCIETY COPYRIGHT OWNER].” Also Lancet special credit - “Reprinted from The Lancet, Vol. number, Author(s), Title of article, Pages No., Copyright (Year), with permission from Elsevier.”

4. Reproduction of this material is confined to the purpose and/or media for which permission is hereby given.

5. Altering/Modifying Material: Not Permitted. However figures and illustrations may be altered/adapted minimally to serve your work. Any other abbreviations, additions, deletions and/or any other alterations shall be made only with prior written authorization of Elsevier Ltd. (Please contact Elsevier at permissions@elsevier.com)

6. If the permission fee for the requested use of our material is waived in this instance, please be advised that your future requests for Elsevier materials may attract a fee.

7. Reservation of Rights: Publisher reserves all rights not specifically granted in the combination of (i) the license details provided by you and accepted in the course of this

licensing transaction, (ii) these terms and conditions and (iii) CCC's Billing and Payment terms and conditions.

8. License Contingent Upon Payment: While you may exercise the rights licensed immediately upon issuance of the license at the end of the licensing process for the transaction, provided that you have disclosed complete and accurate details of your proposed use, no license is finally effective unless and until full payment is received from you (either by publisher or by CCC) as provided in CCC's Billing and Payment terms and conditions. If full payment is not received on a timely basis, then any license preliminarily granted shall be deemed automatically revoked and shall be void as if never granted. Further, in the event that you breach any of these terms and conditions or any of CCC's Billing and Payment terms and conditions, the license is automatically revoked and shall be void as if never granted. Use of materials as described in a revoked license, as well as any use of the materials beyond the scope of an unrevoked license, may constitute copyright infringement and publisher reserves the right to take any and all action to protect its copyright in the materials.

9. Warranties: Publisher makes no representations or warranties with respect to the licensed material.

10. Indemnity: You hereby indemnify and agree to hold harmless publisher and CCC, and their respective officers, directors, employees and agents, from and against any and all claims arising out of your use of the licensed material other than as specifically authorized pursuant to this license.

11. No Transfer of License: This license is personal to you and may not be sublicensed, assigned, or transferred by you to any other person without publisher's written permission.

12. No Amendment Except in Writing: This license may not be amended except in a writing signed by both parties (or, in the case of publisher, by CCC on publisher's behalf).

13. Objection to Contrary Terms: Publisher hereby objects to any terms contained in any purchase order, acknowledgment, check endorsement or other writing prepared by you, which terms are inconsistent with these terms and conditions or CCC's Billing and Payment terms and conditions. These terms and conditions, together with CCC's Billing and Payment terms and conditions (which are incorporated herein), comprise the entire agreement between you and publisher (and CCC) concerning this licensing transaction. In the event of any conflict between your obligations established by these terms and conditions and those established by CCC's Billing and Payment terms and conditions, these terms and conditions shall control.

14. Revocation: Elsevier or Copyright Clearance Center may deny the permissions described in this License at their sole discretion, for any reason or no reason, with a full refund payable to you. Notice of such denial will be made using the contact information provided by you. Failure to receive such notice will not alter or invalidate the denial. In no event will Elsevier or Copyright Clearance Center be responsible or liable for any costs, expenses or damage incurred by you as a result of a denial of your permission request, other than a refund of the amount(s) paid by you to Elsevier and/or Copyright Clearance Center for denied permissions.

LIMITED LICENSE

The following terms and conditions apply only to specific license types:

15. **Translation**: This permission is granted for non-exclusive world **English** rights only unless your license was granted for translation rights. If you licensed translation rights you may only translate this content into the languages you requested. A professional translator must perform all translations and reproduce the content word for word preserving the integrity of the article. If this license is to re-use 1 or 2 figures then permission is granted for non-exclusive world rights in all languages.

16. **Website**: The following terms and conditions apply to electronic reserve and author websites:
Electronic reserve: If licensed material is to be posted to website, the web site is to be password-protected and made available only to bona fide students registered on a relevant course if:
This license was made in connection with a course,
This permission is granted for 1 year only. You may obtain a license for future website posting,
All content posted to the web site must maintain the copyright information line on the bottom of each image,
A hyper-text must be included to the Homepage of the journal from which you are licensing at http://www.sciencedirect.com/science/journal/xxxxx or the Elsevier homepage for books at http://www.elsevier.com , and
Central Storage: This license does not include permission for a scanned version of the material to be stored in a central repository such as that provided by Heron/XanEdu.

17. **Author website** for journals with the following additional clauses:

All content posted to the web site must maintain the copyright information line on the bottom of each image, and the permission granted is limited to the personal version of your paper. You are not allowed to download and post the published electronic version of your article (whether PDF or HTML, proof or final version), nor may you scan the printed edition to create an electronic version. A hyper-text must be included to the Homepage of the journal from which you are licensing at http://www.sciencedirect.com/science/journal/xxxxx . As part of our normal production process, you will receive an e-mail notice when your article appears on Elsevier's online service ScienceDirect (www.sciencedirect.com). That e-mail will include the article's Digital Object Identifier (DOI). This number provides the electronic link to the published article and should be included in the posting of your personal version. We ask that you wait until you receive this e-mail and have the DOI to do any posting.

Central Storage: This license does not include permission for a scanned version of the material to be stored in a central repository such as that provided by Heron/XanEdu.

18. **Author website** for books with the following additional clauses:
Authors are permitted to place a brief summary of their work online only.
A hyper-text must be included to the Elsevier homepage at http://www.elsevier.com . All content posted to the web site must maintain the copyright information line on the bottom of each image. You are not allowed to download and post the published electronic version of your chapter, nor may you scan the printed edition to create an electronic version.

Central Storage: This license does not include permission for a scanned version of the

material to be stored in a central repository such as that provided by Heron/XanEdu.

19. **Website** (regular and for author): A hyper-text must be included to the Homepage of the journal from which you are licensing at http://www.sciencedirect.com/science/journal/xxxxx. or for books to the Elsevier homepage at http://www.elsevier.com

20. **Thesis/Dissertation**: If your license is for use in a thesis/dissertation your thesis may be submitted to your institution in either print or electronic form. Should your thesis be published commercially, please reapply for permission. These requirements include permission for the Library and Archives of Canada to supply single copies, on demand, of the complete thesis and include permission for UMI to supply single copies, on demand, of the complete thesis. Should your thesis be published commercially, please reapply for permission.

21. **Other Conditions**:

v1.6

If you would like to pay for this license now, please remit this license along with your payment made payable to "COPYRIGHT CLEARANCE CENTER" otherwise you will be invoiced within 48 hours of the license date. Payment should be in the form of a check or money order referencing your account number and this invoice number RLNK500990087.
Once you receive your invoice for this order, you may pay your invoice by credit card. Please follow instructions provided at that time.

Make Payment To:
Copyright Clearance Center
Dept 001
P.O. Box 843006
Boston, MA 02284-3006

For suggestions or comments regarding this order, contact RightsLink Customer Support: customercare@copyright.com or +1-877-622-5543 (toll free in the US) or +1-978-646-2777.

Gratis licenses (referencing $0 in the Total field) are free. Please retain this printable license for your reference. No payment is required.

ELSEVIER LICENSE
TERMS AND CONDITIONS

Apr 04, 2013

This is a License Agreement between K M Mostafijur Rahman ("You") and Elsevier ("Elsevier") provided by Copyright Clearance Center ("CCC"). The license consists of your order details, the terms and conditions provided by Elsevier, and the payment terms and conditions.

All payments must be made in full to CCC. For payment instructions, please see information listed at the bottom of this form.

Supplier	Elsevier Limited The Boulevard,Langford Lane Kidlington,Oxford,OX5 1GB,UK
Registered Company Number	1982084
Customer name	K M Mostafijur Rahman
Customer address	414A, 108th Street Saskatoon, SK S7N1P9
License number	3120631488745
License date	Apr 02, 2013
Licensed content publisher	Elsevier
Licensed content publication	Acta Materialia
Licensed content title	Damage evolution in SiC particle reinforced Al alloy matrix composites by X-ray synchrotron tomography
Licensed content author	J.J. Williams,Z. Flom,A.A. Amell,N. Chawla,X. Xiao,F. De Carlo
Licensed content date	October 2010
Licensed content volume number	58
Licensed content issue number	18
Number of pages	12
Start Page	6194
End Page	6205
Type of Use	reuse in a thesis/dissertation
Portion	figures/tables/illustrations
Number of figures/tables /illustrations	9
Format	both print and electronic
Are you the author of this Elsevier article?	No
Will you be translating?	No
Order reference number	

Title of your thesis/dissertation	IN-SITU 3D IMAGING OF STRUCTURE AND FAILURE OF MATERIALS USING SYNCHROTRON RADIATION TOMOGRAPHY
Expected completion date	Apr 2013
Estimated size (number of pages)	80
Elsevier VAT number	GB 494 6272 12
Permissions price	0.00 USD
VAT/Local Sales Tax	0.0 USD / 0.0 GBP
Total	0.00 USD
Terms and Conditions	

INTRODUCTION

1. The publisher for this copyrighted material is Elsevier. By clicking "accept" in connection with completing this licensing transaction, you agree that the following terms and conditions apply to this transaction (along with the Billing and Payment terms and conditions established by Copyright Clearance Center, Inc. ("CCC"), at the time that you opened your Rightslink account and that are available at any time at http://myaccount.copyright.com).

GENERAL TERMS

2. Elsevier hereby grants you permission to reproduce the aforementioned material subject to the terms and conditions indicated.

3. Acknowledgement: If any part of the material to be used (for example, figures) has appeared in our publication with credit or acknowledgement to another source, permission must also be sought from that source. If such permission is not obtained then that material may not be included in your publication/copies. Suitable acknowledgement to the source must be made, either as a footnote or in a reference list at the end of your publication, as follows:

"Reprinted from Publication title, Vol /edition number, Author(s), Title of article / title of chapter, Pages No., Copyright (Year), with permission from Elsevier [OR APPLICABLE SOCIETY COPYRIGHT OWNER]." Also Lancet special credit - "Reprinted from The Lancet, Vol. number, Author(s), Title of article, Pages No., Copyright (Year), with permission from Elsevier."

4. Reproduction of this material is confined to the purpose and/or media for which permission is hereby given.

5. Altering/Modifying Material: Not Permitted. However figures and illustrations may be altered/adapted minimally to serve your work. Any other abbreviations, additions, deletions and/or any other alterations shall be made only with prior written authorization of Elsevier Ltd. (Please contact Elsevier at permissions@elsevier.com)

6. If the permission fee for the requested use of our material is waived in this instance, please be advised that your future requests for Elsevier materials may attract a fee.

7. Reservation of Rights: Publisher reserves all rights not specifically granted in the combination of (i) the license details provided by you and accepted in the course of this

licensing transaction, (ii) these terms and conditions and (iii) CCC's Billing and Payment terms and conditions.

8. License Contingent Upon Payment: While you may exercise the rights licensed immediately upon issuance of the license at the end of the licensing process for the transaction, provided that you have disclosed complete and accurate details of your proposed use, no license is finally effective unless and until full payment is received from you (either by publisher or by CCC) as provided in CCC's Billing and Payment terms and conditions. If full payment is not received on a timely basis, then any license preliminarily granted shall be deemed automatically revoked and shall be void as if never granted. Further, in the event that you breach any of these terms and conditions or any of CCC's Billing and Payment terms and conditions, the license is automatically revoked and shall be void as if never granted. Use of materials as described in a revoked license, as well as any use of the materials beyond the scope of an unrevoked license, may constitute copyright infringement and publisher reserves the right to take any and all action to protect its copyright in the materials.

9. Warranties: Publisher makes no representations or warranties with respect to the licensed material.

10. Indemnity: You hereby indemnify and agree to hold harmless publisher and CCC, and their respective officers, directors, employees and agents, from and against any and all claims arising out of your use of the licensed material other than as specifically authorized pursuant to this license.

11. No Transfer of License: This license is personal to you and may not be sublicensed, assigned, or transferred by you to any other person without publisher's written permission.

12. No Amendment Except in Writing: This license may not be amended except in a writing signed by both parties (or, in the case of publisher, by CCC on publisher's behalf).

13. Objection to Contrary Terms: Publisher hereby objects to any terms contained in any purchase order, acknowledgment, check endorsement or other writing prepared by you, which terms are inconsistent with these terms and conditions or CCC's Billing and Payment terms and conditions. These terms and conditions, together with CCC's Billing and Payment terms and conditions (which are incorporated herein), comprise the entire agreement between you and publisher (and CCC) concerning this licensing transaction. In the event of any conflict between your obligations established by these terms and conditions and those established by CCC's Billing and Payment terms and conditions, these terms and conditions shall control.

14. Revocation: Elsevier or Copyright Clearance Center may deny the permissions described in this License at their sole discretion, for any reason or no reason, with a full refund payable to you. Notice of such denial will be made using the contact information provided by you. Failure to receive such notice will not alter or invalidate the denial. In no event will Elsevier or Copyright Clearance Center be responsible or liable for any costs, expenses or damage incurred by you as a result of a denial of your permission request, other than a refund of the amount(s) paid by you to Elsevier and/or Copyright Clearance Center for denied permissions.

LIMITED LICENSE

The following terms and conditions apply only to specific license types:

15. **Translation**: This permission is granted for non-exclusive world **English** rights only unless your license was granted for translation rights. If you licensed translation rights you may only translate this content into the languages you requested. A professional translator must perform all translations and reproduce the content word for word preserving the integrity of the article. If this license is to re-use 1 or 2 figures then permission is granted for non-exclusive world rights in all languages.

16. **Website**: The following terms and conditions apply to electronic reserve and author websites:
Electronic reserve: If licensed material is to be posted to website, the web site is to be password-protected and made available only to bona fide students registered on a relevant course if:
This license was made in connection with a course,
This permission is granted for 1 year only. You may obtain a license for future website posting,
All content posted to the web site must maintain the copyright information line on the bottom of each image,
A hyper-text must be included to the Homepage of the journal from which you are licensing at http://www.sciencedirect.com/science/journal/xxxxx or the Elsevier homepage for books at http://www.elsevier.com , and
Central Storage: This license does not include permission for a scanned version of the material to be stored in a central repository such as that provided by Heron/XanEdu.

17. **Author website** for journals with the following additional clauses:

All content posted to the web site must maintain the copyright information line on the bottom of each image, and the permission granted is limited to the personal version of your paper. You are not allowed to download and post the published electronic version of your article (whether PDF or HTML, proof or final version), nor may you scan the printed edition to create an electronic version. A hyper-text must be included to the Homepage of the journal from which you are licensing at http://www.sciencedirect.com/science/journal/xxxxx . As part of our normal production process, you will receive an e-mail notice when your article appears on Elsevier's online service ScienceDirect (www.sciencedirect.com). That e-mail will include the article's Digital Object Identifier (DOI). This number provides the electronic link to the published article and should be included in the posting of your personal version. We ask that you wait until you receive this e-mail and have the DOI to do any posting.

Central Storage: This license does not include permission for a scanned version of the material to be stored in a central repository such as that provided by Heron/XanEdu.

18. **Author website** for books with the following additional clauses:
Authors are permitted to place a brief summary of their work online only.
A hyper-text must be included to the Elsevier homepage at http://www.elsevier.com . All content posted to the web site must maintain the copyright information line on the bottom of each image. You are not allowed to download and post the published electronic version of your chapter, nor may you scan the printed edition to create an electronic version.

Central Storage: This license does not include permission for a scanned version of the

material to be stored in a central repository such as that provided by Heron/XanEdu.

19. **Website** (regular and for author): A hyper-text must be included to the Homepage of the journal from which you are licensing at http://www.sciencedirect.com/science/journal/xxxxx. or for books to the Elsevier homepage at http://www.elsevier.com

20. **Thesis/Dissertation**: If your license is for use in a thesis/dissertation your thesis may be submitted to your institution in either print or electronic form. Should your thesis be published commercially, please reapply for permission. These requirements include permission for the Library and Archives of Canada to supply single copies, on demand, of the complete thesis and include permission for UMI to supply single copies, on demand, of the complete thesis. Should your thesis be published commercially, please reapply for permission.

21. **Other Conditions**:

v1.6

If you would like to pay for this license now, please remit this license along with your payment made payable to "COPYRIGHT CLEARANCE CENTER" otherwise you will be invoiced within 48 hours of the license date. Payment should be in the form of a check or money order referencing your account number and this invoice number RLNK500990090.
Once you receive your invoice for this order, you may pay your invoice by credit card. Please follow instructions provided at that time.

Make Payment To:
Copyright Clearance Center
Dept 001
P.O. Box 843006
Boston, MA 02284-3006

For suggestions or comments regarding this order, contact RightsLink Customer Support: customercare@copyright.com or +1-877-622-5543 (toll free in the US) or +1-978-646-2777.

Gratis licenses (referencing $0 in the Total field) are free. Please retain this printable license for your reference. No payment is required.

ELSEVIER LICENSE
TERMS AND CONDITIONS

Apr 04, 2013

This is a License Agreement between K M Mostafijur Rahman ("You") and Elsevier ("Elsevier") provided by Copyright Clearance Center ("CCC"). The license consists of your order details, the terms and conditions provided by Elsevier, and the payment terms and conditions.

All payments must be made in full to CCC. For payment instructions, please see information listed at the bottom of this form.

Supplier	Elsevier Limited The Boulevard,Langford Lane Kidlington,Oxford,OX5 1GB,UK
Registered Company Number	1982084
Customer name	K M Mostafijur Rahman
Customer address	414A, 108th Street Saskatoon, SK S7N1P9
License number	3120640055907
License date	Apr 02, 2013
Licensed content publisher	Elsevier
Licensed content publication	Acta Materialia
Licensed content title	Damage evolution in SiC particle reinforced Al alloy matrix composites by X-ray synchrotron tomography
Licensed content author	J.J. Williams,Z. Flom,A.A. Amell,N. Chawla,X. Xiao,F. De Carlo
Licensed content date	October 2010
Licensed content volume number	58
Licensed content issue number	18
Number of pages	12
Start Page	6194
End Page	6205
Type of Use	reuse in a thesis/dissertation
Intended publisher of new work	other
Portion	figures/tables/illustrations
Number of figures/tables /illustrations	10
Format	both print and electronic
Are you the author of this Elsevier article?	No
Will you be translating?	No

Order reference number	
Title of your thesis/dissertation	IN-SITU 3D IMAGING OF STRUCTURE AND FAILURE OF MATERIALS USING SYNCHROTRON RADIATION TOMOGRAPHY
Expected completion date	Apr 2013
Estimated size (number of pages)	80
Elsevier VAT number	GB 494 6272 12
Permissions price	0.00 USD
VAT/Local Sales Tax	0.0 USD / 0.0 GBP
Total	0.00 USD
Terms and Conditions	

INTRODUCTION

1. The publisher for this copyrighted material is Elsevier. By clicking "accept" in connection with completing this licensing transaction, you agree that the following terms and conditions apply to this transaction (along with the Billing and Payment terms and conditions established by Copyright Clearance Center, Inc. ("CCC"), at the time that you opened your Rightslink account and that are available at any time at http://myaccount.copyright.com).

GENERAL TERMS

2. Elsevier hereby grants you permission to reproduce the aforementioned material subject to the terms and conditions indicated.

3. Acknowledgement: If any part of the material to be used (for example, figures) has appeared in our publication with credit or acknowledgement to another source, permission must also be sought from that source. If such permission is not obtained then that material may not be included in your publication/copies. Suitable acknowledgement to the source must be made, either as a footnote or in a reference list at the end of your publication, as follows:

"Reprinted from Publication title, Vol /edition number, Author(s), Title of article / title of chapter, Pages No., Copyright (Year), with permission from Elsevier [OR APPLICABLE SOCIETY COPYRIGHT OWNER]." Also Lancet special credit - "Reprinted from The Lancet, Vol. number, Author(s), Title of article, Pages No., Copyright (Year), with permission from Elsevier."

4. Reproduction of this material is confined to the purpose and/or media for which permission is hereby given.

5. Altering/Modifying Material: Not Permitted. However figures and illustrations may be altered/adapted minimally to serve your work. Any other abbreviations, additions, deletions and/or any other alterations shall be made only with prior written authorization of Elsevier Ltd. (Please contact Elsevier at permissions@elsevier.com)

6. If the permission fee for the requested use of our material is waived in this instance, please be advised that your future requests for Elsevier materials may attract a fee.

7. Reservation of Rights: Publisher reserves all rights not specifically granted in the

combination of (i) the license details provided by you and accepted in the course of this licensing transaction, (ii) these terms and conditions and (iii) CCC's Billing and Payment terms and conditions.

8. License Contingent Upon Payment: While you may exercise the rights licensed immediately upon issuance of the license at the end of the licensing process for the transaction, provided that you have disclosed complete and accurate details of your proposed use, no license is finally effective unless and until full payment is received from you (either by publisher or by CCC) as provided in CCC's Billing and Payment terms and conditions. If full payment is not received on a timely basis, then any license preliminarily granted shall be deemed automatically revoked and shall be void as if never granted. Further, in the event that you breach any of these terms and conditions or any of CCC's Billing and Payment terms and conditions, the license is automatically revoked and shall be void as if never granted. Use of materials as described in a revoked license, as well as any use of the materials beyond the scope of an unrevoked license, may constitute copyright infringement and publisher reserves the right to take any and all action to protect its copyright in the materials.

9. Warranties: Publisher makes no representations or warranties with respect to the licensed material.

10. Indemnity: You hereby indemnify and agree to hold harmless publisher and CCC, and their respective officers, directors, employees and agents, from and against any and all claims arising out of your use of the licensed material other than as specifically authorized pursuant to this license.

11. No Transfer of License: This license is personal to you and may not be sublicensed, assigned, or transferred by you to any other person without publisher's written permission.

12. No Amendment Except in Writing: This license may not be amended except in a writing signed by both parties (or, in the case of publisher, by CCC on publisher's behalf).

13. Objection to Contrary Terms: Publisher hereby objects to any terms contained in any purchase order, acknowledgment, check endorsement or other writing prepared by you, which terms are inconsistent with these terms and conditions or CCC's Billing and Payment terms and conditions. These terms and conditions, together with CCC's Billing and Payment terms and conditions (which are incorporated herein), comprise the entire agreement between you and publisher (and CCC) concerning this licensing transaction. In the event of any conflict between your obligations established by these terms and conditions and those established by CCC's Billing and Payment terms and conditions, these terms and conditions shall control.

14. Revocation: Elsevier or Copyright Clearance Center may deny the permissions described in this License at their sole discretion, for any reason or no reason, with a full refund payable to you. Notice of such denial will be made using the contact information provided by you. Failure to receive such notice will not alter or invalidate the denial. In no event will Elsevier or Copyright Clearance Center be responsible or liable for any costs, expenses or damage incurred by you as a result of a denial of your permission request, other than a refund of the amount(s) paid by you to Elsevier and/or Copyright Clearance Center for denied permissions.

LIMITED LICENSE

The following terms and conditions apply only to specific license types:

15. **Translation**: This permission is granted for non-exclusive world **English** rights only unless your license was granted for translation rights. If you licensed translation rights you may only translate this content into the languages you requested. A professional translator must perform all translations and reproduce the content word for word preserving the integrity of the article. If this license is to re-use 1 or 2 figures then permission is granted for non-exclusive world rights in all languages.

16. **Website**: The following terms and conditions apply to electronic reserve and author websites:
Electronic reserve: If licensed material is to be posted to website, the web site is to be password-protected and made available only to bona fide students registered on a relevant course if:
This license was made in connection with a course,
This permission is granted for 1 year only. You may obtain a license for future website posting,
All content posted to the web site must maintain the copyright information line on the bottom of each image,
A hyper-text must be included to the Homepage of the journal from which you are licensing at http://www.sciencedirect.com/science/journal/xxxxx or the Elsevier homepage for books at http://www.elsevier.com , and
Central Storage: This license does not include permission for a scanned version of the material to be stored in a central repository such as that provided by Heron/XanEdu.

17. **Author website** for journals with the following additional clauses:

All content posted to the web site must maintain the copyright information line on the bottom of each image, and the permission granted is limited to the personal version of your paper. You are not allowed to download and post the published electronic version of your article (whether PDF or HTML, proof or final version), nor may you scan the printed edition to create an electronic version. A hyper-text must be included to the Homepage of the journal from which you are licensing at http://www.sciencedirect.com/science/journal/xxxxx . As part of our normal production process, you will receive an e-mail notice when your article appears on Elsevier's online service ScienceDirect (www.sciencedirect.com). That e-mail will include the article's Digital Object Identifier (DOI). This number provides the electronic link to the published article and should be included in the posting of your personal version. We ask that you wait until you receive this e-mail and have the DOI to do any posting.

Central Storage: This license does not include permission for a scanned version of the material to be stored in a central repository such as that provided by Heron/XanEdu.

18. **Author website** for books with the following additional clauses:
Authors are permitted to place a brief summary of their work online only.
A hyper-text must be included to the Elsevier homepage at http://www.elsevier.com . All content posted to the web site must maintain the copyright information line on the bottom of each image. You are not allowed to download and post the published electronic version of your chapter, nor may you scan the printed edition to create an electronic version.

Central Storage: This license does not include permission for a scanned version of the

material to be stored in a central repository such as that provided by Heron/XanEdu.

19. **Website** (regular and for author): A hyper-text must be included to the Homepage of the journal from which you are licensing at http://www.sciencedirect.com/science/journal/xxxxx. or for books to the Elsevier homepage at http://www.elsevier.com

20. **Thesis/Dissertation**: If your license is for use in a thesis/dissertation your thesis may be submitted to your institution in either print or electronic form. Should your thesis be published commercially, please reapply for permission. These requirements include permission for the Library and Archives of Canada to supply single copies, on demand, of the complete thesis and include permission for UMI to supply single copies, on demand, of the complete thesis. Should your thesis be published commercially, please reapply for permission.

21. **Other Conditions**:

v1.6

If you would like to pay for this license now, please remit this license along with your payment made payable to "COPYRIGHT CLEARANCE CENTER" otherwise you will be invoiced within 48 hours of the license date. Payment should be in the form of a check or money order referencing your account number and this invoice number RLNK500990093.
Once you receive your invoice for this order, you may pay your invoice by credit card. Please follow instructions provided at that time.

Make Payment To:
Copyright Clearance Center
Dept 001
P.O. Box 843006
Boston, MA 02284-3006

For suggestions or comments regarding this order, contact RightsLink Customer Support: customercare@copyright.com or +1-877-622-5543 (toll free in the US) or +1-978-646-2777.

Gratis licenses (referencing $0 in the Total field) are free. Please retain this printable license for your reference. No payment is required.

K M Mostafijur Rahman <mostafij.mj1310@gmail.com>

Use of figures

Steve Smith <Steve.Smith@tek84.com> Tue, Apr 2, 2013 at 9:51 AM
To: titas_mr@yahoo.com, Stephane Boucher <stephaneb@dsprelated.com>

Hi Mostafijur,
Yes, you may use up to 5 figures from The Scientist and Engineer's Guide to Signal Processing for this purpose. Thanks for asking and let me know if you need to use more. Remember to indicate in the thesis that these are not your own work, and cite where they come from. Good luck on your defense!
Regards,
Steve

Steven W. Smith, Ph.D.
President
California Technical Publishing

Dear Sir,
I want to use some text and figures from this book to illustrate the computed tomography reconstruction algorithm in M.Sc. thesis. For that reason I am seeking for your kind permission to use this book to enrich my thesis content.

Regards,
K M Mostafijur Rahman
Department Mechanical Engineering,
University of Saskatchewan.